# TREES IN A COOL CLIMATE CITY: IMPACTS ON BUILDING CARBON EMISSIONS AND GROWTH RESPONSE TO ENVIRONMENTAL GRADIENTS

by

Tedward Erker

A dissertation submitted in partial fulfillment of
the requirements for the degree of

Doctor of Philosophy

(Forestry)

at the

UNIVERSITY OF WISCONSIN–MADISON

2020

Date of final oral examination: 12/17/2019

The dissertation is approved by the following members of the Final Oral Committee:
    Philip A. Townsend, Professor, Forest and Wildlife Ecology
    Jun Zhu, Professor, Statistics
    Eric L. Kruger, Professor, Forest and Wildlife Ecology
    Christopher Kucharik, Professor, Agronomy
    Annemarie Schneider, Associate Professor, Geography

*To Bridget, Jean, and Maeve*

## ACKNOWLEDGMENTS

I would like to express my sincere gratitude to my advisor, Phil Townsend. Phil accepted me as a student even though I had no research project or grant funding and he helped me to create a research plan, write a proposal and secure funding for my work. Phil, thank you for believing in my potential as a scientist and giving me the freedom me to chose my own path (and fail along the way). I'm sorry for any headaches that I caused you in the process. I loved working with you as a teaching assistant in the forest ecology class and learning remote sensing from our lab meetings and conversations. I had no idea what I was getting into when I signed up, but looking back six years later I am very proud of all I have accomplished, and none of it would have been possible without your support, guidance, and advice. Your dedication to creating an excellent research program, your ability to communicate science, and your capacity to manage a hundred things at once provide a truly impressive example. Thank you for bringing together such a friendly, collaborative, and intelligent lab group from whom I have learned so much.

I am very honored to have an excellent graduate committe: Jun Zhu, Chris Kucharik, Annemarie Schneider, and Eric Kruger. Thanks to each of you for your advice. Thank you Chris for your patience and guidance on the work in my second chapter and letting me take part in the urban heat island work. Thank you Eric for sharing my love of trees and always finding time to discuss them or life in general. Thank you Jun for opening my eyes to the beauty in statistics and encouraging me to complete my master's degree in biometry. I owe much of who I am as a scientist to my interactions with all of you.

Thank you to all the teachers and professors who have inspired me throughout the years. A version of chapter 2 appeared as the final project in Steve Carpenter's Ecosystem Concepts course and his comments improved the final product.

Thank you to all the members of the Townsend lab past and present, in particular, Clayton Kingdon, Shawn Serbin, John Couture, Huan Gu, Ryan Sword, Alex Brito, Robi Phetteplace, Aidan Mazur, Andy Ciurro, Prabu Ravindran, Matt Garcia, Aditya Singh, Andrew Jablonski, Beckett Hills, Zhiwei Ye, Zhihui Wang, Ting Zheng, Sarika Mittra, Erin Wagner, Lei Wang, Sarah Wegmueller, Natalie Queally, Nanfeng Liu, John Clare, Adam

**CONTENTS**

## LIST OF TABLES

## LIST OF FIGURES

## ABSTRACT

Urban trees can provide important ecosystem services and disservices for city dwellers. Their growth and function is in turn altered by the urban environment humans create. We explored aspects of these relationships in the chapters below. First, we developed a method for mapping urban tree canopy cover using NAIP which is freely available for the conterminous US. We then used this tree canopy map in conjunction with energy use data for thousands of single family residential buildings in Madison, WI to show that greater tree cover was associated with an increase in energy use and the associated carbon emissions. Updating on past simulation research, we showed that trees likely increase building energy use and carbon emissions in many cool climate regions, not just Madison. Third, we derived tree height growth rates from multiple years of bias-corrected LiDAR and showed that growth rates could be largely be explained by initial tree height and genus, but foliar canopy traits derived from AVIRIS-NG imaging spectroscopy could explain much of the same variability in growth if genus information was unavailable. Urban tree height growth also varied significantly with urban environmental variables, being greatly reduced for street trees surrounded by high amounts of impervious cover.

# 1   INTRODUCTION

*those who wish to look carefully at the earth should stay at the necessary distance*

— Italo  Calvino, The Baron in the Trees (1959)

By mid-century, more than two out of every three people will live in urban areas (United Nations, 2018). Because of our concentration in cities, these environments have a strong effect on our wellbeing (Liu et al., 2017; Ward et al., 2016), despite covering less than 3% of the earth's land (Liu et al., 2014). Urban forests, the collection of trees within an urban environment, can provide ecosystem services to improve human wellbeing (Young, 2011; Roy et al., 2012; Nowak et al., 2006). However, they also provide disservices (von Döhren and Haase, 2015). Just as the magnitude of the effects of trees on the global carbon cycle and climate change are being debated (Veldman et al., 2019), the role of trees in cities needs a critical investigation to identify how to maximize services (e.g. reducing the urban heat island, reducing atmospheric carbon, and improving air quality) while minimizing disservices (e.g. conflict with infrastructure, increased mosquitos, and allergenic pollen production) (Kabisch et al., 2016; Pataki et al., 2011).

Not only do urban trees affect the urban environment, but the urban environment affects them. Urban trees are heavily managed - pruned to reduce utility conflict and selected for traits such as seedlessness, form, and/or general tolerance to pollution (Poland and McCullough, 2006; Barker, 1975). Urban trees can be more prone to damage from pests and abiotic factors (Cregg and Dix, 2001; Czerniawska-Kusza et al., 2004), and subject to a wide range of modified ecosystem processes (McDonnell et al., 2008).

This dissertation seeks to contribute to the answer of this fundamental question: "How do urban trees affect us and how do we in turn affect them?" Because the spatial distribution of trees mediates their relationship with the urban environment, the first chapter maps urban tree canopy cover for the state of Wisconsin. The second chapter explores one of the effects of trees on us: the modification of microclimates which influences building energy use and carbon emissions. The third chapter explores the potential for remote sensing to estimate urban tree height growth rates and tests for relationships between growth, imaging spectroscopy derived foliar canopy traits, and urban environmental variables.

## 2  A STATEWIDE URBAN TREE CANOPY MAPPING METHOD

## 2.1  Summary

Maps of urban tree canopy are essential to estimate the magnitude and spatial distribution of ecosystem services, and to determine who benefits from them. Our objective was to develop a repeatable method to map urban tree canopy cover for the state of Wisconsin. We compared two types of imagery (pan-sharpened 1.5 m SPOT-6 and 1 m NAIP aerial photography), three classification algorithms, seven segment sizes ranging from single pixels to 105 m$^2$ , three levels of compactness for each segment size, and sixteen subsets of features. NAIP outperformed SPOT. On average across classification algorithms there were no significant differences in map agreement. Pixel-based maps with convolution features performed as well as the best segment-based maps. The best segment size tested was 60 m$^2$ on average, but there was also a local maximum around 15 m$^2$ , which suggests a large range of possible segment sizes must be tested to find the best. The model chosen for application to the whole state was a pixel-level Random Forest classifier with 160 features, and the final state-wide map has five classes: tree/woody vegetation, grass/herbaceous vegetation, impervious surfaces/bare soil, water, and non-forested wetland. Overall accuracy for our state-wide map at the pixel-scale was 79.3% (95% CI: 77.5–81%). Errors occurred due to meter-scale heterogeneity in the urban environment which increases the errors due to spatial misregistration and the number of difficult-to-classify mixed and edge pixels. At larger management level scales, mean absolute error (MAE) decreases to about 10% at the Landsat pixel scale and about 6% at the scale of a city block. Our work is comparable to past efforts to map urban tree canopy, and the open source software and use of imagery that is freely available for all cities in the contiguous US make it broadly applicable.

## 2.2 Introduction

### Importance of Urban Tree Canopy Maps

Many methods exist to estimate canopy cover and the associated ecosystem services/disservices of urban forests. Nowak et al. (1996) reviewed methods from the 1970s to 1990s for quantification of urban tree cover using aerial photo interpretation and provided estimates of canopy cover for 68 cities. Additionally, the i-Tree software suite is a commonly used set of tools for managers and the public to assess a community's tree canopy benefits (itreetools.org). However, often due to lack of resources (time, imagery, expertise), these estimates of services/disservices often use random point sampling and visual interpretation of aerial photography to estimate canopy cover. Such methods yield accurate estimates of canopy cover (Walton et al., 2008), but the final outputs are not spatially explicit maps that indicate where ecosystem services are concentrated, and who benefits (Dobbs et al., 2014).

The location of canopy cover can affect the magnitude of its ecosystem services/disservices, for example: changing building energy use (Heisler, 1986), regulating urban climate (Heisler et al., 2015), using water (Al-Kofahi et al., 2012b), and managing storm water (Thomas et al., 2003). Maps of tree canopy cover are also needed to understand how the forest is shaped by social drivers and demographic characteristics of neighborhoods (Boone et al., 2009; Grove et al., 2014). Maps are thus a critical prerequisite for an accurate and detailed accounting of the effects of tree canopy on a city. i-Tree Landscape now uses 30 m land-cover maps to provide more spatially explicit estimates of ecosystem services. Our work was motivated by the need to develop higher resolution and extensive maps from consistent data sources that can be incorporated into online tools such as i-Tree to allow the public to estimate services at different locations and to identify plantable areas.

### Past efforts to map urban canopy cover

Given the need for urban forest canopy maps, there have been numerous successful efforts to map canopy cover, especially related to methods for working with high-resolution imagery, often comparing or demonstrating new algorithms or sensors. These maps usually have not covered entire cities (e.g. Cleve et al. (2008); Myint et al. (2011)). Other maps have been made with the specific goal of quantifying urban tree canopy impacts (see Table 2.1). Many of these maps are from the Vermont Spatial Analysis Lab (SAL). Vermont SAL has used LiDAR (light detection and ranging) as the primary input to their maps. Combining LiDAR with multiband aerial imagery, other ancillary data and hand editing, Vermont SAL have used object-based image analysis to create highly accurate maps (Ahles et al., 2016).

Table 2.1: Some cities or regions that have had complete urban canopy cover mapped.

| City or Region | Citation and/or Research Group |
|---|---|
| Baltimore, MD | Irani and Galvin (2002)[*] |
| Gwynns Falls, Baltimore, MD | Zhou and Troy (2008) |
| Phoenix, AZ | Walker and Briggs (2007) |
| Hangshou City, Zhejiang, China | Ma et al. (2015) |
| Tsukuba City, Japan | Thapa and Murayama (2009) |
| Dunedin City, New Zealand | Mathieu et al. (2007)[†] |
| New York City, NY | MacFaden et al. (2012), Vermont SAL |
| Syracuse, NY | Myeong et al. (2001) |
| Washington, D.C. | O'Neil-Dunne et al. (2009)[*‡], Vermont SAL |
| Philadelphia, PA | O'Neil-Dunne (2011)[*‡], Vermont SAL |
| Annapolis, MD | Galvin et al. (2006)[*‡], Vermont SAL |
| Des Moines, IA | O'Neil-Dunne (2009)[*‡], Vermont SAL |
| Honolulu, HI | MacFaden and O'Neil-Dunne (2012)[*‡], Vermont SAL |
| New Haven, CT | Pelletier and O'Neil-Dunne (2009)[*‡], Vermont SAL |
| Indianapolis, ID | Vermont SAL[*] |
| Cook County, IL (Chicagoland) | Vermont SAL[*] |
| Delaware | Vermont SAL[*] |
| Pennsylvania | Vermont SAL[*] |
| Boone, Campbell, and Kenton, KY | Vermont SAL[*] |
| Mecklenburg County, NC | Vermont SAL[*] |
| Maryland | Vermont SAL[*] |
| Cambridge, MA | Vermont SAL[*] |
| Chelsea, MA | Vermont SAL[*] |
| Virginia Beach, VA | Vermont SAL[*] |
| Toronto, Ontario, Canada | Vermont SAL[*] |

* no accuracy estimates
† doesn't classify in residential or commercial areas.
‡ not peer reviewed.
More examples at:
`https://www.nrs.fs.fed.us/urban/utc/pubs/`

## Objectives

There is great need for urban tree cover maps, but also limited resources for costly imagery such as leaf-on LiDAR. The objective of this study was to develop a method to map tree canopy cover in an accurate and reproducible way across every urban area in the state of Wisconsin using widely available or free high spatial resolution imagery. Towards that end, we systematically assessed two image types (NAIP and SPOT), 21 segmentation parameter sets, three machine learning classification algorithms, and sixteen feature subsets using open-source software. There is also a need to rigorously evaluate classification methods. Object-based (aka segment-based) classifications are widely used for high spatial resolution imagery because of their ability to aggregate pixels, effectively incorporating spatial information (Lu and Weng, 2007). Such approaches are widely recommended for mapping urban tree canopy (Cleve et al., 2008; Walker and Briggs, 2007; Al-Kofahi et al., 2012a; Zhou and Troy, 2008; MacFaden et al., 2012). However, the superiority of the segment-based approach over a pixel-based approach has often been confounded with other factors such as a change in the classifier used or method of accuracy assessment (pixel versus object scale). Our work tests wheter a pixel-based approach with additional features for spatial context can perform similarly to segment-based approaches.

## 2.3   Methods

We first tested methods using one municipality, Madison, Wisconsin, and then applied the resulting approaches statewide (Fig. 2.1). For Madison, we tested each combination of 2 different images (NAIP digital aerial photography and pansharpened SPOT imagery), 3 machine learning classification algorithms (boosted regression trees, GBM; random forests, RF; and support vector machines, SVM), 7 segment sizes ranging from pixels to 105 $m^2$, 3 levels of compactness for each segment size, and 16 subsets of features. For the pixel-based methods, we also added features created by the convolution of input bands, which gave neighborhood information to pixels. For the segment-based methods, we used the SLIC segmentation algorithm on the first three bands of a principal components analysis (PCA) on the original bands plus relative reflectance and NDVI bands (Achanta et al., 2012). We assessed over 4000 models to identify the best performing approach using independent validation data. For the urban canopy cover map of all of Wisconsin, we collected additional training data from across the state (n = 10,000), and, given our results in Madison, we used the pixel-based approach and NAIP imagery to map all urban areas in the state of Wisconsin. Fig. 2.2 summarizes the workflow.
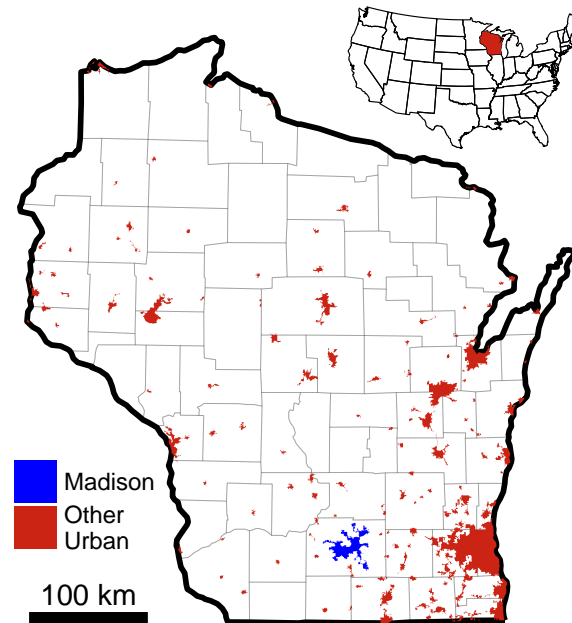
Figure 2.1: Urban areas in the state of Wisconsin as defined by the US Census Bureau (2013).

## Study Area and Spatial Domain

Wisconsin is 3.5% urban (5045 km$^2$; Census Bureau 2013, Fig. 2.1). In 2015, the city of Madison in south central WI (43 N, 89 W) had an estimated population of 248,951 and population density of 1173 people/km2 (Census Bureau, 2017). The dominant vegetation types in the city include turf grass and broad-leaved deciduous trees.

The spatial domain was urban areas (as defined by U.S. Census Bureau at 1:500,000 scale) (Census Bureau, 2013). Agricultural land covers about 7% of urban areas. Since cultivated land switches from bare soil to vegetation within a single year, a single image cannot accurately determine its dominant cover and would likely be wrong at some point in the year - a field that is vegetated in our image might be bare soil for much of the year, or vice versa. We tested a mask of cultivated agricultural areas using the USDA's cropland database (Boryan et al., 2011), however the resolution (30 m) and accuracy of this dataset was such that stakeholders such as the State of Wisconsin Department of Natural Resources deemed the map would be more useful if it included the relatively small amount of agricultural lands that fall in urban areas, rather than possibly incorrectly mask them. The result is a map that does include some agricultural areas, but we excluded these from our accuracy assessment.
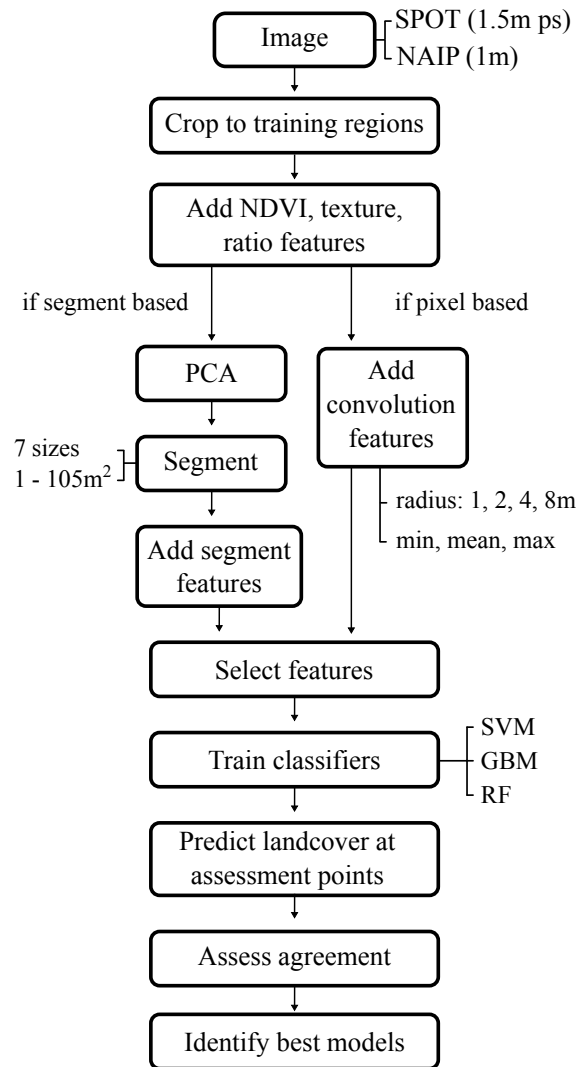
Figure 2.2: Workflow for creation of classifiers

## Classes

We defined five classes: "trees" (trees and shrubs, woody vegetation), "grass" (grass and other herbaceous vegetation), "impervious/soil" (both impervious surfaces and bare soil), "wetland" (non-forested wetlands), and "water". Trees, grass, and impervious were derived from imagery. Wetland and water were derived from vector layers provided by the Wisconsin Department of Natural Resources (DNR) (`ftp://dnrftp01.wi.gov/geodata/`). These vector layers are not perfect, but were important to include for our end users. For example, wetland areas could have be classified as tree or grass, but the functional difference of wetlands from those two cover types would be omitted. Furthermore, the vector layers helped lessen the confusion caused by the darkness of water, which otherwise led to confusion

with shadow covered land. After classifying the imagery as tree, grass or impervious/soil, we reclassified pixels as wetland or water if they fell within the vector layers' polygons.

For our Madison analysis, in which we were interested in finding the best way to map cover from imagery, we assessed the accuracy of the three image derived classes: trees, grass, and impervious/soil. For our state-wide analysis, in which we were interested in the accuracy of the map, we assessed all five classes.

## Imagery

We compared NAIP and SPOT imagery, over Madison, WI to identify an image source for state-wide mapping, considering quality and cost. Commercial SPOT-6 imagery, which has a panchromatic band at 1.5 m resolution and 4 bands (Blue 0.450-0.520 μm, Green 0.530-0.590 μm, Red 0.625-0.695 μm, and Near Infrared 0.760-0.890 μm) at 6 m resolution was acquired in August 2014. We pan-sharpened the SPOT imagery to 1.5 meter resolution using PCI Geomatic's Geomatica software. SPOT-6 has a cost of $3.88 per km for archived imagery over Wisconsin. We selected it as a comparison to NAIP because of is comparable pan-sharpened spatial resolution. To our knowledge SPOT-6 has not been used for city-wide tree canopy mapping.

National Agriculture Inventory Program (NAIP) aerial orthorectified digital photography, which has 4 bands (blue, green, red, and near infrared) at 1 m resolution, was captured over Madison, WI on June 19 and July 4, 2013. In the statewide map we used NAIP imagery across state of Wisconsin which was acquired between June 16 2013 and September 5 2013. Time of day ranged from 8:19 AM to 1:25 PM. See table 2.7 and work from the Vermont Spatial Analysis Lab for other maps derived from aerial photography and NAIP imagery.

## Classification Algorithms

We implemented three classification algorithms: random forests, boosted regression trees, and support vector machines in R (Ridgeway, 2017; Liaw and Wiener, 2002; Karatzoglou et al., 2004). Detailed explantions of the algorithms can be found in Hastie et al. (2009).

## Segmentation

To segment the imagery we used the simple linear iterative clustering algorithm (SLIC) implemented in python's scikit-image (van der Walt et al., 2014). SLIC accepts 3 bands (usually red, green, blue), though we provided the first three principal components of the NAIP imagery. SLIC adapts k-means clustering to create segments which are clusters in

color-image space and is a simple and fast algorithm with only two tuning parameters, average segment size and compactness (Achanta et al., 2012). This makes it easy to assess a large number of segmentations.

## Features/ Input variables

The features, or input variables, used in the classification were the original 4 bands of the imagery (red, green, blue, and near infrared), the relative reflectance of each of the 4 original bands (band / brightness; where brightness = R + B + G + NIR), the normalized difference vegetation index (NDVI), and texture features. For the segmentation approach, the minimum, maximum, and mean of each of these bands were calculated for each segment, and these summary statistics were used as inputs for the classification. For the pixel-based approach we convolved the non-texture features, and added the convolved bands as inputs for the classification. Below we expand on the texture inputs and convolution.

### Texture

Texture features are variables that describe patterns of reflectance within a given window and given direction (Haralick et al., 1973). From the grey-level co-occurrence matrices of the image we calculated 4 texture features: contrast, correlation, entropy, and homogeneity (inverse difference moment). See Haralick et al. (1973) for definitions and Zvoleff (2016) for implementation in R. We tested window sizes of 3x3, 5x5, and 7x7 pixels. Given the directional nature of shadows in the imagery, we calculated textures in four directions: 0, 45, 90, and 135 degrees.

### Additional Pixel Level Features / Convolution

For pixel classifiers we convolved each of the input bands except texture bands since they already are a convolution. Convolution involves passing a moving window over the image, applying a function at each position, and assigning the output value to the center pixel, which creates a new convolved image. The moving windows we used were circles with radii of 1, 2, 4, and 8 meters, and the functions were minimum, maximum, and mean. This created 108 new features to add spatial context to pixel-wise classifiers (context which is inherent to segment-based classifiers).

## Feature Selection

Because of the large number of potentially correlated features created (e.g. glcm texture features), we ranked features according to the Kruskal-Wallis test, and selected the most independent features to build models. For the systematic testing of which image, classification algorithm, segment size, and compactness to use, we tested building models with the top most independent features in increments of 10 from 10 to 100, then increments of 30 up to 240 features. We also tested models that included all features.

## Training data for supervised classification

To collect training data, we drew training polygons over regions of each class on NAIP and SPOT imagery, and, after verification in Google Earth imagery from 2011 or 2014, assigned the class label to pixels or segments that fell mostly within the training polygons. For the statewide classification we stratified the sampling across all months and hours of day that the NAIP imagery was acquired. We sampled from the largest city of each month and hour combination. Validation pixels were collected randomly and independently from the training data. Details on assessment are below.

## Software

All software used was open source, with the exception of PCI Geomatic's software to pansharpen the SPOT imagery. The SLIC algorithm for segmentation was implemented with Python's scikit image (van der Walt et al., 2014). All other computations used the R language (R Core Team, 2016).

## Assessment

We used simple random sampling to assess the agreement of our maps with Google Earth imagery, our reference dataset. We use the term "agreement" instead of "accuracy" because the reference dataset is not perfect.

For Madison, 2500 random points were placed over the greater Madison area and subset to the spatial domain, leaving 584 points. For the assessment of all the urban areas in the state we had 2125 sample points. We determined the majority cover within the $1m^2$ square around each point, corresponding to the support size (a pixel), by human interpretation of Google Earth imagery. All points were independently assessed by two interpreters and disagreements resolved by consensus or a third person. The use of higher resolution imagery as reference is not only faster than visiting reference locations in the field, but also

eliminates bias that would arise from the limited access to reference points in urban areas dominated by private property.

We used reference imagery from the date closest to the acquisition of the input imagery (most often June 2014). We also assessed the cover on the input NAIP imagery at each reference point to estimate how these differences in imagery dates and spatial registration might affect estimates of agreement.

In Madison our objective was to find the best method of classifying imagery into a map. We therefore only assessed the classes that were derived from imagery: tree, grass, and impervious/soil. We excluded wetland and water since they are derived from vector layers and independent of the imagery. For the statewide assessment, we assessed the accuracy of all 5 cover classes.

Segment-based maps are sometimes assessed at the segment level. However, since users could ask a question and apply the map at the smallest spatial unit of the map, a pixel, they should know the agreement of the map at the pixel level and we performed our assessments to select models accordingly (Myint et al., 2011).

Pixel-level assessment sets the floor of a map's agreement with the reference dataset; it probably does not provide estimates of agreement at the most relevant spatial scale for users. Most analyses that use this map will consider larger spatial scales. To assess how agreement changed as the unit of spatial analysis changes, we overlaid 50 grids of points on top of the map and reference. We created five 50 m x 50 m grids, 26 100 m x 100 m grids, 10 150 m x 150 m grids, and 5 200 m x 200 m grids. Points were spaced 7.14m apart in each grid and the reference cover was determined at each point. Starting in the northwest corner of each grid, we compared the estimates of percent tree cover from the successively larger grid subsets (2x2 points, 3x3 points, …, 20x20 points) with the map's estimate of percent tree cover in the successively larger square region below the grid of points ($\sim$50 m$^2$, $\sim$200 m$^2$, …, $\sim$30,000 m$^2$). We summarized the agreement at this scale using the coefficient of determination ($R^2$), Mean Absolute Error (MAE), and the Agreement Coefficient (AC of Ji and Gallo 2006). The AC provides a symmetric, bounded, and non-dimensional metric of agreement. It can also be partitioned into systematic agreement ($AC_{sys}$), and unsystematic agreement ($AC_{uns}$) (see Riemann et al. 2010 and Ji and Gallo 2006).

## 2.4 Results

### Madison, WI: Developing the classification approach.

**Imagery: NAIP and pansharpened SPOT**

Maps derived from NAIP imagery always outperformed maps derived from pan-sharpened SPOT imagery, all else being equal (e.g. segment size, compactness, classification algorithm) (Supple. data "madison-models-details.csv" and Supple. Fig. 2.3). Across all pairs of models tested, maps derived from NAIP had on average 19% greater agreement with reference imagery than those derived from SPOT (the range of the difference was 5-33%. Because NAIP always outperformed SPOT, subsequent results are limited to NAIP imagery.
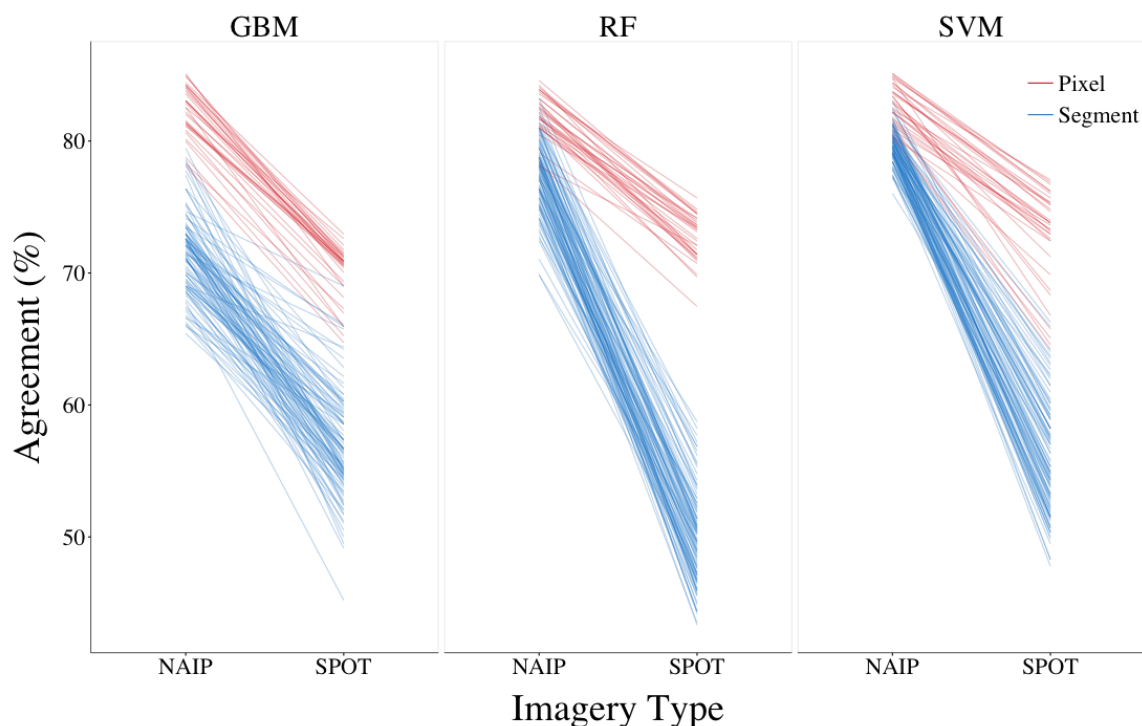


Figure 2.3: Agreement of maps derived from NAIP and pansharpened SPOT imagery with human interpreted Google Earth imagery. Lines connect models that are identical in all factors except which imagery is used. The negative slope of each line shows that –controlling for other factors such as segment size, classification algorithm, etc – maps derived from NAIP always outperform those derived from pansharpened SPOT. There is a three-way interaction between imagery type, classification algorithm, and segmentation. When comparing segment-based maps, maps that used Random Forests (RF) and Support Vector Machines (SVM) show a steeper drop in accuracy than maps that used Generalized Boosting Models (GBM). Additionally, pixel-based maps generally have higher agreement

than segment-based maps and that this difference is larger for SPOT derived maps than it is for NAIP derived ones.

## Classification Algorithms: Random Forests (RF), Support Vector Machines (SVM), and Boosted Regression Trees (GBM)

There were no significant differences in the mean or maximum performance of the 3 classification algorithms used. GBM has greater variability than RF and SVM due to a large decline in agreement for models with segment sizes of 20 $m^2$ and 30 $m^2$. Also, in the notable case of a pixel-based map with the original 4 bands/features, SVM did much better than GBM and RF (Fig. 2.4).
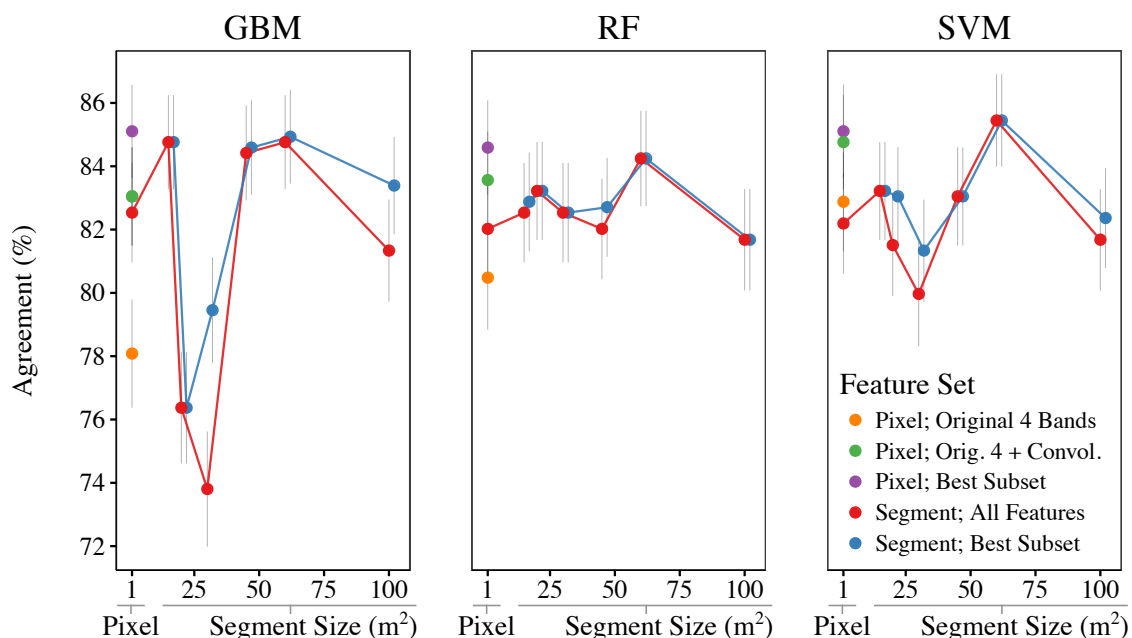


Figure 2.4: The effect of segment size on agreement by classification algorithm and feature subset for maps made from NAIP imagery. Vertical lines show the standard errors. "Segment; Best Subset" points are shifted slightly to prevent overplotting in the cases where the best subset was also the full feature set.

## Segment Size: From pixel to 105m$^2$

Agreement improves slightly from a segment size of 1 $m^2$ (a single pixel) to 15 $m^2$ ("Segment: All Features" in Fig. 2.4). For GBM and SVM, agreement decreases at segment sizes of 20 $m^2$ and 30 $m^2$. Agreement then increases to a local maximum around 60 $m^2$, then declines

at 105m$^2$. Agreement at finer scales is thus maximized at 15 m$^2$ and at coarser scales at 60 m$^2$.

## Comparison of Feature Subsets

For RF and GBM, the models with highest agreement both used 160 features. For SVM, the model with highest agreement used all features. Depending on the classification algorithm and the segment size selected, the increase in agreement due to feature selection ranged from 0% to 5%, but was most often below 1% (Fig. 2.4, and see Supple. data "madison-models-details.csv").

## Best Segment-based versus Pixel-based Classifications

There was no significant difference in agreement between the best pixel-based maps (with convolved features) and the best segment-based maps (Fig. 2.4). However, when the pixels were treated as segments of size 1m$^2$, that is, they underwent the segment workflow without the additional convolution features, the best segment-based methods outperformed these 1 m$^2$ sized segments by about 2.2% to 3.3% depending on the classification algorithm. However, segmentation often caused a decline or no improvement in agreement (e.g. the large drop in agreement around 30 m$^2$).

## Selection of the best model

With 584 sample assessment points, the 95% confidence interval around the estimate of agreement for single map is about ± 3.2% ($1.96\sqrt{\frac{(.2)(.8)}{584}}$, assuming a model agreement of around .80). This means that dozens of models were statistically indistinguishable from the top model's agreement with the reference image. A sample size of over 32,000 would be required to test for statistically significant differences between two maps using McNemar's test for paired proportions (assuming β=.2, $\alpha$ = .05, and similar map differences as in this study). The standard unpaired proportion test would require an even larger sample size. This over 50-fold increase in effort would yield relatively little information - knowing one model outperforms another by 0.5% is of little real significance.

Given the diminishing returns of additional assessment points, we sought to select a classification method with our existing points and according to three criteria: 1) overall agreement with reference, 2) the amount of tree bias (over or under classification of tree cover), and 3) the degree to which the model captures real objects in the image.

The map with the highest overall agreement (85.4%) was made with SVM and had an average segment size of 60 m$^2$ (Fig. 2.5, panel B). While the point estimate of this map's

overall agreement was highest, it underestimated our reference data estimate of total tree cover by approximately 1.2%. It also made some surprisingly large classification errors, creating patches of impervious cover in what should have obviously been tree.
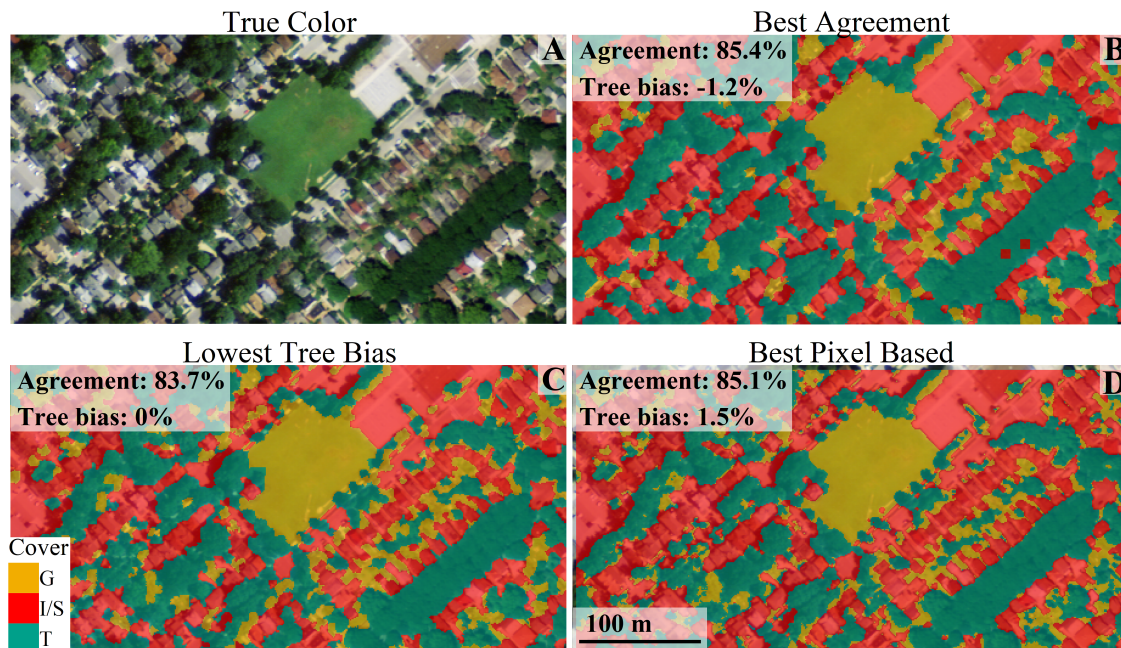


Figure 2.5: A) true color NAIP image; B) Map with best overall agreement (SVM, 60 m$^2$ segment size). C) Map with lowest bias in estimation of tree cover within 1% of the top model (GBM, 45m$^2$ segment size). D) Best pixel-based map, within 1% of the top model (GBM).

The map with smallest bias in estimation of tree cover used GBM and had an average segment size of 45 m$^2$. Its estimated overall accuracy was 83.7% and had no tree bias (Fig. 2.5, panel C). The best pixel level map used GBM and had an estimated overall agreement of 85.1% and overestimated tree cover by approximately 1.5% (Fig. 2.5, panel D).

We combined overall agreement and tree bias into a single metric by subtracting the absolute tree bias from the overall agreement (see Supple. data "top-madison-models-agreement-withBias.csv" for comparisons). This weights overall agreement and tree bias equally. Using this metric, the top model is segment-based with 60 m$^2$ sized segments. The best pixel-based method is about 1% worse, but is again statistically indistinguishable.

After we identified the top models we visually assessed them. The pixel-based map captured the small (few meters squared) objects, which are common in urban environments and which the maps with segment sizes of 60 m$^2$ on average missed. We needed to select a model to apply to the whole state and picked the pixel-based approach for the finer scale patterns it identified. However, a segment-based approach would have similar agreement

statistics and could have been selected if overall agreement and tree bias were the only criteria.

**Agreement at management scales**

To compare models, we assessed agreement using the spatial unit of a 1m$^2$ square, a pixel. While this scale is appropriate for a map with 1m$^2$ pixels, it is not the most relevant reporting scale for managers since urban forests are managed at the scale of neighborhoods. Using a pixel-based model, we found that at the scale of the entire city, our estimates of percent cover were very close to the estimates from the reference Google Earth imagery. So while there was only about an 85% chance of any single pixel agreeing with the interpreted cover in the Google Earth imagery, the estimates of cover for the whole city were within 1.5% of the validation data for the entire city (Table 2.2). The results were similar for other top models.

Table 2.2: Madison estimates of cover from Google Earth Imagery and one of the best maps (n=584). Absolute differences are all less than 1.5%.

|  | Google | Map | Difference |
| --- | --- | --- | --- |
| Grass | 35.8 | 35.1 | -0.7 |
| Impervious/soil | 35.6 | 35.1 | -0.5 |
| Tree | 28.6 | 29.8 | 1.2 |

Error decreases as one assesses percent tree cover from the pixel scale to progressively larger areas (Fig. 2.6A). At the scale of an average house parcel (700 m$^2$) or a Landsat pixel (900 m$^2$), mean absolute error decreases to around 9.7%, with essentially no bias (Fig. 2.6B). This scale is relevant because a house parcel is perhaps the smallest possible management unit, and Landsat is the source for the National Land Cover Dataset (NLCD), which is a commonly used, nationally available percent tree cover product Homer et al. (2015). At the scale of a city block on average estimates of tree cover are off by about 6%. Almost all of this disagreement between the map and Google Earth interpretations is unsystematic. That is, on average, tree cover is not over or underestimated.

## Every Urban Area of Wisconsin: Extending the classification approach.

**A Model for Wisconsin**

When we applied the selected Madison model (pixel-level GBM, 160 features, agreement 85.1%) to the whole state, agreement was 76.7%. We then created a new statewide model using the formulation from the Madison model, but that included training data from
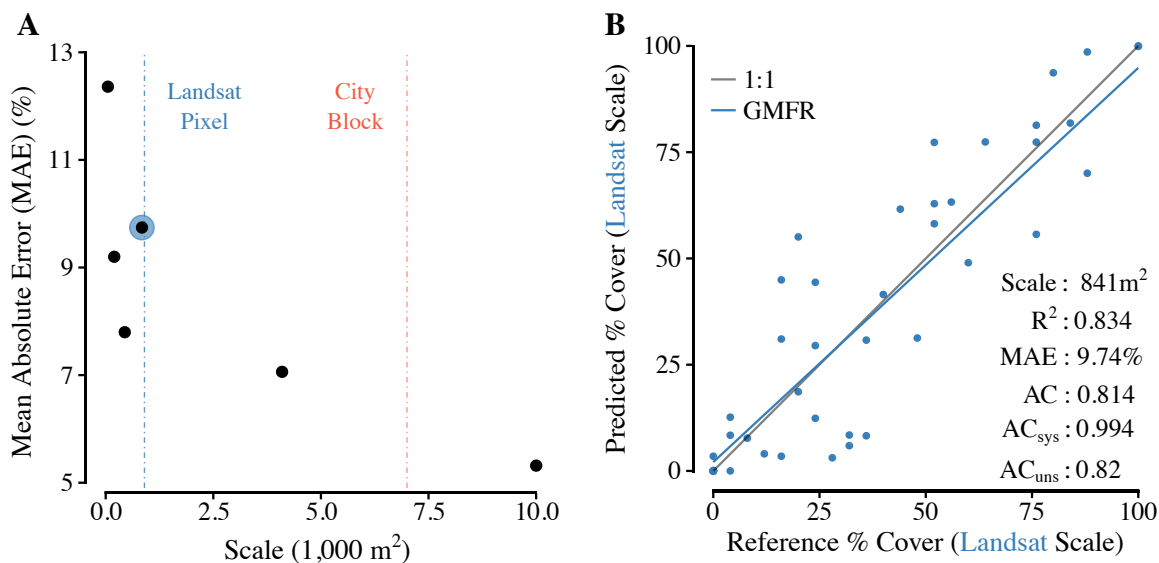
Figure 2.6: A) Decrease in mean absolute error with increasing scale. B) Predicted versus reference derived estimates of percent tree cover in 841 m² regions. The geometric mean functional relationship (GMFR) line, which assumes error in both the reference and predicted, is very close to the 1:1 line. Systematic agreement coefficient ($AC_{sys}$) is .994. The mean absolute error (MAE) is 9.74%, and the unsystematic agreement coefficient ($AC_{uns}$) is .820.

representative locations in the state and additionally included month and solar angle during image acquisition as independent variables. Using the same criteria for selection of the Madison model (high overall agreement and minimal tree bias), we selected a random forest model with 145 features. Overall accuracy was 79.3% (see Table 2.3 for the confusion matrix and Supple. data "WholeState-top20models.csv" for results of the top 20 whole state models). Similar to the Madison analyses, this map did not differ significantly in overall agreement from other top maps created by varying training data size, classification algorithm, and feature subset size. With a sample size of 2125, the standard error for map agreement with the reference was less than 1%.

**Partitioning Disagreement**

Partitioning the sources of disagreement between the map and the reference Google imagery revealed the factors contributing to map error. Of the 440 disagreement points in Table 2.3, we further evaluated 171 to determine the sources of disagreement. The top-level reasons for disagreement between the map and the reference imagery were that 1) the source imagery, NAIP, did not agree with the reference imagery, Google Earth, due to registration errors, parallax, shadows, etc. (38.5%), 2) the vector layers used to classify wetland and

water were imperfect (12.3%), and 3) the classifier model mislabeld pixels (52%) (Table 2.6). Excluding wetland and water areas, agreement rises slightly rises to 80.7%. If the wetland and water masks were perfect and retained in the assessment, agreement would increase to 83.2%.

18.7% of disagreement was due to shadows in the imagery. 6.4% of the errors were because the human could not correctly identify the land cover in the shadow–NAIP image quality was too poor for proper interpretation. For 12.3% of errors, the human interpreting NAIP imagery could correctly identify the land cover, but the classification model could not. Shadows were a smaller problem for the Madison model than the whole state model: imagery from much of the state was acquired early in the morning and long shadows were prominent. Shadows reduce agreement by up to about 3.9%.

The highly heterogeneous urban environment means that spatial misregistration of a few meters, mixed pixels, and edge pixels on the border of land cover types are a large source of disagreement. These pixels account for almost half of all disagreement (48.5%). 25.1% of errors were due to spatial misregistration between NAIP and Google imagery. The majority of this results from parallax, where tall objects are shifted in space because of the sensor's viewing angle. If NAIP and Google imagery had no spatial misalignment, agreement between the map and google imagery could increase by 5.2%. Pixels that are close to the edge of cover type are far more likely to be incorrectly classified than those in the interior (Fig 2.7A) with 50% of all pixels in the imagery less than 5m from a different cover type (Fig 2.7B).

## 2.5  Discussion

### Imagery: NAIP versus SPOT

At the outset of this work we wanted to know whether any improvement a map made from SPOT imagery (e.g., radiometric consistency) would be worth the cost of commercial SPOT vs. free NAIP data. The NAIP images produced more accurate maps than the pan-sharpened SPOT. Pan-sharpening increases the multispectral resolution of SPOT from 6m to 1.5m, but the resulting pixels appeared to have pan-sharpening artifacts and were larger than NAIP pixels. In every paired comparison of NAIP and SPOT, NAIP outperformed SPOT (Supple. Fig. 2.3 and data "madison-model-agreement-details.csv").

The NAIP imagery has numerous benefits. It is free, available since the early 2000's, covers the contiguous US, and is acquired every 2-3 years, potentially enabling automation of mapping with each new collection. This record also allows for change detection studies,
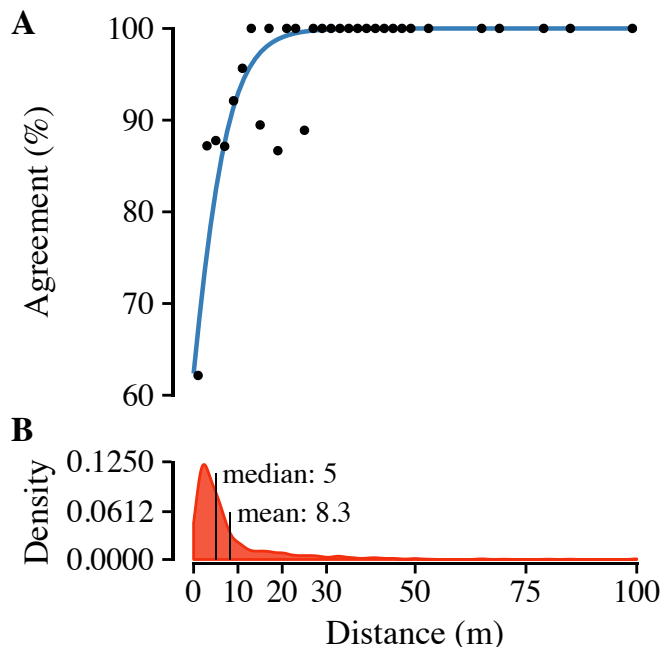
Figure 2.7: A) Distance to a different cover type versus agreement. Black points are average agreement for every 2m bin. Blue curve is logistic fit between distance and agreement for every assessment pixel. B) Approximate density of the distance to a different cover type.

which are needed to assess the trajectory of canopy cover through time (Hostetler et al., 2013). Leaf-off LiDAR can create higher quality maps (Table 2.7), but is costly and not available widely, making NAIP good alternative. Other fine resolution (1 m) commercial satellite data sources are not practical for statewide mapping due to limited swath widths. There are several limitations to NAIP as well. Timing of flights varies between and within years which affects image quality and consistency. NAIP imagery is orthorectified, but not true orthrectified. This leads to tree and building "lean", which obscures ground cover and can increase error in cover estimates. The shadows in the imagery are also problematic, and especially so for city centers with large buildings. Wisconsin has no megacities and our approach may not be as effective in these areas.

## Selecting Segmentation Parameters

Segmentation parameters are usually determined by trial and error, adjusting until the segments fit the image being tested according to an often subjective criterion (Al-Kofahi et al., 2012a; Myint et al., 2011; Cleve et al., 2008; Möller et al., 2007). The speed of the SLIC algorithm made the test of 21 different segmentation parameter sets possible. This is a grid search across parameter space, and is generally less efficient than an optimization

algorithm (which an expert user might approximate when performing the trial and error approach). One benefit of the grid search is that it assess a wide range of parameter space. This was important because we found a nonlinear relationship between segment size and map agreement, with two local maxima around 15 m$^2$ and 60 m$^2$ (RF does not show this trend, but SVM and GBM do). These two spatial scales may represent common sizes of objects in the image, explaining why the classifier performs better at these scales. We did not find a large influence of the compactness parameter on map agreement. Generally, larger compactness did better for larger segment sizes, and smaller compactness did better at smaller segment sizes.

The effect of segment size on agreement depends on the classifier used. The presence of two local maxima in the relationship between segment size and agreement suggests that in practice, a wide range of segmentation parameters should be tested; otherwise a local maximum may be utilized and the global maximum missed. Similarly, there may be this risk for optimization algorithms that seek the best segmentation parameters. Care should be taken to test multiple starting points in parameter space.

## Segment versus Pixel

The segment-based approach is widely reported to outperform the pixel-based approach because of the ability to leverage spatial information (Lu and Weng, 2007), but the underlying basis for these conclusions has often not been rigorously tested. Stow et al. (2008) report that the segment-based approach is qualitatively better, but did not do a formal comparison. In two papers that explicitly compared the segment-based and pixel-based approaches, the authors used different classifiers for the pixel-based and object-based approaches, which confounds the approach with the classifier (Myint et al., 2011; Cleve et al., 2008). Ouyang et al. (2011) did control for different classifiers and feature sets between segment-based and pixel-based approaches. In the four pairs of models they built comparing segment-based to pixel-based methods (holding other factors constant) they found no difference in one of the pairs, a 2% superiority of the pixel-based approach in one of the pairs, and a 5% and 1% superiority of the segment-based apprach in the two remaining pairs. This would suggest on average a small superiority of the segment-based approach over the pixel-based, but they do not provide any description of sampling that would allow for a statistical test of differences in the methods. Ultimately their best model was segment-based and used a hierarchical apprach to which their was no direct pixel-based comparison. This hierarchical approach requires iterative trial and error to select segmentation parameters. This means segment-based maps involve a greater effort than the pixel-based maps, and this variable

effort should be considered in comparisons too. Furthermore, comparisons in accuracy should only be done if the spatial support is the same. See Żaneta Kaszta et al. (2016) for an example of assessment at different supports and Ye et al. (2018) for a description of the challenges in assessing the accuracy of object-based maps.

If the objective is simply to create the best map possible, this confounding is irrelevant. But before we can generalize about segment-based always outperforming pixel-based, we must account for the change in classifier and variable effort.

We compared pixel-based maps to segment-based maps, keeping as many factors as constant as possible so as to make a valid comparison. When we treated pixels as segments of size 1 m$^2$, agreement was often lower than it was for maps made with larger segments ("Segment: All Features" in Fig. 2.4). This is because a segment of 1 pixel has no information about its neighborhood. This result is very similar to the conclusions of Żaneta Kaszta et al. (2016), who found segment-based methods always out performed pixel-based methods, regardless of the classifier used.

There may be evidence from their work that the segment-based approach can leverage additional features, use more information (all the pixels in a segment rather than just one for training the model), and benefit from expert selection of segmentation parameters. This makes it superior to pixel-based approaches which cannot leverage much spatial context.

However, our work showed segmentation also could also cause decreases in agreement when poor segmentation parameters are chosen. At segment sizes of 20 m$^2$ and 30 m$^2$ agreement was lower than for segments of size 1m$^2$ (Pixel), 15m$^2$ and 105m$^2$ (for GBM and SVM classifiers). Overall, this finding was consistent with past findings that segmentation improves map agreement, but highlights that the improvement is dependent on the selection of the correct segmentation parameters and that not all segment-based maps are better than pixel-based maps.

There are other ways to include spatial information to a classifier besides segmentation. One method often used to resolve the salt and pepper effect is a majority filter (a convolution with a window of a 3x3 block of pixels and the mode function) applied post classification. For example, Myeong et al. (2001) found a majority filter improved the accuracy from 81% to 84%.

We leveraged similar convolutions of our input bands *before* classification to improve pixel-based performance. This reduced salt and pepper effects but preserved the information in the single pixel needed to capture small objects that segment-based approaches can miss. This method might outperform segmentation for two reasons. First, each pixel was assigned information about its own neighborhood, not just information about its segment. Pixels on the edges of segments did not have information about their neighbors,

which could be important. Second, in segmentation, individual pixels lost their pixel-level information and instead were aggregated. This aggregation is a loss of information. In the pixel-based approach with convolved features, pixels have both the pixel-level features and the convolved features, which supplies them information at multiple spatial scales.

Our results show that the agreement difference between pixel-based maps with convolved features and the best segment-based maps was less than 1%, with a confidence interval that includes 0, no difference (n = 2125). When pixel-based maps used features that incorporate spatial information, they performed essentially as well as segment-based maps. Moreover, pixel-based maps retained the ability to identify smaller objects than a segment in the imagery and for this reason we selected this approach for the state-wide maps.

The major benefit of segmentation is the inclusion of spatial context, but the selection of appropriate segmentation parameters requires an interative trial and error approach by an expert. Our work suggests that the addition of convolved features can provide spatial context to a pixel and achieve similar quality maps without the need for expert selection of segmentation parameters.

## Disagreement

The heterogeneity of the urban environment explains approximately half of all disagreements between the map and reference imagery. There is significant spatial mismatch between Google and NAIP imagery due to registration and parallax, and mixed and border pixels can be difficult to classify correctly as a result. This effect is inconsistent and highly variable across a large number of airborne NAIP scenes due to flight and solar characteristics.

Only assessing pixels that occur in homogeneous regions, for example a 3x3 grid of pixels following Russell G. Congalton (1999), would improve reported agreement, but the proportion of the scene actually being assessed would greatly decrease. About 10% of all pixels are within 1m of a different cover type (Fig. 2.7), and removing these from assessment increases agreement to 85.1% (86.3% if wetland and water are excluded). About 25% of all pixels are within 2m of a different cover type, and removing these from assessment increases agreement to 88.7% (90.4% if wetland and water are excluded). By assessing agreement at pixels regardless of whether or not they fall in a homogeneous region, our goal is not to be overly critical in our assessment of map usefulness (Foody, 2008), but rather to thoroughly evaluate the challenges of heterogeneity in urban classification. Our assessment at larger spatial scales addresses the disagreements due to spatial misregistration and provide

managers with estimates of agreement that are relevant for scales such as the city-block (94% agreement) that are used by managers.

After mixed and border pixels, the most common source of disagreement was confusion between trees and grass. The leaves of trees and grass can have similar reflectance spectra and would be difficult to distinguish with a 4-band sensor were it not for the structure of the plants. Short grass often transmits the spectral signature of soil, while taller trees create shadows. Human interpreters of 1m resolution imagery often struggle to distinguish a tree from grass unless they can see its shadows created by the complex structure of a tree canopy. Computer classifiers tend to depend on simply the pixel values or perhaps gather textural features within a small window. Without the benefit of the greater context available to humans, classification algorithms struggle to accurately discriminate tall, coarsely textured grass from bright finely textured tree canopies. Even humans can struggle to accurately separate tree from grass with 1 m imagery in the highly heterogeneous urban environment. As noted by MacFaden et al. (2012), LiDAR can be beneficial for accurately separating short and tall-structure classes (Table 2.7), but leaf-on LiDAR are rarely available at statewide extents and generally do not have repeat imaging such as NAIP.

As mentioned above, there was error in the wetland and water classes. Being derived from vector layers created at different times and spatial precision than the imagery, they occassionally incorrectly reclassified land cover. While they were crucial to prevent confusion between shadows and water, and between trees and herbaceous wetlands, the hard post hoc reclassification of the imagery introduced errors particularly at edges of polygons. In future work, the vector layers should be included as an additional feature in the classification, rather than a mask.

We did not quantitatively assess accuracy by state region, but there were qualitative differences between the less urbanized north and the more urbanized south. This was likely due to two factors: 1) image quality was generally higher in the south, and 2) there was more urban area in the south and so the classifier weighted these areas more. Overall accuracy was maximized by better performance in the more urban south than the less urban north. Our estimate of accuracy applies to the state scale, but there is considerable variability in accurracy that makes our map more or less useful depending on the local site. Local scale analyses should evaluate the quality of the map at their location since our estimates of accuracy do not apply.

**Comparison to other studies**

Table 2.7 compares our work to that of others. It is clear that fewer classes and more input data yield higher overall accuracy. LiDAR can improve the classification of trees by around 10%. As Lu and Weng (2007) also noted, eCognition is a popular choice of software for segmentation. This tool is clearly effective, but its prevalence raises the question of how methods may be constrained by tools. For example, eCognition segment-based maps are almost always classified with user defined membership functions. These functions create a relatively simple classification tree and could arguably be improved with an ensemble method such as random forests, which could learn the best multivariate thresholds to separate classes. Our results do not use eCognition for segmentation, which on one hand broadens knowledge and the set of segmentation algorithms used to map urban tree canopy, but on the other makes comparison harder. Further work needs to be done to compare a variety of segmentation algorithms (such as eCognition, Orfeo Toolbox and RSGISLib) to pixel-based maps with convolved features as in this study.

## 2.6 Conclusion

We have created a map of land cover for every urban area in the state of Wisconsin at the 1m scale, greatly improving on the detail available from widely used Landsat derived 30m resolution maps. We found that NAIP was superior to pan-sharpened SPOT imagery. We found that pixel-based maps with convolved features perform just as well as segment-based maps, but there is room for additional studies to test a greater range of segmentation algorithms and parameter values.

Considering differences in the number of classes and input data, our map seems to perform similarly to others. The inclusion of LiDAR would greatly improve discrimination of trees from other vegetation, but this data source is not available state-wide. What our method lacks in input data quality is made up for by its applicability to places or times (the past) where LiDAR is not available. The agreement of the map with reference imagery is very good at the pixel level and increases with spatial scale. Importantly, our map has very little bias and estimates canopy cover across large areas well (but manual QA/QC are needed at local scales to ensure reliability). This map will be included in iTree Landscape and accessible for managers and the public to use to inform decision-making.

Table 2.3: Overall Accuracy = 79.29%; 95% CI = (77.5%, 81.0%); kappa = .7075

| Prediction | **Reference** Grass | Imper./Soil | Wetland | Tree | Water | Total |
|---|---|---|---|---|---|---|
| Grass | 465 (21.9%) | 56 (2.6%) | 2 (0.1%) | 114 (5.4%) | 0 (0%) | 637 (30%) |
| Imper./Soil | 44 (2.1%) | 598 (28.1%) | 1 (0%) | 23 (1.1%) | 0 (0%) | 666 (31.3%) |
| Wetland | 11 (0.5%) | 1 (0%) | 31 (1.5%) | 11 (0.5%) | 0 (0%) | 54 (2.5%) |
| Tree | 114 (5.4%) | 28 (1.3%) | 4 (0.2%) | 518 (24.4%) | 8 (0.4%) | 672 (31.6%) |
| Water | 0 (0%) | 3 (0.1%) | 20 (0.9%) | 0 (0%) | 73 (3.4%) | 96 (4.5%) |
| Total | 634 (29.8%) | 686 (32.3%) | 58 (2.7%) | 666 (31.3%) | 81 (3.8%) | 2125 (100%) |

Table 2.4: Whole State Map: Table of User's Accuracy (1-Commission Error) and Producer's Reliability (1-Omission Error). 95% CI in parentheses.

| Cover | User's (1-Commission Error) | Producer's (1-Omission Error) |
|---|---|---|
| Grass | 73.0 (69.4, 76.4) | 73.3 (69.7, 76.7) |
| Impervious/Soil | 89.8 (87.2, 92) | 87.2 (84.4, 89.6) |
| Wetland | 57.4 (43.2, 70.8) | 53.4 (39.9, 66.7) |
| Tree | 77.1 (73.7, 80.2) | 77.8 (74.4, 80.9) |
| Water | 76.0 (66.3, 84.2) | 90.1 (81.5, 95.6) |

Table 2.5: Comparison of percent cover estimates for all urban areas in the state. The map shows very little systematic under or over estimation of cover.

| Cover | Google (Reference) | Map (Prediction) | Difference |
|---|---|---|---|
| Grass | 29.8 | 30.0 | 0.2 |
| Impervious/Soil | 32.3 | 31.3 | -1.0 |
| Wetland | 2.7 | 2.5 | -0.2 |
| Tree | 31.3 | 31.6 | 0.3 |
| Water | 3.8 | 4.5 | 0.7 |

Table 2.6: Identifying reasons for diagreement between map and reference. Note that a few points have multiple conditions so the total does not sum to 100%

| Disagreement Description | Est. % of Disagreements | Total |
|---|---|---|
| **NAIP $\neq$ Google Earth** | | |
| NAIP image quality | 7.0 | |
| Shadow | 6.4 | |
| Spatial Misregistration (Parallax) | 19.3 | |
| Spatial Misregistration (ground) | 5.8 | 38.5 |
| **Imperfect Vector Layers** | | |
| Imperfect wetland mask | 7.6 | |
| Imperfect water mask | 4.7 | 12.3 |
| **Classifier Wrong** | | |
| Shadow | 12.3 | |
| Classification error, mixed or border pixel | 23.4 | |
| Coarse herbaceous vegetation called tree | 1.2 | |
| Brown grass called impervious | 0.6 | |
| Dark grass called tree | 5.8 | |
| Light tree called grass | 6.4 | |
| Just plain wrong, unknown reason | 2.3 | 52.0 |

Table 2.7: Summary of results for other tree canopy studies at 1m resolution or less.

| Paper | Overall | κ | Classes | Input Data | Method | Pix. or Seg. | Software | Scope |
|---|---|---|---|---|---|---|---|---|
| This study | 79 | 71 | 5 | 1m RGBN AP; anc | RF | Pixel | R, Python | State |
| Cleve et al. (2008)[*] | 62 | 48 | 4 | .15m RGB AP | ISODATA | Pixel | eCognition | 1 mi$^2$ |
| Cleve et al. (2008)[*] | 80 | 71 | 4 | .15m RGB AP | NN; UDMF | Segment | eCognition | 1 mi$^2$ |
| Walker and Briggs (2007) | 81 | 63 | 2 | .61m RGB AP | UDMF | Segment | eCognition | City |
| Al-Kofahi et al. (2012a) | 89 | 85 | 4 | .15m RGB AP | NN | Segment | ENVI | City |
| Zhou and Troy (2008) | 92 | 90 | 5 | .6m RGBN AP; 1m L; anc | UDMF | Segment | eCognition | Watershed |
| MacFaden et al. (2012)[†] | 96 | 95 | 7 | .15m RGBN AP; .7m L; anc | UDMF | Segment | eCognition | City |

Table 2.8:  Key for Table 7

| Column | Code | Item |
|---|---|---|
| Input Data | RGBN | Red, Green, Blue, Near Infrared |
| | AP | Aerial Photography |
| | L | LiDAR |
| | anc | Ancillary Datasets (e.g building footprints, water boundaries) |
| Method | ISODATA | Iterative self-organizing data analysis |
| | NN | Nearest Neighbor |
| | UDMF | User Defined Membership Functions |
| | RF | Random Forest |
| notes | * | Shadow is a class |
| | † | manual editing |

# 3 TREES IN COOL CLIMATE CITIES MAY INCREASE ATMOSPHERIC CARBON BY ALTERING BUILDING ENERGY USE

## 3.1 Summary

Urban trees are a critical part of the "green infrastructure" intended to make our growing cities more sustainable in an era of climate change. The potential for urban trees to modify microclimates and thereby reduce building energy use and the associated carbon emissions is a commonly cited ecosystem service used to justify million tree planting campaigns across the US. However, what we know of this ecosystem service comes primarily from unvalidated simulation studies.

Using the first dataset of actual heating and cooling energy use combined with tree cover data, we show that that contrary to the predictions of the most commonly used simulations, trees in a cool climate city increase carbon emissions from residential building energy use. This is driven primarily by near east (< 20m from building) tree cover. Further analysis of urban areas in the US shows that this is likely the case in cool climates throughout the country, encompassing approximately 39% of the US population and 62% of its area (56%, excluding Alaska). This work adds geographic nuance to our understanding of how urban shade trees affect the carbon budget, and it could have major implications for tree planting programs in cool climates.

## 3.2   Introduction

Two global trends of the 21st century, climate change and increasing urbanization, have deepened our need to make cities more sustainable. Urban trees are often championed as a means to that end. Several large cities in the U.S. have recently committed to large tree planting programs (see Million Trees New York City and Million Trees Los Angeles). Spending hundreds of millions of dollars, these cities hope that the environmental benefits, particularly the reduction in building energy use and the associated carbon (**C**) emissions from power plants, will outweigh the cost (Young, 2011).

A single urban tree has a much stronger impact on the carbon cycle than a non-urban counterpart because an urban tree induces or reduces more C emitting human behaviors than a rural one does. Both trees sequester C from the atmosphere, but the urban tree requires more management (planting, watering, pruning, removal, chipping) and, by modifying the microclimate, it can alter building energy use and the associated C emissions (**ACE**) from power plants.

Trees primarily alter microclimates by 1) shading, 2) reducing wind speed, and 3) cooling via transpiration. With the exception of transpirative cooling, which is mostly active in summer, these effects can both increase or decrease ACE. Shading to the west of buildings greatly reduces summer cooling loads, but shading to the south of buildings, even by deciduous trees, may increase winter heating loads (Heisler, 1986). Reduced wind speeds have complex effects. They: 1) decrease convective heat loss, which is beneficial for winter heating but detrimental for summer cooling, 2) decrease air infiltration which decreases both heating and cooling energy use, and 3) decrease natural ventilation, increasing the need for mechanical cooling (Huang et al., 1990). The strength of the effect of a tree on ACE attenuates with distance to a building. Trees far from a house have little affect on ACE via shading and wind reduction, but they likely affect ACE via evapotranspiration and the associated reduction in temperature (Ziter et al., 2019).

Whether the net effect of trees is to increase or decrease ACE depends on the balance of beneficial and detrimental effects on heating and cooling energy use. This is largely mediated by the location of tree cover, the prevailing climate (e.g. number of heating- and cooling- degree days), building characteristics (orientation, insulation, size and surface area, etc.), occupant behavior and the C content of a kWh, which varies depending on the fuel mix in the electrical grid.

Our current understanding of how trees affect building energy use and ACE suggests that there are contexts in which trees may increase ACE. But despite this potentially detrimental effect of trees, it is often not mentioned in the literature (a gray literature

exception is Nowak et al. (2010)). In an extensive review of the effect of the urban forest on $CO_2$ emissions, Weissert et al. (2014) did not consider that trees could increase ACE. In a paper critical of many ecosystem services provided by trees, Pataki et al. (2011) nevertheless state that trees reduce energy use and ACE. Our work here builds on past simulation studies and uses empirical energy use data from thousands of houses in a city to demonstrate that trees may actually increase ACE in cool climate cities.

## 3.3   Previous research

Decades worth of research primarily by two research groups, the US Forest Service (USFS) and the Lawrence Berkeley National Lab Heat Island Group (LBNL), have reported that, on average, trees reduce C emissions. In 2002, Akbari published a paper summarizing their group's findings: "Shade trees reduce building energy use and $CO_2$ emissions from power plants". In 1999, McPherson and Simpson wrote a technical report that was the basis of the iTree software, which has been used by thousands of communities around the U.S. to estimate ACE avoided. Their methodology was recently applied to estimate the effects of trees on ACE for the entire conterminous US (Nowak et al., 2017). Despite the number of publications on the topic, the length of time we have been researching the matter, and the many large cities with massive tree planting initiatives, our uncertainty about the effects of trees on building energy use is actually quite high (Pataki et al., 2006; McPherson and Simpson, 1999). The effect of trees on nearby building energy use is difficult and expensive to measure directly and complex to model.

Direct measures of the effect of trees on building energy use are rare, focused on cooling energy use, and limited in their ability to be extrapolated. To our knowledge, there are the only 5 studies that test the effect of trees on measured building energy use data (Akbari et al., 1997; Donovan and Butry, 2009; DeWalle et al., 1983; Parker, 1983; McPherson et al., 1989). Only two of these studies were of actual houses (not mobile homes nor models) and both are from Sacramento, CA and did not measure heating energy use (Akbari et al., 1997; Donovan and Butry, 2009). Only one of the studies was from a cool, heating dominated climate (typical of much of the US) and it studied a single mobile home in a forest (DeWalle et al., 1983).

Given the challenges inherent in collecting direct measurements, simulation studies are useful attempts to extend our understanding of how trees affect building energy use and ACE. But these simulations necessarily contain simplifications and generalizations which are sometimes unrealistic or untestable due to lack of data.

The work from LBNL assumes: millions more trees are planted in an urban area

(extremely ambitious); trees are planted to the west and south of buildings (ideal placement for reducing cooling loads); and winter tree canopy transmissivity is 0.9 (0.7 is more realistic, Heisler, 1986). In later work, microclimate wind effects are ignored (Akbari and Konopacki, 2005), and in earlier work, they use a three parameter equation fit to four data points to estimate how wind speed is reduced by canopy cover (Heisler, 1990; Huang et al., 1990). Finally, the LBNL work uses potential evapotranspiration to predict cooling, and their model uses parameters derived from crops. Given these assumptions, the authors note that their work provides an upper boundary for the indirect effect of trees (Akbari and Konopacki, 2005; Huang et al., 1987).

USFS studies assume: lookup tables for the effect of tree shade on building energy use are reliable (even though they may deviate from more detailed simulations by up to 10%, Simpson, 2002); wind reduction only affects heating use in the winter, even though we know cooling use is also affected; and they also use an overfit summertime leaf-on equation from Heisler (1990). Evergreen trees are modeled as if they are windbreaks for rural farmhouses in winter, even in suburban neighborhoods where other buildings and trees already block significant winds; and estimated evapotranspirative cooling is optimistically high, higher even than the self declared upper limit of Huang et al. (1987) (McPherson and Simpson, 1999).

The consequence of these assumptions is that simulations may overestimate the energy reducing power of trees. What little validation we have has confirmed the general effects of trees on energy use that we expect in hot climates, but also highlight the imprecision of simulations as well as occasional discrepancies from empirical observations. Simulations of Akbari et al. (1997) were off by 2-fold, though trees were about twice as beneficial as predicted for the two houses studied. Donovan and Butry (2009) found trees to the north actually increasing electricity use, unlike the predictions of McPherson and Simpson (1999).

Despite providing estimates for the effects of trees on building energy use and ACE for anywhere in the country (Akbari and Konopacki, 2005) and the entire country (Nowak et al., 2017), we still have no empirical validation of the effect of urban trees in a cool climate. More than 3 out of every 4 people in the U.S. live in places with more heating degree days than cooling degree days, and Americans use much more energy for heating than for cooling (U.S. Department of Energy, 2009). To properly assess simulations of the role of urban trees in the C budget, comprehensive analyses are needed to test the relationship between tree location and energy usage (both heating and cooling). Our work in Madison, WI was the first to begin address this need. In 2016, we downloaded average annual energy use data for approximately 32 thousand single family residential homes and built a regression model between the amount of tree cover near each house and the C

produced from electricity and natural gas use, controlling for other factors such as building characteristics.

## 3.4   Methods

### Building Energy Use

In April 2016, we obtained the annual energy use summary table (April 2015 - April 2016) from Madison Gas and Electric's publicly available website for approximately 32 thousand single family residential houses in Madison, WI. This included average monthly gas and electricity use. This period exhibited a much warmer than average December (about 6º C) and had low snowfall. We removed from our sample outliers that used fewer than 120 therms (which is less than the 0.5% quantile) or fewer than 240 kWh (which is less than the 0.05% quantile) annually. We included only buildings that used natural gas for heating and had central air conditioning. Our final sample size used to build models was 25095.

### Carbon Emissions

We converted energy use to C emissions using emission factors published by the US EPA's Emissions & Generation Resource Integrated Database, eGRID (Emissions & Generation Resource Integrated Database, 2016). 100% of the carbon in natural gas is oxidized to $CO_2$ when burned for heating. The carbon coefficient for natural gas is 1.446 kg C / therm (United State Environmental Protection Agency, 2017). For electricity, Madison, WI is a part of the Midwest Reliability Organization East (MROE) region of the North American electric grid. The estimated carbon coefficient for power generated in this region is 0.2063698 kg C/kWh (Emissions & Generation Resource Integrated Database, 2016). We had originally used emission factor for MROE from 2012 (.1567988 kg C / kWh) and by switching to the updated and higher 2016 emission factor (0.2063698 kg C/kWh), the overall detrimental effects of trees on ACE was diminished from about 3.4% to 2.5%.

### Building Characteristics

Energy use is strongly determined by building characteristics. For every address in the city, the City of Madison releases the assessor's property information, which includes information on building age, size, materials, type of heating and cooling, as well as which schools serve the address. We removed any houses that had bad or missing data. Many of the covariates, such as size and price, were strongly correlated. Given that our primary

Figure 3.1: Simulated shadows of trees on a house at the latitude of Madison, WI. In the summer, trees to the west of buildings provide the most effective shade since solar angles are lower and cooling demand highest in the afternoon. In winter, even deciduous trees can significantly reduce solar gain.

interest was how tree cover affected building energy use, not how building characteristics affect building energy use, we reduced the dimensionality of building characteristics using principal components analysis. This reduced the number of building covariates from 20 (Lot area, length of water frontage, year built, number of stories, number of bedrooms, number of bathrooms (full and half), number of fireplaces, living area on each floor, finished attic area, finished basement area, total basement area, crawl space area, year roof was replaced, number of stalls in each garage, land value, improvement value) to 5 orthogonal vectors, accounting for 55% of the variance.

## Tree Canopy

For tree cover we used a 1m resolution land cover map derived from 2013 National Agriculture Inventory Program (NAIP) visible and near-infrared digital aerial imagery with an accuracy of 85% (Erker et al., 2019). Using building footprints from the Dane county, for each house for which we had energy use data, we divided the space around it into 8 regions defined by 2 buffers around the house of distance 20 m and 60m and 4 rays from the building's centroid. Tree cover closer than 20m was considered near, tree cover farther than 20m and closer than 60m was considered far. These buffers were subdivided into north, west, south, and east regions by rays of angles 57, 123, 237, 303 degrees from north. These angles are within 1 degree of the azimuth angle of sunrise and sunset at the two solstices. This defines the south region as the region that is exposed to direct sunlight year-round, and the north region as the region that is never exposed to direct sunlight (this relationship is approximate and complicated by individual building geometry). Within each of the eight regions we summed the area covered by trees, and then use the tree cover in each region as predictors in our models.

We tested buffers of different widths (every 3m from 3m to 60m), but found because of the observational nature of our data that we needed to aggregate regions to remove multicollinearity that caused unstable coefficient estimates. Using a distance of 18, 21, or 24 m instead of 20m to separate "near" from "far" cover only slightly changed coefficient estimates. By fitting a model with all tree cover close to a house aggregated into one variable and then a model with the tree cover separated into 8 variables defined by distance and direction we tested the overall association of ACE with tree cover and then tested for specific associations by distance and direction.

## Building Cover

Nearby buildings likely also affect the energy use of a building. To test this hypothesis we calculated the area of buildings in each of the eight regions around every building and included these as covariates in our modeling. We used building footprints from Dane County which consists of structures the size of a single car garage or larger. The horizontal accuracy is +/- 6.6 feet for well-defined points, at a ninety percent confidence level.

## Modeling

We fit linear models where the response was log transformed annual ACE for gas use, for electricity use, or for gas and electricity combined (net). Because a separate model was built to explain net C emissions, coefficient estimates for the net model were not precisely the sum of the coefficients from the electricity and gas models. ACE was log transformed to meet assumptions of normality and diagnostic plots were assessed to check other model assumptions and potential sensitivity to influential observations. Our first models aggregated all tree cover near buildings into one variable, and subsequent models separated tree cover based on direction and distance into eight variables. In addition to tree cover, variables in our model were: 5 principal components of building characteristics, building cover in each of the 8 regions, and a random effect for elementary school which might capture neighborhood characteristics such as culture. We used AIC as a variable selection criterion and in our final models only used the first 5 building characteristics principal components and we dropped all the building cover covariates. Estimates for the coefficients of tree cover were not sensitive to the inclusion or removal of these covariates, but model fit improved. Although some tree cover covariates increased AIC, we kept all tree cover covariates in the model because we wanted estimates of their effects, however uncertain they might be. We also fit models We fit models using the R package lme4 (Bates et al., 2015).

## Interpreting coefficients

To improve interpretability of coefficients, we back transformed them to the original scale and expressed the multiplicative effects as a percentage (Gelman and Hill, 2007). We then multiplied this percent change by the median ACE (a better estimator of the central tendency because of the right skew in our data) to estimate the typical effect in absolute C terms. To get typical effects of tree cover, we multiplied median tree cover in each region by its coefficient estimate and back transformed to the original scale.

## Estimating C storage and sequestration of a green ash with 100m$^2$ canopy

To estimate C storage and sequestration by a single green ash tree with a canopy cover of 100m$^2$, we used allometric equations to estimate that tree's diameter at breast height (DBH) and mass and then, assuming an annual DBH growth of 0.61 cm, predicted the change in mass to get C sequestration Nowak and Crane (2002); McPherson et al. (2016).

## Extending Analyses from Published Literature

To compare our work to past simulation studies we converted results that were in Therms or kWh to kg C. We did this for Thayer Jr and Maeda (1985), McPherson et al. (1988), and Huang et al. (1990) using updated emission factors corresponding to each study city's eGrid subregion (Emissions & Generation Resource Integrated Database, 2016). To extend Akbari and Konopacki (2005), we joined climate data (heating and cooling degree days) from the nearest NOAA weather station to census tract centroids U.S. Census Tract Centroids (2010); Arguez et al. (2012). It was from this join of climate and census data that we determined that 77% of the U.S. population lives in places with more heating than cooling degree days. Then for each census tract we predicted the effect of trees and increasing roof albedo on the energy use of a pre-1980's building with gas heating following their table that bins houses according to heating degree-days and using emission factors corresponding to the eGrid subregion containing the census tract centroid. Separating out the indirect effects of trees from the indirect effects of increasing roof albedo was not possible because these were not modeled separately. However, the general trend would be similar, but with a decreased electricity savings and a decreased heating penalty. Akbari and Konopacki (2005) found the effect of tree shade to be stronger than the indirect effects of increased roof albedo and transpirative cooling.

## Code

All of the code and data for these analyses are present on Github (`https://github.com/TedwardErker/energy`). Code is provisional pending review.

## 3.5 Results

### Effect of trees on building associated C emissions

Trees increased C emissions associated with residential building energy use (**ACE**) in Madison, WI. This effect was the result of a trade-off between their electricity (cooling) saving and gas (heating) penalty. We estimated that 100m$^2$ of tree cover within 20m of a house increased ACE from gas use by 0.77% (95% CI: 0.68%, 0.85%), and decreased ACE from electricity use by 0.21% (95% CI: 0.34%, 0.080%). Our model for net ACE estimated that 100m$^2$ of tree cover increased ACE by 0.17% (95% CI: .09%, .27%).

The magnitude and direction of the effect depended on tree location relative to the building. Figure 3.2 shows the percent change in the ACE from 100m$^2$ of tree cover. Trees reduced ACE from electricity for all near regions except the east. Trees increased ACE from gas for all regions, especially in the near south and east. For net ACE, tree cover in the near east was the most important, having the only estimate with a 95% CI that excluded 0.
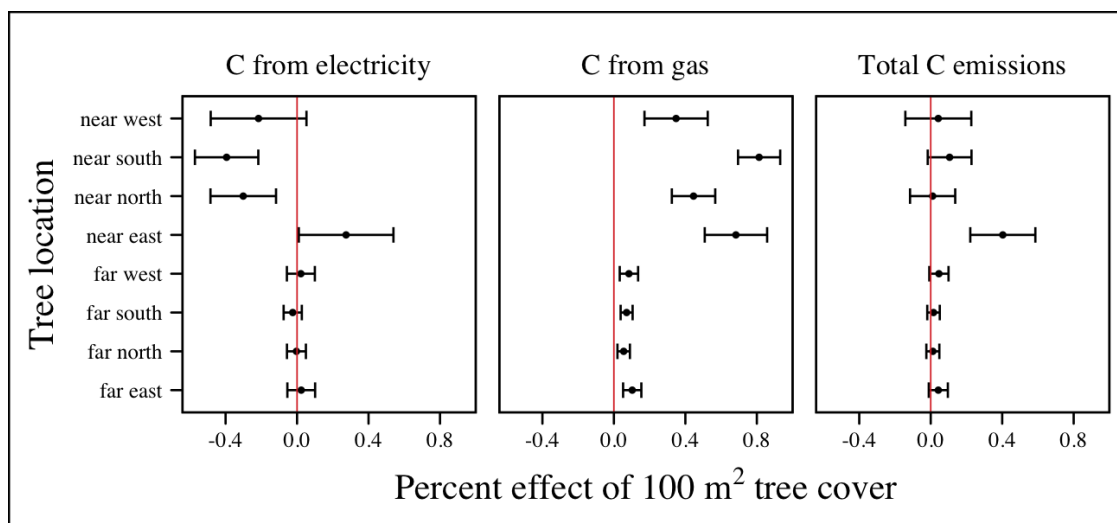


Figure 3.2: The percent effect of 100m$^2$ tree cover in different locations on C emissions from residential building energy use. n = 25095, bars indicate standard errors.

### Effect of existing tree cover on a typical house

The median house in our sample was responsible for 1084 and 954 kg C annual emissions due to electricity use and gas use, respectively. Multiplying the median tree cover in each region (see table 3.1) by its coefficient we estimated the effects of typical tree cover on a typical house in Madison: electricity C emissions were reduced by 33.8 kg C / yr (95%

CI: 14.7, 52.7), but gas C emissions were increased by 102.3 kg C / year (95% CI: 92.9, 111.8). Our combined model estimated the net effect of existing tree cover is to increase C emissions by about 62 kg C/year (95% CI: 38.7, 85.3) for a typical house. This is 2.5% of the median house's annual ACE.

Table 3.1: Summary statistics for amount of tree cover ($m^2$) in each region around houses in Madison, WI.

| Region | min | mean | median | max |
|---|---|---|---|---|
| near west | 0 | 193 | 179 | 742 |
| near south | 0 | 372 | 363 | 1443 |
| near north | 0 | 357 | 345 | 1197 |
| near east | 0 | 193 | 179 | 764 |
| far west | 0 | 974 | 960 | 2640 |
| far south | 0 | 1676 | 1653 | 4376 |
| far north | 0 | 1673 | 1661 | 4602 |
| far east | 0 | 967 | 955 | 2677 |

While tree cover in far regions had smaller per unit area effects than in near regions, there was more tree cover in farther regions, so when median tree cover was multiplied by the smaller coefficients some of the farther regions had larger typical effects than near ones (figure 3.3). Typical tree cover in the far east and far west regions had a greater estimated effect than cover in the near north and near west.

## Comparing C emissions from energy use due to trees to C stored and sequestered.

For comparison, consider a green ash tree with a crown area of 100m$^2$. This tree would store approximately 1360 kg C in above ground biomass and it could sequester around 34 kg C / year. That same tree in the near east region of a typical house in Madison was estimated to increase C emissions by 9.8 kg C/yr (95% CI: 6.7, 12.9). In the near west the estimated effect was 1.0 kg C/yr (95% CI: -2.1, 4.1). Therefore, the transfer of carbon from atmosphere to the biosphere (sequestration) is an order of magnitude larger than the transfer from the lithosphere to atmosphere (emissions).
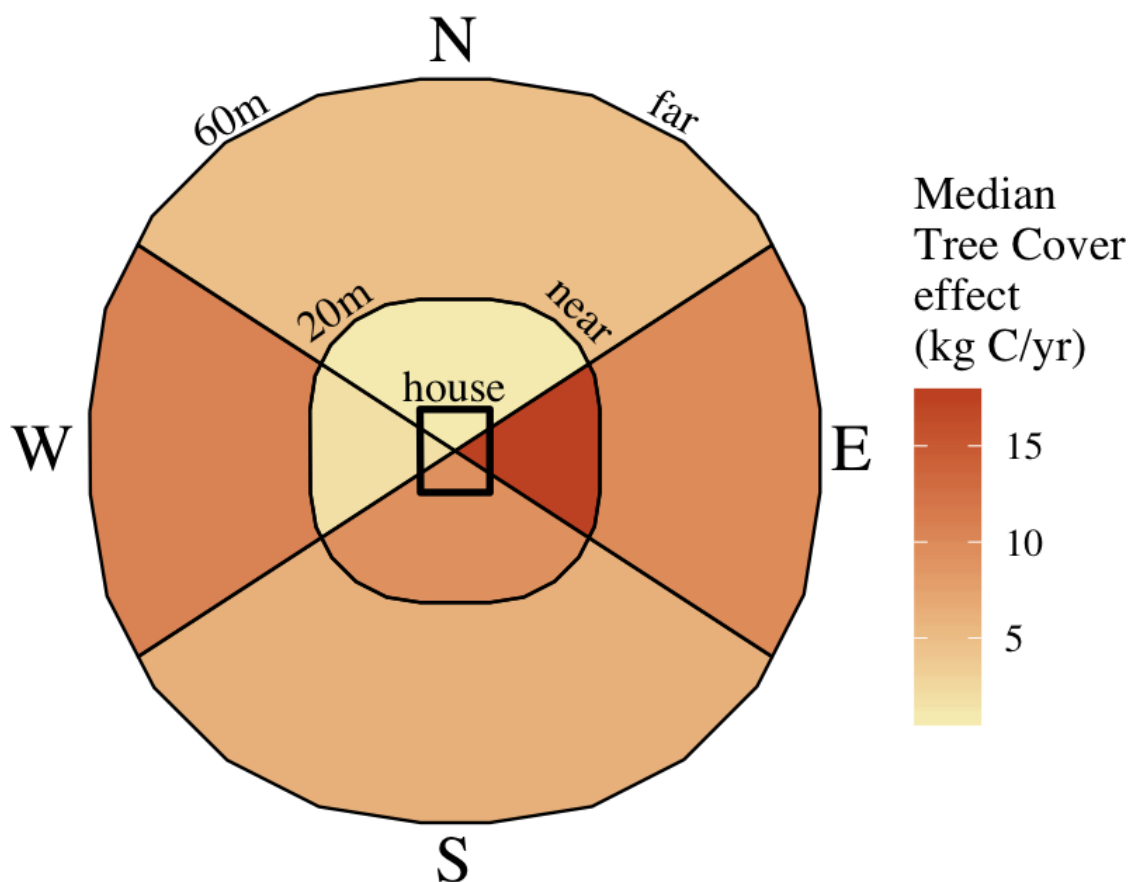
Figure 3.3: Effect of typical tree cover on a typical building's C emissions.

## 3.6   Discussion

### Interpreting Tree Effects

In the cool climate city of Madison with 7283 heating degree days, 597 cooling degree days and a electricity emission factor of 0.206 kg C / kwh, the relationship of trees with ACE was clear: trees increased ACE from gas use more than they decreased ACE from electricity use, resulting in a net increase in ACE.

According to past studies, if shade were the only effect on ACE (winter wind speed reduction was not included) trees in cool climate cities would cause an increase in ACE.

Since we found an increase in ACE with increased tree cover this suggests that shading was the most important process and that whatever gas savings trees may have provided in winter by reducing wind speeds was swamped by the penalty of reduced solar radiation.

By separating tree cover into different locations, it appeared that for the most regions, the beneficial effects of trees on electricity ACE *mostly* canceled out the detrimental effects of trees on gas ACE, with the exception of the near east. This suggests that trees to the east may have been responsible for most of the net increase in ACE. Eastern trees did not provide electricity savipngs since houses require less cooling in the morning hours, but still caused an increased gas use in winter. This agrees with Donovan and Butry (2009) who also found trees to the east had no effect on electricity use.

As expected, trees to the near south had a strong effect on electricity savings, but they also had a stronger gas penalty. Trees in the near west and near north had the weakest gas penalty, which may have been due to the savings they provided by reducing wind speed. Somewhat surprising was the weakness of the estimated electricity savings of trees in the near west, which all simulations have predicted has the strongest effect. Also surprising was that trees to the north are associated with an increase in gas use, something no other study has predicted. Since tree cover is measured north of each building's centroid, it could be that there is still some shading from trees on the northern roof. It is also possible that there could be some transpirative cooling occuring during the early spring and late fall when trees have their leaves and it is still the heating season in Madison.

The inability to discern causation and identify clear mechanisms is one of the limitations of this observational study. While the overall association between tree cover and ACE is clear, uncertainty increases when distance and direction of tree cover are considered. Where our coefficents disagree with past studies, they should be considered cautiously.

## Comparing to past work

Our findings agreed with some though not all of the past simulation studies, and the modeling of wind is the main cause of discrepancies. Thayer Jr and Maeda (1985) modeled the shading effects of south trees on building energy use and reported that trees increased emissions in cities with more heating degree days than cooling degree days. McPherson et al. (1988) investigated the shading and wind effects on building energy use in 4 cities, one of which was Madison, WI. Converting their results into C, trees in Madison caused a small increase in emissions, though their method for modeling wind was later criticized and abandoned (Simpson and McPherson, 1998). Akbari and Konopacki (2005) developed a method to predict the effect of a tree planting program and increasing roof albedo for any

city in the U.S. Figure 3.4 illustrates an application of their method to every census tract in the conterminous US for pre-1980s houses using updated energy emission factors. They identify places where trees increase ACE and others where trees decrease ACE, however they are most often cited for the average effect found: "Shade trees reduce building energy use and $CO_2$ emissions from power plants", the title of from Akbari's 2002 paper. Clearly climate largely drives the relationship between ACE and trees at large scales, but there is significant regional variation due to differences in electricity C emission factors. Trees are more beneficial in places with "dirtier" (more C per kWh) electricity and less beneficial in places with "cleaner" (less C per kWh) electricity. For example, despite its cool climate, trees in Chicago reduce ACE because the electricity has more C per kWh and therefore the electricity reduction benefit of trees leads to a greater reduction in C than in places with cleaner electricity.

About 40% of the US population live in areas where the Akbari and Konopacki (2005) model predicts that trees increase C emissions. While their methods were limited as mentioned above, and they modeled theoretical, not existing, tree cover, their work suggests that many large cities especially in New England, the Northwest, the Mountains and the Upper Midwest would need to carefully consider the C implications of large tree planting programs.

Our empirical findings disagree with those simulation studies that model the relationship between tree cover and wind speed following Heisler (1990) and McPherson and Simpson (1999). When the beneficial effects of wind are excluded for models of several cool climate cities: Toronto (Akbari and Taha, 1992), Chicago (Jo and McPherson, 2001), Minneapolis, Sacramento, and Washington (Huang et al., 1990), trees either have no effect or increase energy use and ACE, which agrees with our general findings. The iTree model which uses the methods of McPherson and Simpson (1999) predicts that the shading effects of a large deciduous tree in the Northern Tier, North Central, Mountains, Pacific Northwest, and California Coast regions increases ACE of a 1950-1980 vintage house by 0.136 to 9.52 kg, depending on the region. This is comparable to our results. However, the wind effect in the iTree model of that same tree on the same house decreases heating ACE by 1.23 to 66.14 kg depending on the region and existing canopy: an order of magnitude greater savings for gas ACE from wind reduction than the penalty from shading. Given that our model coefficients show that trees increases ACE, it suggests that shading is a more important process than wind speed reduction. In other words, our results agree with the shading but not wind reduction effects proposed by others, and therefore may suggest that shading is being more accurately modeled than wind in existing simulations. McPherson and Simpson (1999) note that the uncertainty in their methods was high, and, given our contradictory
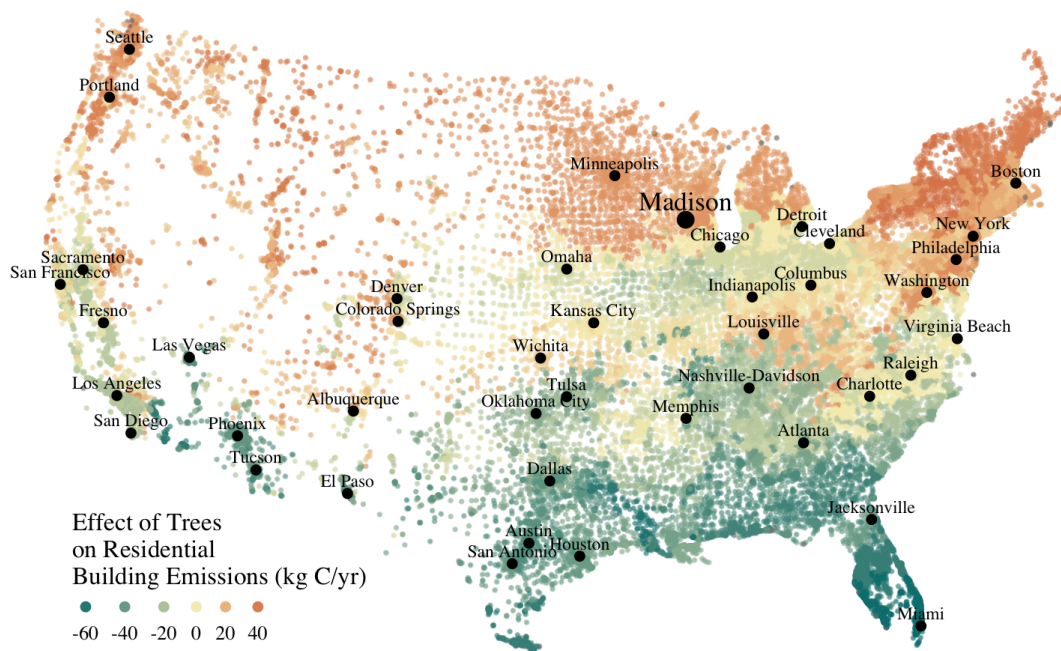
Figure 3.4: Each census tract in the conterminous US shaded by magnitude of building C emissions effect of trees planted to west and south of a pre-1980's home and increasing roof albedo. Differences in regional emission factors (C/kWh) cause deviations from climate trend. New England has especially high ACE for the climate because their electricity is cleaner (low C/kWh). About 40% of Americans live in places where trees increase ACE. Model based on Akbari and Konopacki (2005).

findings, it is clear that more data and improved models are needed to better parameterize the complex and uncertain relationship between tree cover, wind, and building energy use.

## Considering the larger C cycle

The effect on ACE of a tree with a 100 m$^2$ canopy area is an order of magnitude smaller than that tree's C sequestration. However, it is important to make the distinction between different pools of C. Discounting increased ACE as irrelevant because C sequestration more than compensates, fails to recognize that ACE is an input of fossilized C while sequestration is a temporary transfer of C from the atmosphere to biosphere. In the short term, sequestration may assist in climate change mitigation, but unless forested land is permanently expanded or wood products are forever prevented from decay, in the long run (hundreds of years) sequestration by trees can never offset fossil C emissions. Indeed this same conclusion was made for fossilized C emissions due to tree management

(Nowak et al., 2002). The avoided ACE from trees has been estimated to more than offset these management emissions in a life-cycle analysis of the Million Trees Los Angeles program (McPherson and Kendall, 2014). However, our results suggest that for cool climate communities, shade trees actually increase ACE and, especially when combined with the C emissions from management, are atmospheric C sources in the long term.

## Trees relative to other factors that affect ACE and the ACE effect of trees relative to other ecosystem services/disservices.

Considering all of the factors that determine building energy use and ACE, trees play a very minor role, which we estimated to be about 2.5% of the ACE of a median house. As buildings become better built and insulated the effect of trees on ACE will decrease. Far greater ACE savings are possible with improved construction and savvy occupant behavior. However, the effect of trees on energy use and ACE is one of the most often cited ecosystem services of trees (Roy et al., 2012), and evidence that ACE is increased by trees highlights the large uncertainty in software used by thousands of communities to justify urban forest costs.

Still, effects on ACE are just one of the ecosystem effects that trees have in cities. Trees may also improve air quality, reduce stormwater runoff, reduce noise, and provide wildlife habitat. The aesthetic value of trees is often far greater than the value of the ecosystem services or disservices provided (McPherson et al., 2005). Even after publishing that trees reduced ACE on average, Akbari (2002) noted that this benefit alone may not justify the cost of tree planting. Our opposing results have a similar caveat: even after finding the detrimental impacts of trees on ACE in cool climates, management decisions need to consider these results as just one of the many benefits and costs of trees. Our results suggest that trees planted on all but the near east side of a house are net neutral in terms of ACE, so that the other benefits of tree planting, such as aesthetics, could be accomplished in cool climates through careful selection of planting locations.

## Future work

Using actual energy use data from over 25,000 houses, we provide a much needed complement to simulation models of tree effects on ACE in cool climates. However, there is need for continuing work to address remaining shortcomings. The observational nature of our data is strengthed by the size of the dataset, but ultimately causal inference depends on our physical knowledge of how trees alter building energy use. Not all coefficients in our model agree with our existing physical understanding of how trees affect building energy

use. For example, it is surprising that trees to the near west have such a weak effect on electricity use and that trees to the north increase gas use. While the overall association between greater tree cover and greater ACE in Madison is clear from our work, how that relationship changes with distance and direction is less clear. Our work is an important complement to simulation studies and highlights the need for more experimental studies especially in cool climate cities.

Our data on tree cover was also limited by a lack of information about tree height, which means we could not address how adjusting the size of trees planted in an urban area affects ACE. Incorporating LiDAR could provide more accurate estimates of tree shading and wind reduction. Furthermore, the scale of the effects that our study could detect is much smaller than the city-wide effects many simulation studies address. Ultimately, this work is a sample of one year from one city with the accompanying limitations. The warm December during the sampling period may mean the effect of trees is even more detrimental than we report, but more years are needed to say. The location of Madison near the boundary that Akbari and Konopacki (2005) identified between trees being a sink and a source is useful, but more cities are needed to empirically determine this boundary.

Our work presents more evidence for a known, but too often overlooked, result in urban ecology. Many studies only report that trees reduce ACE (Pataki et al., 2011; Weissert et al., 2014). While this may be true in most of the US, and the potential ACE reduction is larger than the potential ACE increase, it ignores geographic variation (Akbari and Konopacki, 2005). In many ways it is not surprising, given the climatic diversity across the country, that the effects of trees on ACE might also vary and that our prescriptions for how to plant trees to minimize ACE could be different between Los Angeles and New York City. Our study is only the first study to use a large number of both gas and electric energy use observations, and the first study of its kind in a cool climate. Much more work with observed energy use is needed to identify where trees switch from increasing to decreasing ACE.

## 3.7  Conclusion

Using observed energy use data, we have shown that trees near residential houses in Madison, WI are associated with increased energy use and ACE. Near east tree cover appears to have the strongest net relationship. Extending past simulation studies, we show that this is likely the case for a large area of the US and cool climate regions generally. The magnitude and direction of the association is dependent on tree location relative to buildings, climate, building characteristics, occupant behavior, and the C content of electricity. Disagreements between our results and past work may be due to how wind

effects are modeled and much more work is needed to better understand this process. While we do not invalidate past simulation studies of how trees affect building energy use and ACE, our empirical results raise questions about simulation assumptions and highlight the need for more research. We add critical geographic nuance to research that could have major implications for tree planting programs in cool climates.

## 3.8   Acknowledgments

# 4 URBAN TREE HEIGHT GROWTH RATES EXPLAINED BY THE URBAN ENVIRONMENT AND FOLIAR CANOPY TRAITS DERIVED FROM IMAGING SPECTROSCOPY

## 4.1 Summary

Urban trees alter the urban environment, potentially providing important services to humans in cities. Many of these services are a function of tree growth, and therefore better estimates of tree growth will lead to a better understanding of the impact trees have on our wellbeing. We used 4 years of LiDAR data from 2005, 2009, 2016, and 2017 over the city of Madison, WI to estimate 7,124 tree heights. Using an innovative maximum height bias correction technique, we corrected heights and estimated tree height growth rates for each tree. We then derived indices of foliar canopy traits from imagining spectroscopy data and used these, along with other environmental covariates, to explain variation in tree height growth using multiple linear regression. Genus and initial height were the strongest predictors of urban tree height growth, but if genus was excluded from the model, remotely sensed foliar traits explained nearly as much variability in growth as genus. Trees growing near other trees and buildings grew higher faster than open grown trees, possibly in response to competition for light. Percent impervious cover interacted at multiple scales to affect tree height growth: while impervious cover was generally associated with decreased growth, trees with low impervious cover within 20 m maintained relatively high growth rates even if impervious cover was high in the surrounding 100 m. Four foliar canopy traits predicted from imaging spectroscopy - nitrogen, lignin, total phenolics, and chlorophyll were significantly related to growth. Nitrogen, lignin, and total phenolics had negative coefficients and chlorophyll had a positive coefficient. Topography is significantly related to tree height growth, but effects are small.

## 4.2 Introduction

With over half the human population living in urban areas, planting urban trees to provide ecosystem services is seen as a way to make the environment that most people interact with more pleasant and sustainable. These ecosystem services include habitat for wildlife, stormwater runoff reduction, air quality improvement, carbon sequestration, and aesthetics (Roy et al., 2012).

All these services are a function of growth, either directly or indirectly. Carbon uptake

occurs as a direct result of growth. Reductions in stormwater runoff and improvements in air quality are functions of tree size, which results from growth (Nowak et al., 2014, 2013). Therefore, understanding urban tree growth is essential to estimating and projecting ecosystem services into the future. The factors that contribute to the growth of trees in general are well understood. What we do not understand as well is how the complex urban environment alters these factors, thereby altering the growth of trees.

Urban trees grow differently than their non-urban counterparts because of the challenges they face surviving among urban infrastructure and as a consequence of being cultivated by humans (but not for their wood). For example, street trees are subject to damage from vehicles, pedestrians, soil compaction and poor nutrition (Day et al., 2010); urban trees tend to be more open grown than forest trees; urban trees are pruned to accommodate powerlines or for aesthetics, many urban trees are irrigated and/or fertilized; and the species composition in a city is often different than surrounding native forests (Zipperer and Guntenspergen, 2009). Urban conditions are not only unique, but they are also more heterogeneous, which creates variability in the growth of the urban forest at fine spatial scales.

Remote sensing technology can efficiently estimate tree height growth and quantify traits that explain patterns in that growth for tens of thousands of trees across this heterogeneous landscape. Sufficient sample size is required to detect effect sizes that may be small relative to the variability found in the urban environment. Here we use two technologies that have only recently become more available, repeat airborne laser scanning (LiDAR, also called light detection and ranging) and imaging spectroscopy.

LiDAR has been used extensively for years in forestry applications (Dubayah and Drake, 2000). Laser pulses are sent from an airborne platform to the ground below and, when the reflected light returns with sufficient intensity, the height of the objects below are recorded. The result is a 3 dimensional point cloud that can be used to characterize forest structure, including height (Lim et al., 2003). Repeat LiDAR is a promising technology for measuring tree height growth, but handling differences between LiDAR acquisitions remains a challenge, see for example Duncanson and Dubayah (2018). Our work uses multiple years of historical LiDAR data, in conjunction with an innovative height bias correction, to estimate the heights of trees and their growth rates.

Leaf spectroscopy uses the reflectance of light to predict foliar traits and has been used for decades in remote sensing (Martin and Aber, 1997; Asner, 1998). These foliar canopy traits can help to understand ecosystem function (Ustin et al., 2004), including in urban environments (Gu et al., 2015; Alonzo et al., 2016). NASA's Airborne Visible / Infrared Imaging Spectrometer - Next Generation (AVIRIS-NG) measures the reflectance

of light in hundreds of narrow wavebands from 400 to 2500 nm. We used the spectra from the imagery to create indices of canopy foliar traits which then in turn we used to explain height growth. As the photosynthetic tissues of trees, leaves are responsible for capturing the carbon necessary for growth and the foliar traits of a species show various tradeoffs between factors such as photosynthetic capacity and longevity (Wright et al., 2004). Traits such as percent nitrogen by mass and chlorophyll concentration are related to photosynthetic capacity and productivity (Reich, 2012). Lignin is related to leaf structure and recalcitrance, and can be synthesized in response to ozone (Cabané et al., 2004). Total phenolics are related to defense against herbivory or other stressors (Martin and Aber, 1997; Lindroth and Batzli, 1984; Mellway et al., 2009).

In addition to canopy foliar traits, we also included variables that have been shown to influence tree biology: topography, land cover, tree height, mean height of a tree's surroundings and whether or not the tree was a street tree and whether or not it had overhead utilities. Current tree height has a strong effect on the potential for the tree to continue growing upward (Ryan and Yoder, 1997). Topographic variables such as elevation, slope, and aspect influence the formation of soils and the soil temperature and moisture, which in turn affect tree growth (Chapin III et al., 2011). Trees continue growing upwards in response to competition for light (King, 1990). Trees surrounded by tall objects (both buildings and other trees) will need to grow tall to capture light energy. Impervious surfaces and utility presence are associated with poor tree growth, pruning, and mortality (Jim, 1998; Day et al., 2010), but also enhanced growth and longer growing seasons (Searle et al., 2012; Pretzsch et al., 2017; Zipper et al., 2016).

The objectives of our study were to:

- evaluate the effectiveness of multiple years of terrain optimized leaf-off LiDAR with variable pulse densities to estimate urban tree height growth;

- evaluate whether canopy foliar traits estimated from remotely sensed imaging spectroscopy can explain tree height growth; and

- evaluate how urban tree height growth is altered by environmental factors common to all trees (e.g. topography) as well as environmental factors specific to the urban environment (e.g. impervious cover, streets, and utility lines) by exploiting existing datasets.

## 4.3 Methods

### Overview

In our study city, Madison, WI, we combined remote sensing measurements of urban terrestrial vegetation with environmental factors derived from a geographic information system (GIS) to explore the potential for these to explain urban tree height growth. Using four years of LiDAR data (2005, 2009, 2016, and 2017) and an innovative height bias correction method, we estimated the height growth of trees over a 12 year period. We used two street tree inventories (one from the city of Madison and one from the village of Shorewood Hills, which is within the city) and two complete inventories of the trees in Madison's Atwood and Hill Farms neighborhoods to provide taxonomic information of trees. In September 2015, NASA's Airborne Visible / Infrared Imaging Spectrometer - Next Generation (AVIRIS-NG) imaged the majority of Madison. Using predictive equations developed following Singh et al. (2015), we mapped canopy foliar traits: Nitrogen (% mass), N; leaf mass per area (g m$^{-2}$), LMA (g m$^{-2}$); lignin (% mass), chlorophyll (mmol m$^{-2}$), and total phenolics (% mass), then converted these trait predictions to scaled indices. In addition to foliar traits, we calculated other covariates such as percent impervious cover at two scales (within 20m and within 100m, as derived from Erker et al. (2019), Chapter 1), topographic variables, and the mean height of the surroundings within 20 m of a tree (see table 4.1 for all covariates).

For the purposes of estimating coefficients more reliably and minimizing spatial dependence, we subset our data for statistical analyses so that no two trees of the same genus were closer than 200 m to one another. This reduced our sample size from 21,247 to 7,124, but also reduced spatial dependence that could potentially bias coefficient estimates or inflate confidence that coefficient estimates were different from zero. We fit several multiple linear regressions with growth rate as a response and all covariates as predictors with plausible interactions. We used AIC to help with model selection, but did not test very many interactions, instead we were primarily guided by our objectives and the goal of finding a model that was straightforward to communicate. Details on the selected models are in results.

### Study Area

Madison is a small city (population ~260,000, metropolitan ~500,000) in south central Wisconsin, USA, (figure 4.1, cite:Madison$_{WIQuickFactsUSCensus}$. The dominant forest type is broadleaf deciduous. Pre-European settlement forests were dominated by oaks (Quercus),
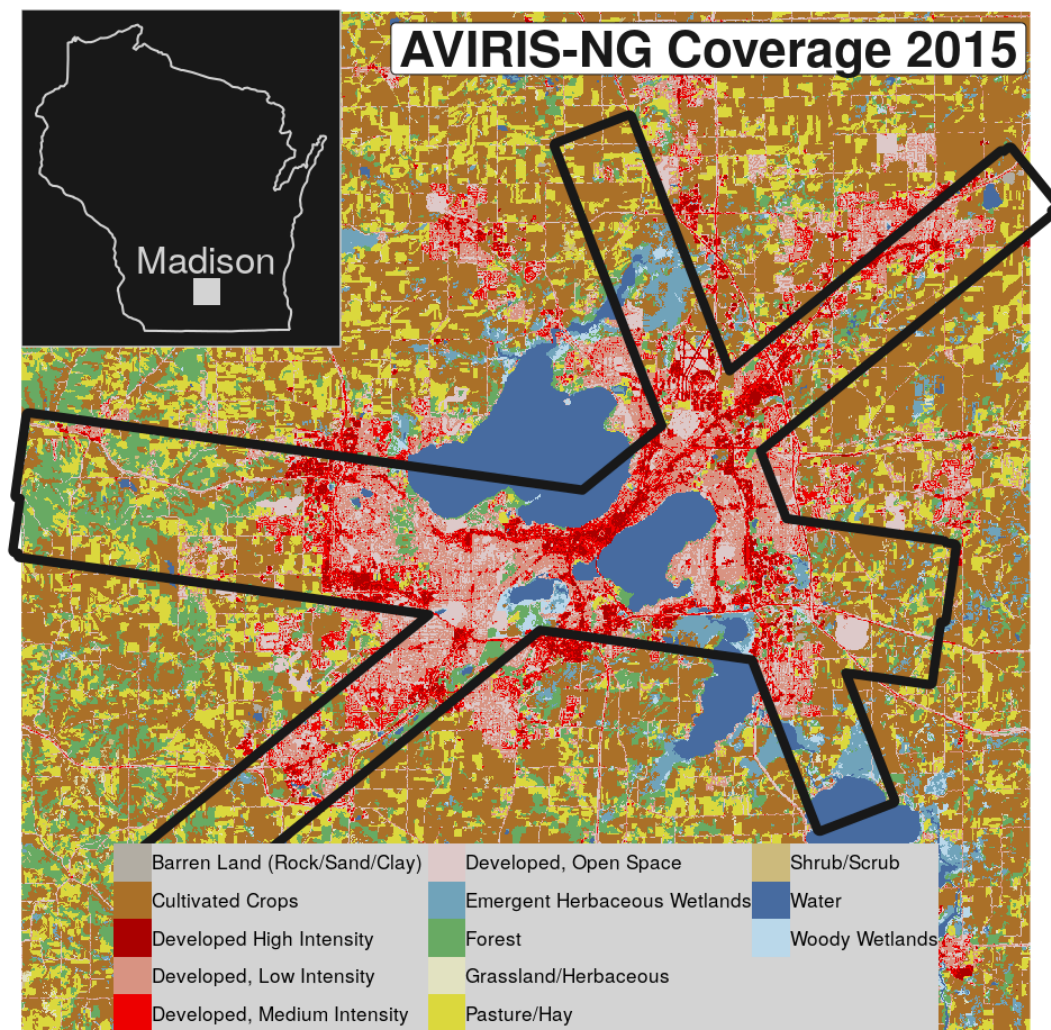
Figure 4.1: AVIRIS-NG coverage overlaid on the National Land Cover Database map for Madison.

maples (Acer), and basswood (Tilia) Mollenhoff (2003). Now the most common street tree genera are Fraxinus, Acer, Gleditsia, and Tilia, making up over 70% of all street trees. Other common genera in neighborhoods include: Picea, Thuja, Betula, and Pinus.

## Data

### Tree inventories

In our analyses, we used four tree inventories – a 2011 City of Madison street tree inventory; a 2012 inventory of the Atwood neighborhood located on Madison's east side, a 2015-2016 inventory of the Hill Farms neighborhood on Madison's west side, and a 2015 Village of Shorewood Hills street tree inventory (Figure 4.2). All inventories recorded species as well as diameter and all trees were been geolocated with differential GPS and/or using high resolution imagery. The street tree inventories also provided information on presence of overhead utility lines. Species were aggregated to genus for analysis. Conversations with the Hill Farms inventory organizers suggested this was needed to increase the reliabililty of identification in this largely volunteer-run inventory. Aggregating to genus also increases the sample size of each taxonomic unit.

In our analysis below, we defined trees in our database as either "street trees" (those from street tree inventories), further subdivided as either having power utilities infrastructure overhead or not, or "neighborhood trees", those growing in yards and parks (those from the Hill Farms and Atwood neighborhood inventories).

### Airborne laser scanning (LiDAR)

We used four years of airborne laser scanning (LiDAR) to estimate tree heights for height growth rate estimation. The LiDAR was acquired in springs of 2005, 2009, 2016, and 2017. The intended use of LiDAR was for digital elevation modeling and so was flown in leaf-off conditions. Over this 12-year period LiDAR measurement technology improved significantly leading to increases in pulse density from an average of 0.20 pulses m$^{-2}$ in 2005 to an average of 4 pulses m$^{-2}$ in 2017. LiDAR data were downloaded from the wisconsinview ftp server.

We extracted LiDAR point clouds surrounding the tree points in the tree inventories using a 2.4 m buffer. The buffer width was selected to be large enough to provide enough points to estimate height, but also to be small enough so that points not a part of the tree were excluded. This worked well for the vast majority of trees because the GPS locations for most of the trees were in the center of the crown. We dropped trees from the analysis that had been removed during the study period or were too close to other trees to not be readily
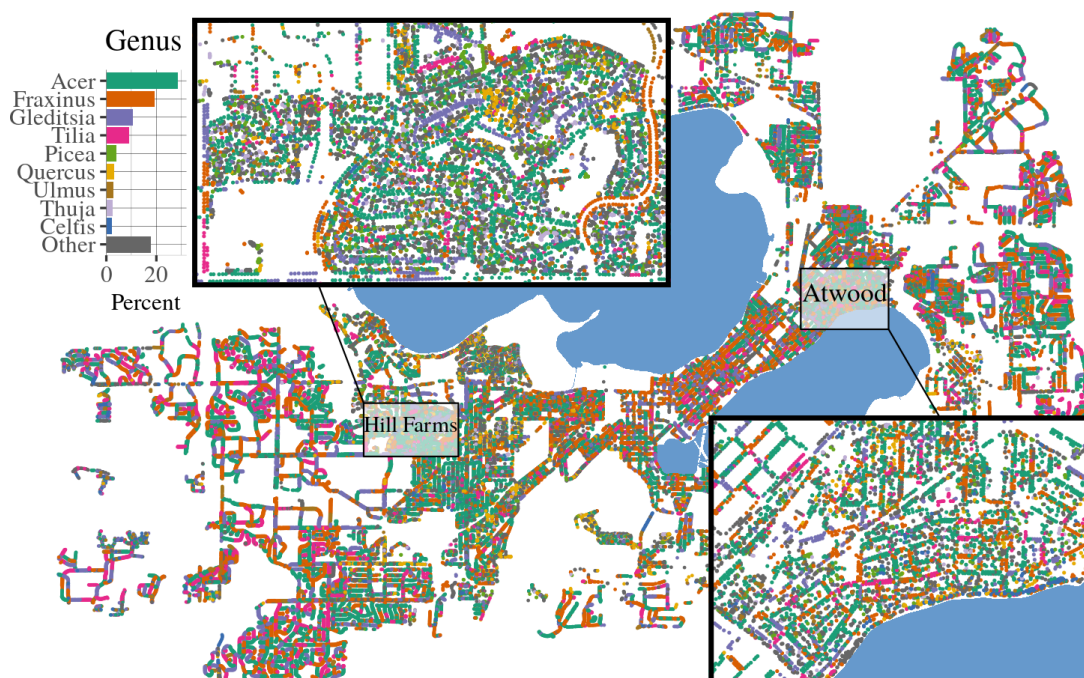
Figure 4.2: Tree inventories of Madison.

distinguishable in the imagery. If two trees were within 5 m of each other we selected the tree with the larger bole diameter.

We analyzed the LiDAR data using the R package `lidR` (Roussel and Auty, 2018). To create a variable that would be related to light availability for a tree, we first created a 1 m canopy height model using the 2016 LiDAR (points to raster method), and then found the average height of that canopy height model within 20 m of each tree. Trees surrounded by buildings or other trees would therefore have high values and open grown trees would have low values.

**Imaging Spectroscopy**

NASA's Airborne Visible / Infrared Imaging Spectrometer - Next Generation (AVIRIS-NG) collected imagery over the majority of Madison on Setember 3, 2015. AVIRIS-NG measures reflected solar radiance in 5 nm bands from 400 nm to 2500 nm. Images were flown at an altitude above mean ground level of 4,600 m resulting in a pixel size of 4.6 m. Atmospherically corrected reflectance images were downloaded from AVIRIS-NG data portal. Data were pre-processed consistent with methods reported in Singh et al. (2015).

Using predictive equations developed following Singh et al. (2015), we predicted canopy foliar traits: Nitrogen (% mass), N; leaf mass per area (g m$^{-2}$), LMA (g m$^{-2}$); lignin (% mass), chlorophyll (mmol m$^{-2}$), and total phenolics (% mass). Singh's work included data from

Madison and the region, but were built using AVIRIS-Classic imagery. We re-developed the models to AVIRIS-NG wavelengths and added three new traits (sugars, phenolics, chlorophyll) for which calibrations had been developed since Singh et al. (2015). Trait predictions from adjacent images were normalized to each other using regression on the overlap areas. Because we used models developed from other datasets (albeit with consistent processing methods) and not validated on our images, we converted these trait predictions to indices standardized by dividing by their standard deviation.

We extracted the trait values at every tree. To ensure that we did not include mixed pixels, we used the 2016 canopy height model derived from LiDAR to mask any pixels that had a mean height lower than 8 meters. This removed some of the smaller trees from our dataset, but was important because the relatively large spatial resolution of the AVIRIS-NG imagery that made distinguishing crown boundaries on small trees difficult.

**Other covariates**

Topographic variables were derived from the 2009 Dane county digital elevation model (DEM). Topographic position index, aspect, and slope were all calculated using the `terrain` function in the R package `raster` (Hijmans, 2016). The DEM was originally at approximately 1.5 m (5 ft) scale. We calculated topographic covariates at this scale and also at the large aggregated scale of 61 m (200 ft). We transformed aspect using sin(angle + 45) + 1 so that trees in the cool wet northeast aspect had a value of 2 and trees in the warm dry southwest aspect had a value of 0.

Using a 1 m land cover map for the city of Madison (Erker et al., 2019), we calculated the percent impervious cover within 20 m and within 100 m of each tree.

# Height bias correction and estimation of height growth rates

### Corrections for maximum height and estimating tree growth

The estimated maximum height of trees derived from LiDAR is always lower than the true maximum height, that is, it is biased downward Roussel et al. (2017). The magnitude of this bias is a function of the interaction between LiDAR characteristics (e.g. pulse density, footprint size, scan angle) and the tree architecture (e.g. branch leaf and gap distribution). Greater density of LiDAR pulses will have less bias since the probability of hitting a branch near the top of the tree increases. Trees with less conical and flatter tops (i.e. those with weak apical dominance) will have less bias because there are more branches close to the highest branch of the tree (Roussel et al., 2017). Branch and twig size and distribution may also play a role Romanczyk et al. (2012). Generally, taxa with thinner twigs have denser

branching. A single twig may not reflect enough energy from a LiDAR pulse to trigger a return, but there may be many more twigs close together leading to a greater return density if the footprint size is large enough. Taxa with thicker twigs will have stronger returns, but since thicker twigs tend to be less dense, the probability of hitting a thick twig is lower. Exactly how these negatively correlated traits (twig thickness and density) interact to influence the bias in maximum height estimates is mediated by the algorithms used to convert full waveform LiDAR into point clouds. Thus, in our attempt to correct for the bias in maximum height estimation and - by extension across multiple years - tree height growth, we used a bootstrap resampling technique to estimate bias at different pulse densities for each genera in our dataset. Other characteristics of the LiDAR, such as footprint size are important in correcting bias, but we did not have this information for all our datasets and could not correct for it (Andersen et al., 2006).

Our goal in the bias correction is to obtain an improved estimate of tree growth from multiple years of data, but tree growth and the size of the bias are confounded (Figure 4.3). In 2005, average pulse density was very low and so bias was large. By 2017, average pulse density had increased and so bias decreased. The challenge therefore is to identify how much of the observed maximum height difference is due to growth over those 12 years and how much is due to a decrease in bias.
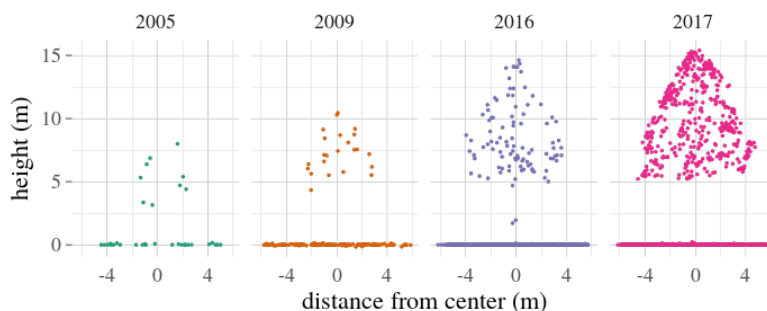


Figure 4.3: Example Tilia tree illustrating the confounding interaction of both considerable tree growth and increased pulse density through time.

To do this, we estimated the bias for trees that were no longer growing (e.g. Figure 4.4) and then applied the bias correction to all other trees. We selected the tallest trees of each genus that had essentially reached their maximum height and stopped growing (differences in observed maximum height between 2009, 2016, and 2017 were all less than 1 meter). We then combined all returns across years for each tree, assuming that other than pulse density all else was equal across LiDAR acquisitions. We then sampled 1000 times with replacement from each tree's point cloud samples of size 1 to the original size. For each
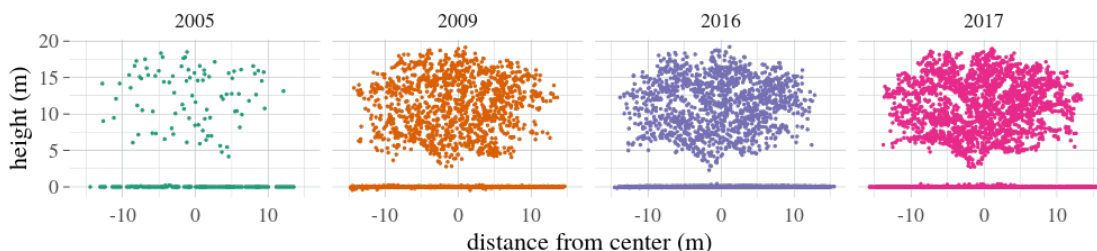
Figure 4.4: Illustration of increasing pulse density through time on a very large Quercus tree with little or no height growth. We assume that any difference in height between years is due to measurement error primarily driven by pulse density.

of the 1000 samples at each sample size, we calculated the maximum height. Averaging the maximum heights across the 1000 samples for each sample size we estimated how bias changes with sample size / pulse density (Figure 4.5).

We then averaged the bias curves for each genus (Figure 4.6) and applied this mean bias correction to each tree by genus and number of pulses. We also averaged the standard deviation of the bias estimates and assigned them to each tree to provide information on the amount of uncertainty in each correction. Bias corrections for each genus at each pulse density are available in supplementary materials.

This method assumes that the relationship between pulse density and bias is the same for large trees as it is for small trees of the same genus. This assumption may not be true, but it is difficult to test with the existing data. We also tested estimating the bias correction for each tree individually, so that the bias by sample size curve was specific to that tree. This may have minimized the issue with the assumption that bias is not a function of tree height, but bias and growth were confounded. Nevertheless, results from both corrections were similar, suggesting that our findings are robust to the method of correction. Recognizing that there is a bias in the observed maximum height and that the uncertainty in the bias is a function of sample size is what appears to be crucial to estimation of height change through time. The final product of the bootstrap analysis was an estimation of bias corrected height per year and its uncertainty.

**Weighted regression for height growth rates**

To predict annual growth rate, fit a weighted linear regression for each tree with height as the response and year as the predictor. Weights were inversely proportional to the variance of each bias-corrected height. The result was an estimate of annual growth rate for each

tree (Figure 4.7). The advantage of the weighted regression is that we were able to include data points in the regression even if they were highly uncertain rather than removing them completely. LiDAR from 2005 generally is very sparse in density, but there were some trees for which the sample size was sufficiently large to provide some information on growth.

Due to the nature of the measurement error and correcting for the mean bias, at times the height of a tree may have been over- or under-corrected, especially in 2005. Over-correction may explain some of the slightly negative growth rates, while under-correction likely explains some of the high growth rates. On average we assume these errors cancel out.

## Modeling growth rates

Considering our objectives above, we sought to test for relationships between growth rates and our covariates. We spatially subset our data so that all trees of the same genus were at least 200 m apart to reduce spatial dependence. This approach drastically simplified modeling and likely reduced bias in coefficient estimates. We used multiple linear regression with growth rates as a response and all covariates as predictors. We included and excluded groups of covariates in several model fits to test their relative contributions. Since growth rate is known to vary nonlinearly with height we added polynomial terms of height to account for this. We expected that growth rates would differ between street trees and neighborhood trees, potentially due to greater disturbance, exposure to salt and herbicides, pruning and soil compaction for street trees, and the more open grown environment and fertilizer for neighborhood or yard trees. We also interacted tree type (neighborhood or street with or without overhead utility lines) with height since the relationship between height and growth rate by vary depending on the trees context (for example trees with overhead utilities might suddenly stop growing upwards because of repeated pruning). We tested for interactions between the two scales of percent impervious cover, hypothesizing that as long as trees had low impervious cover locally (within 20 m), they might not be negatively impacted (or possibly even benefited, Pretzsch et al. 2017) by impervious cover more broadly (within 100 m). Our goal was a relatively parsimonious model and so we did not test for interactions between trait variables, land cover variables, and topographic variables. We did fit models with interactions by genus, since the relationships between growth and these covariates likely has genetic control.

## 4.4 Results

### Tree Height Bias Correction and Growth Rate Estimation

Height bias increases in magnitude as pulse density decreases (Figure 4.5). Bias curves were created for 17 genera with sufficient sample size in our data set. All genera showed similar trends, but there was significant variability in the mean bias curves across genera (Figure 4.6). Estimated bias for every genus at every pulse density is available in supplementary materials.
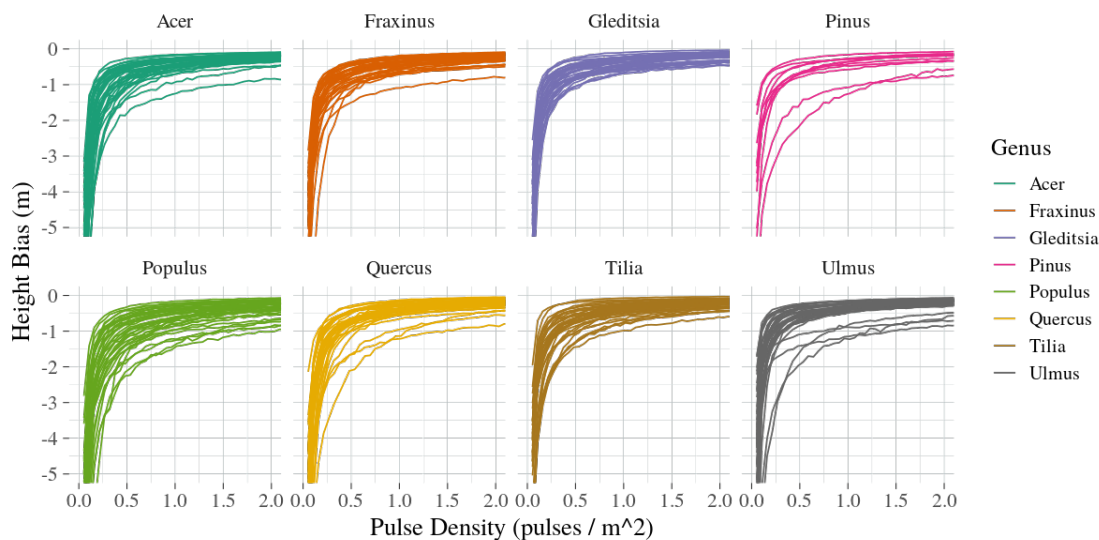


Figure 4.5: Empirical height bias by pulse density curves for individual trees across 1000 bootstrapped samples of eight example genera.

Bias correction and growth rate estimation was applied on a tree-by-tree basis (see Figure 4.7 for results from example trees illustrating the consequences of bias correction on growth estimation). The underestimation of height in 2005 due to low pulse density is evident in most trees by the large drop in height compared to the trend from the other three years ("ST89566" is a particularly stark example). The red bias corrected lines appear to be more realistic growth rates than the gray uncorrected lines. However, over-correction of bias is evident (see "ST03542" and "ST20636" in Figure 4.7), which can result in estimates of negative growth rates ("ST03542" in Figure 4.7). Weighting years in the regression by their bias correction uncertainty diminished the over-correction issues, but some years were over-corrected (likely "ST05216") and some were be under-corrected). See supplementary materials for a similar plot of a random sample of 80 trees.
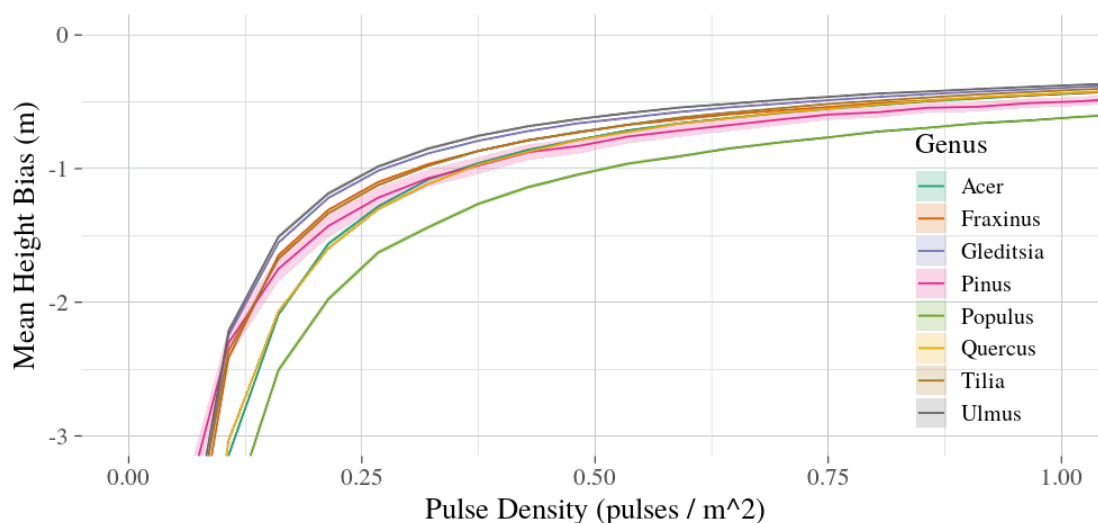
Figure 4.6: Mean height bias by pulse density curves for individual trees of eight example genera. Colored regions are +/- 1 standard error for the mean bias curve. Pinus has the largest standard error because of the smaller sample size.
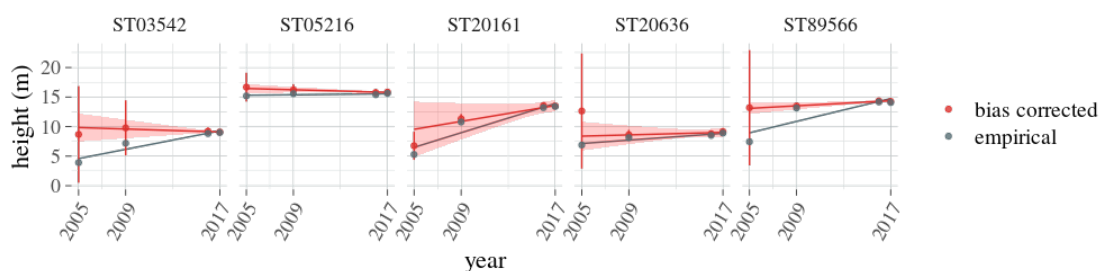


Figure 4.7: Heights of 5 trees in 2005, 2009, 2016, and 2017. Grey points are observed height from LiDAR; grey line is unweighted linear regression for the observed heights. Red points are bias-corrected heights; red line is weighted linear regression trend line for the corrected heights. Tree "ST03542" and "ST20161" are Gleditsia, "ST20636" and "ST89566" are Acer, and "ST05216" is Fraxinus.

## Growth Rates

The mean height growth rate of the 7,124 trees in our sample was 12.8 cm yr$^{-1}$ with a median of 10.1 cm yr$^{-1}$. Performing an unweighted regression for each tree with no bias correction, the growth rate was 22.8 cm yr$^{-1}$. Without the weighted regression but with the bias correction the mean growth rate was 8.7 cm yr$^{-1}$. We only analyzed in depth the bias corrected weighted regression growth rate estimates, but the direction and significance of most model coefficient estimates were the same regardless of which estimates of growth rates were used (bias-corrected results below, results for unweighted and non-bias correct not shown).

Figure 4.8 shows the distribution of growth rates. The large variability and biologically unlikely estimates (e.g. -10 cm yr$^{-1}$) point to: 1) potential LiDAR measurement error influencing projected growth rate; 2) overcorrection of the point density based bias adjustment, or 3) true declining heights, e.g. due to pruning or other management for which information was unavailable.
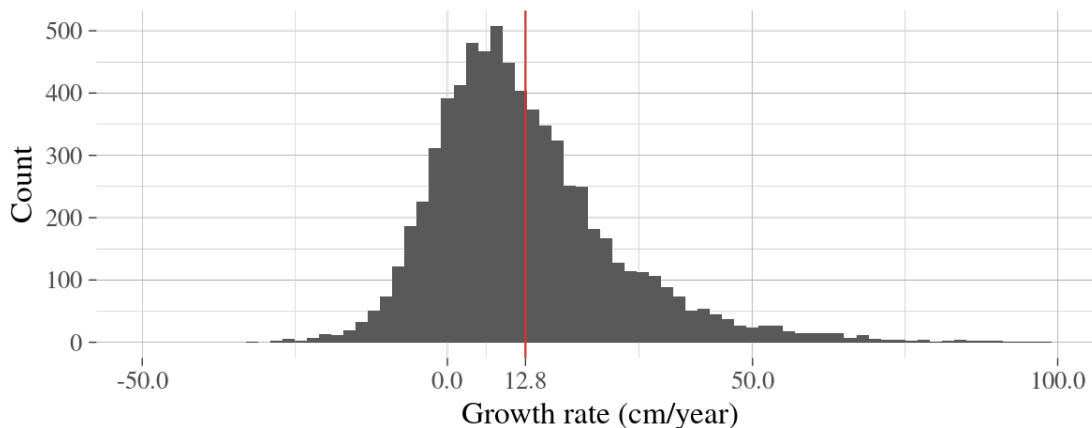


Figure 4.8: Histogram of estimated growth rates for over 7,124 urban trees. The sample mean growth rate is 12.8 cm yr$^{-1}$ with a median of 10.1 cm yr$^{-1}$.

## Multiple linear regression: trait and landscape drivers of growth

We tested multiple model formulations and considered several combinations of interacting variables before settling on two models to report. The first contains interactions between some covariates, but remains simple. The second model adds interactions between genus and many of the covariates to the first model. The first model contained a fourth order polynomial term for the 2005 height covariate, an interaction between 2005 height and the neighborhood/street/utility line indicator variable, and an interaction between the two

scales of percent impervious cover. It identified broad patterns between covariates and growth rates for all trees in our sample, independent of taxonomic identity (genus)

For the second model we interacted the genus covariate with the intercept and all the covariates except those derived from topography. Including genus addresses the likelihood that different taxa respond differently to environmental drivers, and that the biochemical/trait profiles important to growth also differ among species/genera. The second model that included genus had a much improved AIC (662 lower with 315 more parameters) and a higher adjusted $R^2$ (.569 compared to .506) (Table 4.2).

26 parameters were used in the first model (Table 4.3). In allowing the coefficients of non-topographic traits to vary by genus, the second model had 342 parameters (`full_model_summary.txt`). The importance of including genus in as an interaction term was apparent not just in the lower AIC and higher adjusted $R^2$, but also in revealing variability in the covariate coefficients by genus.

We likely could have found a model that had an even lower AIC by fitting more interaction terms and performing exhaustive model selection, but we aimed to keep the model within our existing hypotheses and easily explainable.

## Height in 2005 by street/neighborhood tree interaction

The strongest predictor of growth rate was the initial tree height, i.e. the bias corrected height of a tree in 2005 (Figure 4.9). Neighborhood trees grew significantly faster than street trees (about 3 - 8 cm more per year across the range of tree heights observed). Overhead utility lines did not have a significant effect on growth rates when averaging across all genera. At a height of 8m, neighborhood trees grew at an estimated 35 cm yr$^{-1}$ and street trees at an estimated 28 cm yr$^{-1}$. Depending on the type of tree, asymptotic heights are different. For street trees it occurred at heights around 25 m; for neighborhood trees around 27 m. Different genera also had different asymptotic heights, ranging from about 25 m for *Tilia* to over 30 m for Pinus (low sample size of tall trees makes estimates of asympotitic height uncertain).

## Impervious surfaces

There was a significant interaction between the percent of impervious cover within 20 m and within 100 m of a tree. Trees with little impervious cover at either scales had growth rates of around 13 cm / year. Trees with very high impervious cover at either scale had low growth rates, as low as 2.5 cm yr$^{-1}$. But trees with low impervious cover locally were able to maintain high growth rates despite having over 50% impervious cover within 100m.
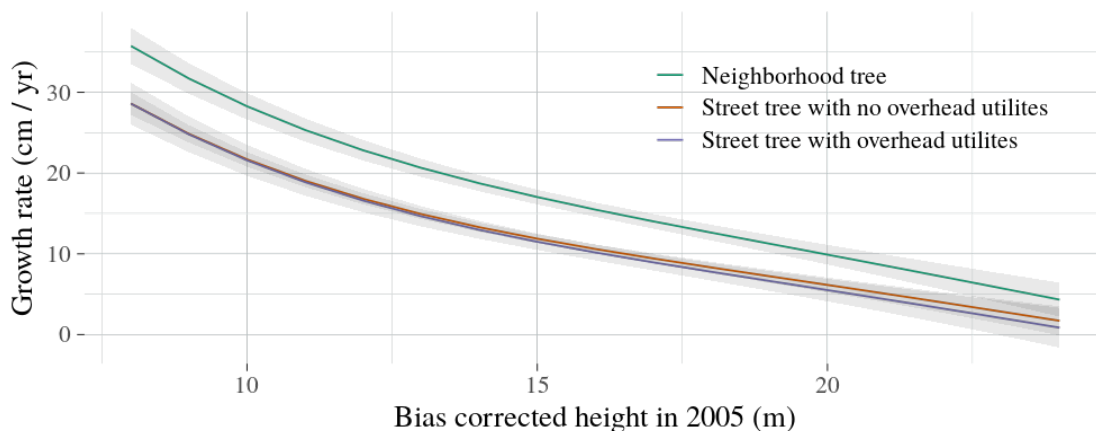
Figure 4.9: Estimated growth rate by 2005 bias corrected height for neighborhood trees and street trees with and without utility lines overhead. All other covariates are set at median values.

For example, this situation might occur for trees in small parks or large yards surrounded by built up surfaces. Growth rates of trees with little impervious cover within 100 m are similar regardless of the impervious cover within the nearest 20 m. But the growth rates of trees with much impervious cover within 100 m are very strongly influenced by the local impervious cover within 20 m.
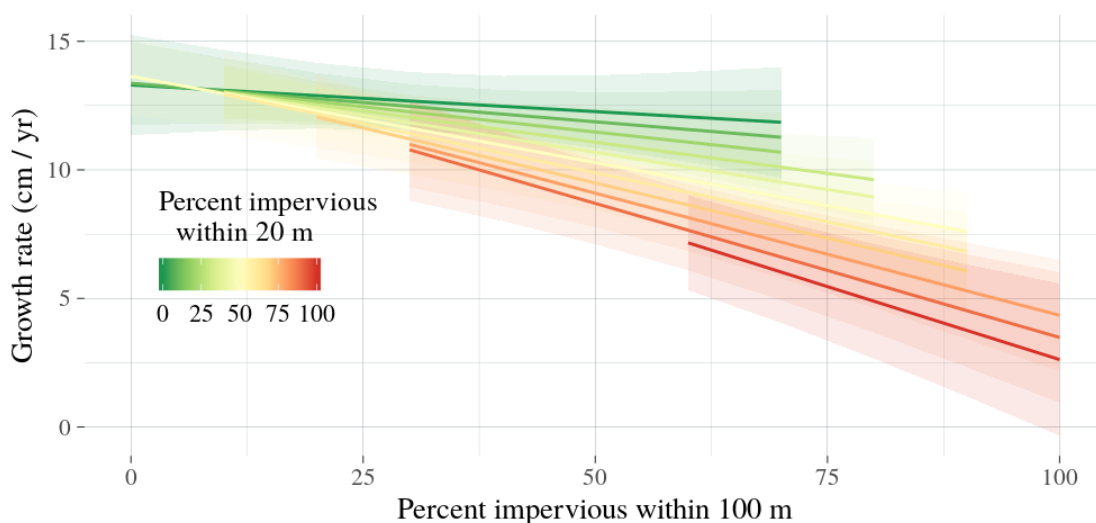


Figure 4.10: Estimated height growth rates for trees with varying percent impervious land cover within 20 m and within 100m. All other covariates are at their median values. Impervious cover is associated with decreased height growth rates with it is high at both scales, but trees with low impervious cover locally can maintain fast growth despite high impervious cover more broadly.

## Topography

Topographic variables had statistically clear, but small effects on tree height growth rates (Figure 4.11). Elevation in Madison ranges from 250 m to 350 m and had a positive association with growth rate. Our model estimated that trees growing in the highest parts of the city grew about 2.2 cm yr$^{-1}$ more than trees growing in the lowest parts of the city. While trees at higher elevations grew faster than trees at lower elevations, higher values of the topographic position index (a scale of local wetness or dryness, with higher values indicated higher relative topographic position) were associated with less growth. At the scale of 1.5 m, for every 1m that trees are higher than their surroundings they grew an estimated 2.5 cm less per year. Slope was not significant at the 61 m scale, but at the 1.5 m scale trees on steeper slopes grew more slowly than trees on flatter ground. Surprisingly, aspect had opposite effects depending on the scale: at the 1.5 m (local) scale trees in the cooler wetter northeast aspect grew faster than trees in the warmer drier southwest aspect by almost .75 cm yr$^{-1}$, while at the 61 m scale the effect was nearly opposite.
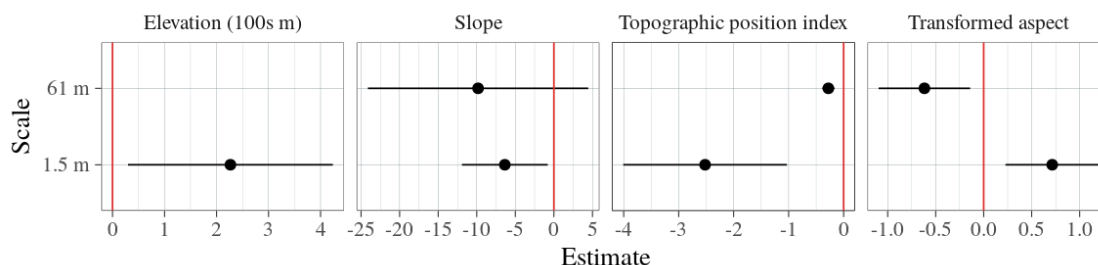


Figure 4.11: Coefficient estimates for topographic covariates at two scales (pixel sizes of 1.5 m and 61 m).

## Mean height within 20m

We had hypothesized that trees surrounded by tall trees or buildings would have greater growth rates due to competition for sunlight. This was substantiated by mean height within 20 m of a tree having a strong association with growth rates and confirms that trees that must compete for light allocate more resources to height growth. For every meter increase in mean height around a tree, the growth rate increased by .85 cm. For example, we estimated an open grown tree in a park would grow about 8 cm less per year than a tree grown in an area with a mean height of about 10 m (for example near buildings and other trees).

Too much competition for light would lead to a decrease in growth rates, but we did not see this in our data. We tested if the quadratic term for mean height within 20m was significant and it was not. This is likely because our sample did not include any trees that were suppressed or over-topped as they would not be visible to the imagery.

Figure 4.12 shows coefficient estimates for mean height within 20 m with 95% confidence intervals for the first model ("overall") and for each genus as included in the second model. There is substantial variability, but no clear difference in the effect of the mean height within 20 m by genus.
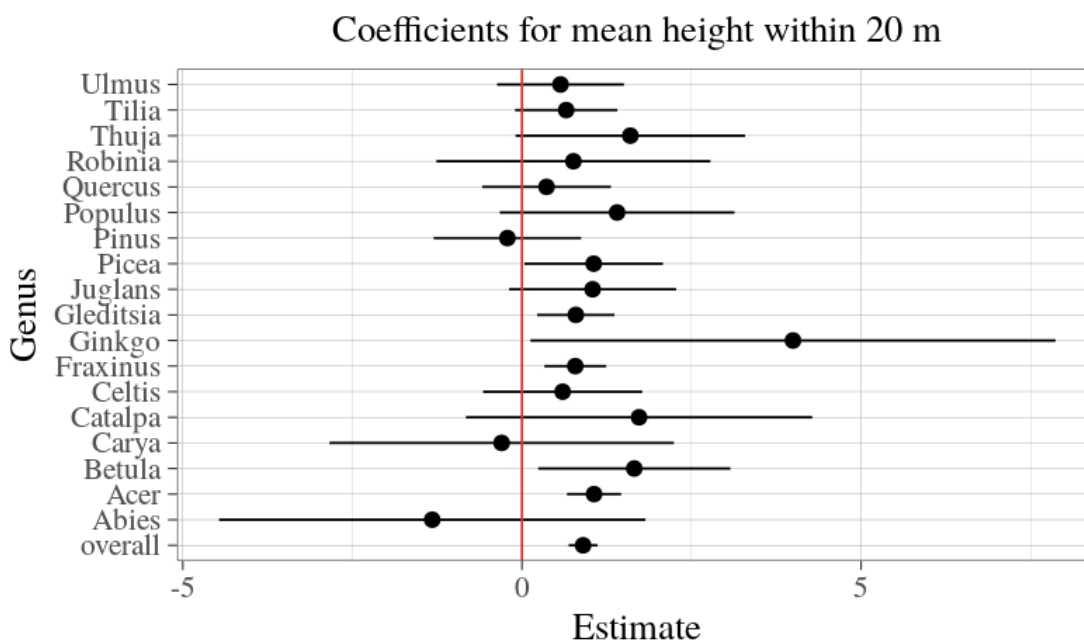


Figure 4.12: Coefficients for mean height within 20 m of a tree by genus and overall.

## Foliar canopy traits

Four of the six foliar canopy traits were significantly related to tree height growth. Total phenolics, lignin and nitrogen had a negative association with growth; chlorophyll had a positive association, sugar and leaf mass per area (LMA) had no association. There is considerable variability by genus in the trait coefficients (Figure 4.13). Applying Tukey's correction for multiple comparisons, most of the pairwise differences are not statistically clear, but that there exists variability in trait coefficients by genus is apparent. Since we scaled the trait values, we are not able to interpret the coefficients in absolute units of the variable. Estimates correspond to growth rate change with one standard deviation change in the trait index.

Growth rates are significantly related to some of the traits, but they have modest predictive power in our model when genus is known. Importantly, the contribution of traits to the model greatly depends on whether or not genus is included. Including traits slightly increases the adjusted $R^2$ from 0.54 to 0.56 for the model with genus, but they increase the adjusted $R^2$ from 0.12 to 0.50 for a model without genus (but with other covariates). If traits are the only covariates the adjusted $R^2$ is just 0.04. Therefore traits alone cannot explain height growth, but they can explain much of the variability explained by genus. This tells us that when genus is known, it can be generally sufficient to predict growth along with landscape predictors. However, in most settings, the taxonomy of trees will not be known or mapped, meaning that traits are an effective surrogate for taxonomic classification in order to predict growth rates.
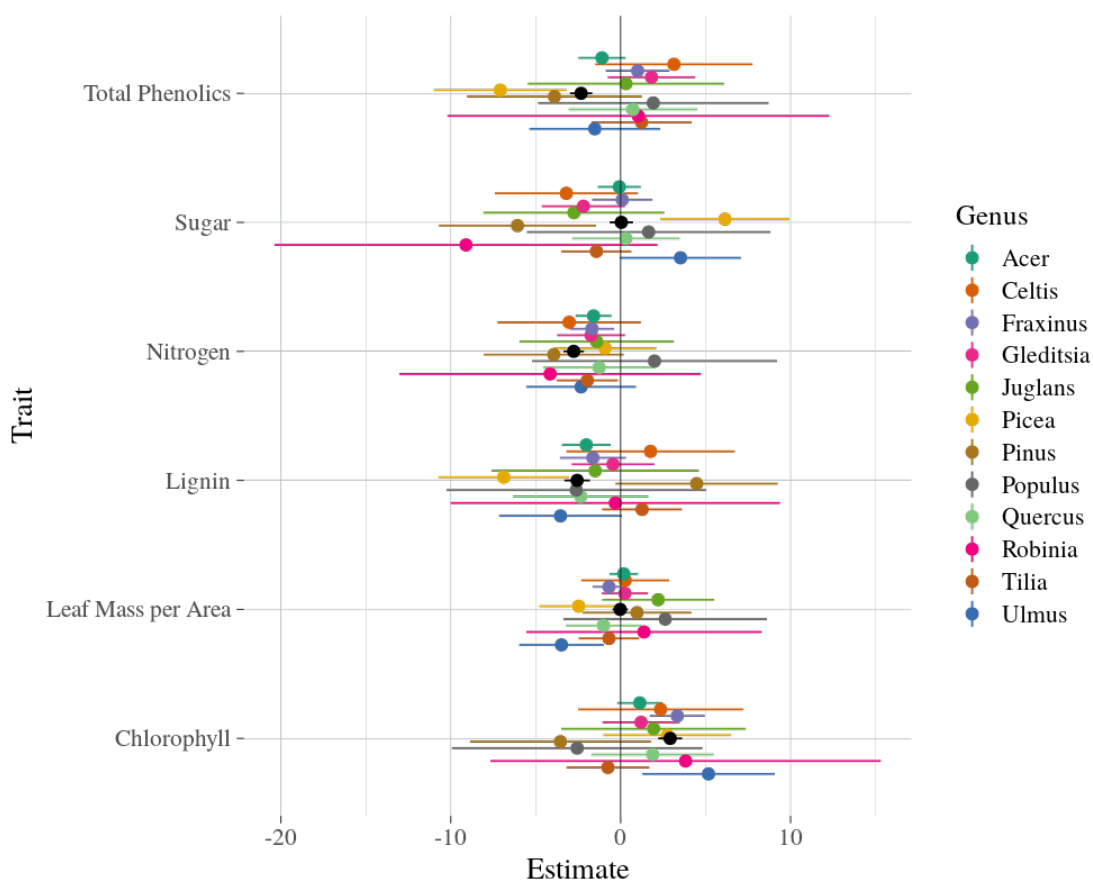


Figure 4.13: Coefficients of imaging spectroscopy derived foliar traits as predictors of height growth. Estimates from the model without genus are shown in black. Estimates by genus are colored.

## Marginal Means by Genus

Much of variation in height growth rates can be explained by the genus. Marginal mean growth rates by genus illustrate the range of variation by genus (Figure 4.14). The three gymnosperms in the dataset, *Pinus*, *Picea* and *Ginkgo*, have some of the highest estimated growth rates (all over 20 cm yr$^{-1}$, although *Ginkgo* has high uncertainty). Other fast growing genera are *Ulmus*, *Tilia*, *Populus*, *Catalpa* and *Carya* (estimated marginal growth rates over 17.5 cm yr$^{-1}$). *Quercus*, *Juglans*, *Celtis* and *Acer* had slower growth (estimated marginal growth rates less than 12 cm yr$^{-1}$.
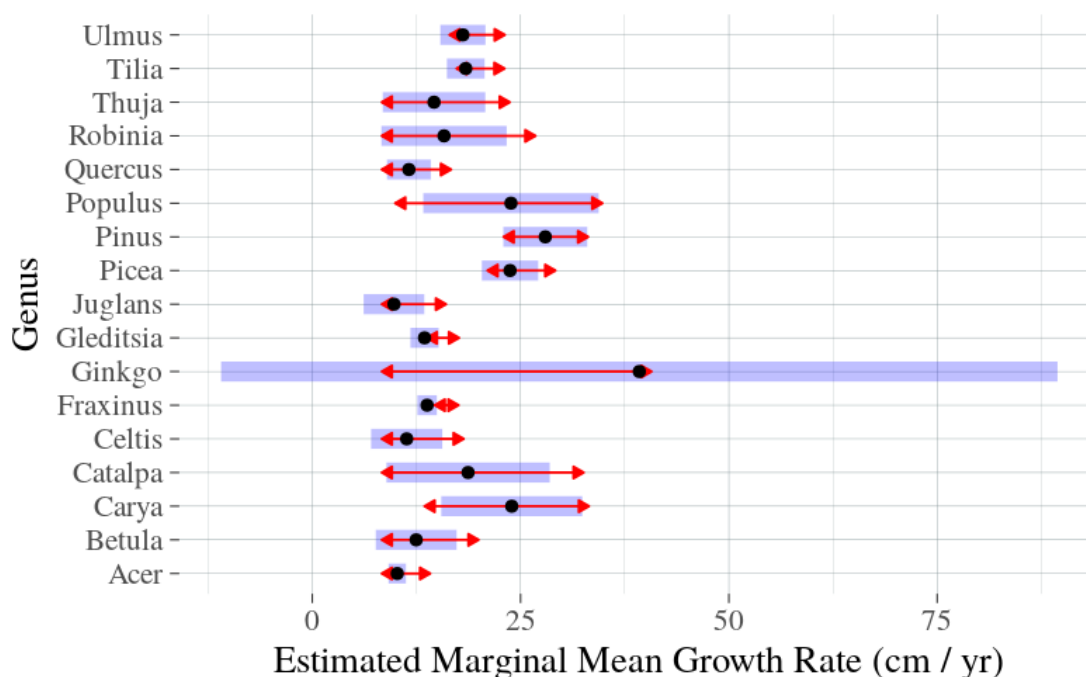


Figure 4.14: Estimated marginal mean growth rates by genus. Shaded bars are 95% confidence intervals and red arrows control for multiple comparisons should be used for pairwise comparison.

## Genus by Height predicted growth rates

Marginal mean growth rates by genus illustrate overall differences, but growth rates also varied with initial height (bias corrected 2005 height) and tree type (neighborhood vs street tree) (Figures 4.15 and 4.16).

Growth rate decreases with increasing height but the nature of the decline varies by genus (Figure 4.15). *Populus* has the fastest estimated growth at 8 m heights, while *Pinus* – the taxon in our data with the tallest potential height – has the fastest growth at 20 m

heights. *Ulmus* and *Quercus* are fast growing when trees are small, but rapidly decline in growth rates as height increases.

There is a three way interaction between genus, height, and type of tree (neighborhood, street with utility line, or street without utility line) (Figure 4.16)). For example, while the relationship between growth rate and height is very similar for *Acer*, *Fraxinus*, and *Gleditisia* if they are neighborhood trees, if the trees are planted on streets *Acer* differs considerably from *Fraxinus* and *Gleditsia*. When a tree is planted on a street growth rates are lower than for neighborhood trees, but the difference is greatest for *Acer* followed by *Fraxinus* and then *Gleditsia*. Overhead utility lines had little association with decreased height growth (except perhaps for *Pinus*, data not shown).
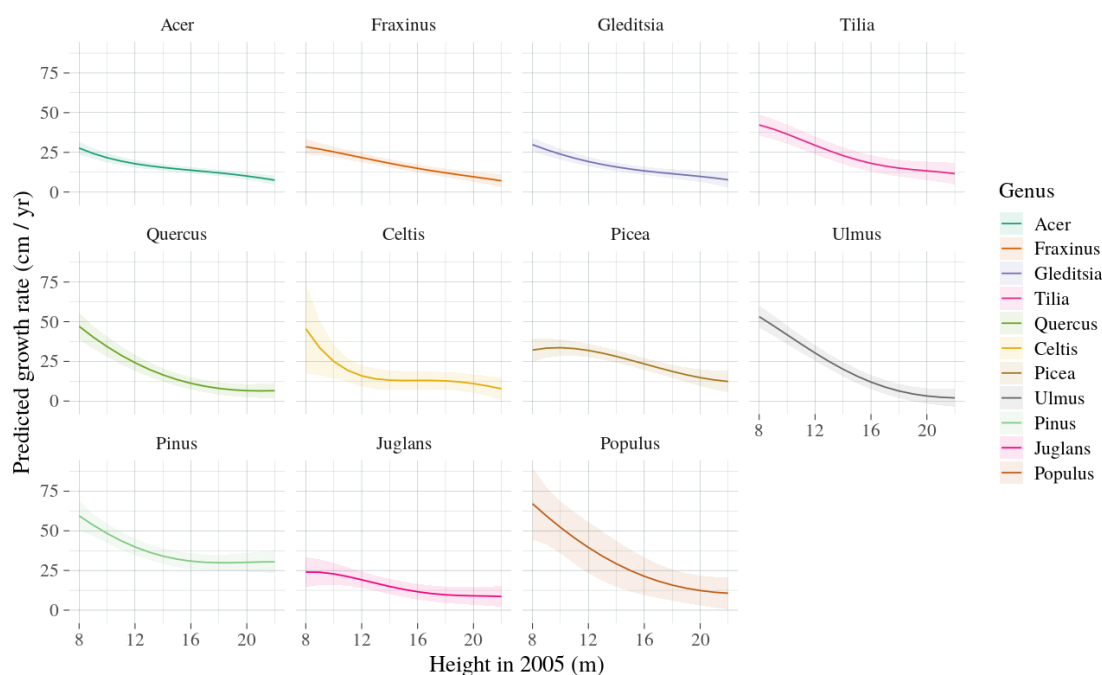


Figure 4.15:  Growth rate by bias corrected height in 2005 for 12 Genera.

## 4.5   Discussion

### Bias correction and growth rate estimates

There is considerable interest in the use of LiDAR data to characterize aboveground biomass in forests, as well as biomass growth, and the primary data sets available at present for such work are the extensive leaf-off LiDAR collections originally developed for topographic mapping and floodplain delineation.  Time series of LiDAR provide an opportunity to
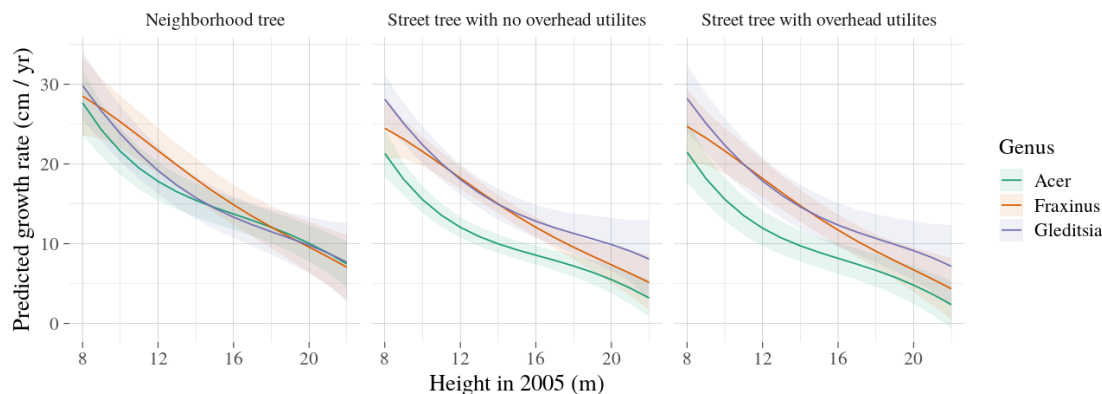
Figure 4.16: Growth rates are associated with a three way interaction between initial height in 2005, genus, and type of tree.

characterize tree growth, but as LiDAR technologies progress and data collection becomes more dense, there will be a need to consider data collection characteristics when performing change detection. The negative bias in height estimates from LiDAR is well known and creates challenges in using multi-temporal LiDAR (Marinelli et al., 2019), especially for individual trees compared to larger forest stands (Paris and Bruzzone, 2015; Roussel et al., 2017). However, the bias is not always corrected.

Song et al. (2016) estimated canopy height growth of urban trees in Osaka, Japan using repeat LiDAR. Like our study their later collections had higher pulse densities (in their case, 52 pulses $m^{-2}$ versus 11 pulses $m^{-2}$). They found mean growth from 2008-2010 (when pulse density was 52 pulses $m^{-2}$) was $2 \pm 19$ cm $m^{-2}$ $yr^{-1}$, and from 2004-2008 (when pulse density increased from 11 to 52 pulses $m^{-2}$) mean growth was $37 \pm 14$ m $m^{-2}$ $yr^{-1}$. So when pulse density was constant they found almost no growth, but when pulse density increased growth was over a third of a meter per year. Unfortunately the authors did not investigate the potential effect of pulse density change on growth rate and instead explained the pattern by other means.

Our method for maximum height bias correction is similar to one described by Roussel et al. (2017). They proposed using a high resolution point cloud to help correct a low resolution point cloud. But a high resolution point cloud is usually not available. They proposed using an area of high pulse density as a reference and then applying the bias correction relationship to areas of low pulse density. They pointed out that not only is there bias in height for multi-temporal LiDAR, but also within single date LiDAR because of the variation in pulse density across space due to variable overlap between flight lines. They mostly described the nature of the bias, but leave application of correction to others.

Our method assumes that point clouds from multiple years for trees that are likely not

growing can be combined into one higher resolution point cloud and then resampled to estimate what the bias might be. We then applied this genus specific bias curve to all trees, assuming that the relationship held for smaller trees that were still growing.

Although we did not have validation data in the form of independently measured heights for trees from 2005 to 2017, from first principles our method appeared to be an improvement over doing nothing. There is a clear negative bias in the maximum height when pulse density is low, especially in 2005. Future work should use historical field data if it is available to validate this method, but it is worth noting that in application, height data will rarely be available for most landscape and larger scale applications of LiDAR data.

Our height bias by pulse density curves showed differences across genera. As expected, trees with stronger apical dominance such as gymnosperms, had greater bias (Roussel et al., 2017). It also appeared that twig size may be related to the amount of bias. Gleditsia and Ulmus have generally thinner twigs and had smaller bias than most other genera. Populus and Quercus have generally thicker twigs and had greater bias. This relationship warrants more rigorous assessment.

While pulse density is a key factor in height bias, there are other important sources of bias that were not accounted for in our method, namely LiDAR pulse footprint size. We did not have footprint size information for the 2005 LiDAR and future work should include it in bias corrections. Some of the residual spatial structure in the data could be explained by these differences.

## Traits

Foliar canopy traits predicted from imaging spectroscopy were significantly related to tree height growth, and they appeared to encode much of the information included in a tree's genus. This is similar to results of McNeil et al. (2008) who found species functional traits explained much of the variation in forest function (N cycling). Models that contained genus as a term had the greatest explanatory power, however taxonomic information is often not available when assessing tree growth in urban areas, especially for trees on private property, and is almost never available if a method such as this were applied to forests in a natural environment. The foliar canopy traits show promise in improving canopy height growth predictions when genus is not known.

Most of the coefficients of foliar canopy traits were in expected directions. Chlorophyll, the key light harvesting molecule for photosynthesis, was positively associated with growth, which is consistent the reduction in chlorophyll concentrations that occurs when plants are stressed (Carter and Knapp, 2001).

Lignin and total phenolics, compounds generally associated with plant investment in leaf construction and defense, were negatively associated with growth. This is expected since allocation of resources to leaf structure and defense implies less allocation to growth (Stamp, 2003; Amthor, 2003). The urban environment contains numerous stressors that might increase phenolic compound production, making these compounds indicative of stressed trees (Mellway et al., 2009).

The coefficient for nitrogen was negative, which was counter to our expectations. First, about 20% - 30% of foliar nitrogen is in Rubisco, the enzyme responsible for carbon fixation (Feller et al., 2007). Plants with higher nitrogen generally grow faster (up to a point). Second, nitrogen had a strong positive correlation to chlorophyll, which had a positive coefficient. But dropping chlorophyll or other traits from the model did not affect the directionsign of the nitrogen coefficient, suggesting that multicollinearity was not the reason for the negative relationship between nitrogen and height growth.

Although it is possible that the predictive models from imaging spectroscopy are faulty, a biological explanation could be that nitrogen availability is very high in an urban setting due to nitrogen deposition (e.g. nitrogen saturation, (Aber et al., 1995) and/or excess fertilizer application (Law et al., 2004)). Numerous urban forest fertilization studies have shown no or very little increased growth in response to increased soil nitrogen (Shoup et al., 1981; Neely, 1980; Harris et al., 2008). In these cases, nitrogen may not be limiting growth and foliar nitrogen thus may be indicative of other processes affecting growth. For example, the deposition of nitrogen could be accompanied by other pollutants that negatively impact growth. The negative association of nitrogen with growth does not appear to be a statistical anomaly, but the driver behind the relationship is not clear and should be further investigated.

## Environmental effects on tree height growth.

We tested the relationship between three groups of variables on tree height growth: mean height of a tree's surroundings (including trees and buildings), nearby impervious land cover proportion, and topography. All three had statistically significant effects, though the effect of topography was relatively small.

We found that the average height of the objects in the surrounding 20 meters (mostly buildings and other trees) had a strong positive association with growth rates. Over-topped and suppressed trees were not in our sample and so we did not find that being surrounded by too many tall objects reduced growth rates. This is the expected response to trees in competition for light (King, 1990). Indeed, across the city of Madison, the tallest trees are

found in dense forest patches where they are competing for light, but also where there is less human interaction. Most trees in yards and along streets are more open grown and are shorter. Future work should separate out buildings from trees in the surroundings of a tree and test whether the faster height growth is in response to nearby buildings as well as trees, i.e. testing competitive interactions.

The association between impervious surface cover and growth rates shows the complex relationship between the built environment and tree growth. Broadly impervious cover decreased height growth, probably because it is associated with a number of stressors like poor, compacted or insufficient soil (Day et al., 2010). However, we found that trees that had little impervious cover within 20 m and much impervious cover within 100 m could maintain relatively fast growth. This could possibly be because trees had sufficient soil locally and may have been receiving increased water from runoff or were responding positively to the elevated temperatures in the broader surroundings (Pretzsch et al., 2017; Searle et al., 2012).

Topographic relationships with growth rate seem to be due to water: trees on less steep slopes, and lower elevation relative to their immediate surroundings all exhibited greater height growth. Why trees at higher elevations grew more than trees at lower elevations is not clear, but in this particular case the response may be due to a correlated geographic factor. This may be a surrogate for the variation from the relatively lower eastern half of the city to the relatively higher and hillier western half of the city. This variation is likely expressed in differences in soil properties, such as texture and depth.

Aspect had opposite effects depending on the scale. Trees in general tend to grow better in the cooler and wetter northeastern aspects (Stoeckeler et al., 1960). However we did not find this was the case at the coarser scale. It could be that the expected aspect-growth relationship is disrupted in the urban environment of a city without very large variation in topography.

## Future work

Our work has shown that urban tree height growth rates can be explained relatively well by variables derived from remote sensing, and the results provide the foundation for additional studies to provide new understanding or improve the analyses presented here. First, our height bias correction method is an improvement over no correction, but could be improved by considering more characteristics of the LiDAR that lead to bias. Second, we only consider tree height growth, rather than other ecologically relevant characteristics such as tree diameter incremental growth or total biomass growth. Height growth is much

easier to estimate from LiDAR, but provides an incomplete picture, especially for taller trees or more open grown, which may still be growing but not allocating resources to height. Nevertheless, height and biomass growth are generally correlated until the asymptotic height maximum is achieved.

Third, our subsampling of the data to remove trees of the same genus that were closer than 200 m to each was used to reduce spatial dependence in our data. Modeling the spatial covariance structure of our observations could better control for this dependence. When we fit the model with all 21,247 available observations, we found residuals of the model had strong spatial structure, suggesting there remain important factors in the urban environment that we are missing in our model (e.g. soils).

## 4.6   Conclusion

There are three major contributions of our work. First, we demonstrated a method to correct for maximum height bias that results from low LiDAR pulse density and more accurately estimate tree relative height growth with multiple years of LiDAR. Second, we show that for urban trees, as for all trees, height growth is significantly related to both initial height and genus. Important for broader applications, we show that if genus information is not available, foliar canopy traits derived from imaging spectroscopy can explain much of the variation in height growth rates that would otherwise be explained by genus. Third, we show that the urban environment, namely the height of a tree's surroundings, the percent impervious, and topography all are associated with changes in tree height growth rates.

Urban trees alter the urban environment, potentially providing city dwellers with ecosystem services. Our work has shown that the growth of trees - and the growth related services - may in turn be affected by the urban environment designed by humans, particularly impervious cover. Trees are dynamic parts of the urban ecosystem and their function can vary considerably, meaning managers cannot simply plant a tree and expect it to provide a certain benefit without considering the tree's context.

## 4.7   Acknowledgements

## 4.8   Supplementary materials

### Bias correction

Figure 4.6 shows the mean maximum height bias by pulse density curves by genera for an example 8 genera. Table 4.4 provides bias by pulse density values for all genera at 4 pulse density levels.

All the bias correction values for every genera used to adjust heights based on pulse density are available in the R binary file: `no_growth_bias.rds` in the paper's github repository, `https://github.com/TedwardErker/hgt`.

### Full model

The full summary of the model with genus included can be found in `full_model_summary.txt`

### Figures
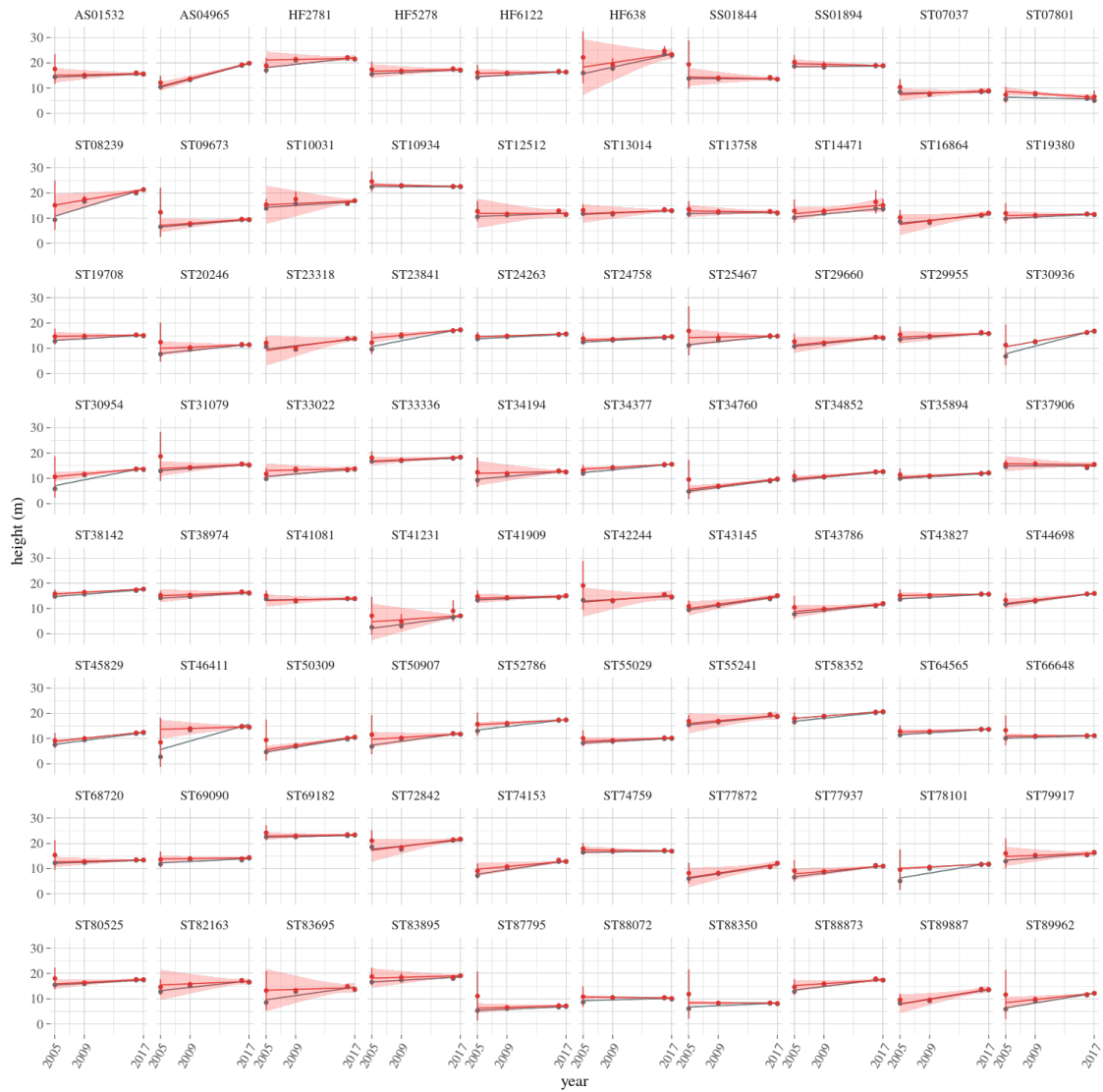
Figure 4.17: As in figure 4.7 but with a random sample of 80 trees.

Table 4.1: Covariates used in analysis

| Covariate | pixel size (m) | Source | method |
| --- | --- | --- | --- |
| Bias corrected height in 2005 (m) | - | LiDAR | this paper |
| Mean of height within 20 m (m) | - | 2016 LiDAR | this paper |
| Genus | - | tree inventories | |
| neighborhood or street tree w/ or w/o overhead utilities | - | tree inventories | |
| elevation (hundreds of meters) | 1.5 | Digital Elev. Model (DEM) | (Hijmans, 2016) |
| slope at 1.5 m (5 ft) scale | 1.5 | DEM | (Beers et al., 1966) |
| transformed aspect at 1.5 m (5 ft) scale | 1.5 | DEM | (Hijmans, 2016) |
| topographic position index, TPI at 1.5m (5 ft) scale (m) | 1.5 | DEM | (Hijmans, 2016) |
| slope at 61 m (200 ft) scale | 61 | DEM | (Beers et al., 1966) |
| transformed aspect at 61 m (200 ft) scale | 61 | DEM | (Hijmans, 2016) |
| topographic position index, TPI at 61 m (200 ft) scale (m) | 61 | DEM | (Hijmans, 2016) |
| Sugar (standardized index) | 4.6 | AVIRIS-NG | (Singh et al., 2015) |
| lignin (standardized index) | 4.6 | AVIRIS-NG | (Singh et al., 2015) |
| chlorophyll (standardized index) | 4.6 | AVIRIS-NG | (Singh et al., 2015) |
| leaf mass per area (standardized index) | 4.6 | AVIRIS-NG | (Singh et al., 2015) |
| total phenolics (standardized index) | 4.6 | AVIRIS-NG | (Singh et al., 2015) |
| nitrogen (standardized index) | 4.6 | AVIRIS-NG | (Singh et al., 2015) |
| percent impervious within 20 m | 1 | land cover map | (Erker et al., 2019) |
| percent impervious within 100 m | 1 | land cover map | (Erker et al., 2019) |

Table 4.2: Summary of models with and without genus

| model | parameters | AIC | adj. $R^2$ |
|---|---|---|---|
| no genus | 26 | 57978 | 0.506 |
| with genus | 341 | 57316 | 0.569 |

Table 4.3: Summary of first model coefficients excluding genera.

| term | estimate | std.error | statistic | p.value | p.value |
|---|---|---|---|---|---|
| neighborhood tree | 89.13 | 10.9 | 8.2 | <0.001 | <0.001 |
| street tree, no utilities overhead | 79.74 | 10.7 | 7.4 | <0.001 | <0.001 |
| street tree, with utilities overhead | 80.15 | 11 | 7.3 | <0.001 | <0.001 |
| height 2005 | -14.1 | 2.6 | -5.5 | <0.001 | <0.001 |
| height $2005^2$ | 0.91 | 0.2 | 3.9 | <0.001 | <0.001 |
| height $2005^3$ | -2.8 (-2) | 9.2 (-3) | -3.1 | <0.001 | 0.002 |
| height $2005^4$ | 3.3 (-9) | 1.3 (-4) | 2.6 | <0.001 | 0.011 |
| street tree, no utilities overhead:height 2005 | 0.28 | 0.1 | 2.4 | <0.001 | 0.018 |
| street tree, with utilities overhead:height 2005 | 0.23 | 0.2 | 1.4 | <0.001 | 0.16 |
| mean height within 20 m | 0.9 | 0.1 | 8.3 | <0.001 | <0.001 |
| percent impervious within 20 m | 0.68 | 2.4 | 0.3 | 0.31 | 0.78 |
| percent impervious within 100 m | -2.07 | 2.5 | -0.8 | 0.12 | 0.407 |
| % impervious 20m : % impervious 100m | -9.29 | 4.2 | -2.2 | <0.001 | 0.027 |
| total phenolics | -2.33 | 0.3 | -6.9 | <0.001 | <0.001 |
| nitrogen | -2.76 | 0.3 | -9 | <0.001 | <0.001 |
| sugar | 0.04 | 0.4 | 0.1 | 0.4 | 0.911 |
| leaf mass per area | -0.03 | 0.2 | -0.1 | 0.52 | 0.9 |
| lignin | -2.56 | 0.4 | -6.7 | <0.001 | <0.001 |
| chlorophyll | 2.92 | 0.4 | 8.1 | <0.001 | <0.001 |
| topographic position index (1.5 m) | -2.52 | 0.8 | -3.3 | <0.001 | 0.001 |
| transformed aspect (1.5 m) | 0.71 | 0.2 | 2.9 | <0.001 | 0.004 |
| slope (1.5 m) | -6.36 | 2.8 | -2.2 | 0.004 | 0.025 |
| topographic position index (61 m) | -0.28 | 0.1 | -4.9 | <0.001 | <0.001 |
| transformed aspect (61 m) | -0.62 | 0.2 | -2.5 | 0.38 | 0.011 |
| slope (61 m) | -9.83 | 7.3 | -1.3 | 0.14 | 0.177 |
| elev | 2.27 | 1 | 2.3 | 0.01 | 0.024 |

Table 4.4: Maximum tree height bias (bias) and mean bootstrap standard deviation (sd) for all genera at varying pulse densities (dens).

| Genus | dens ($m^{-2}$) | bias (m) | sd (m) | Genus | dens ($m^{-2}$) | bias (m) | sd (m) |
|---|---|---|---|---|---|---|---|
| Abies | 0.5 | -0.7 | 0.53 | Picea | 0.5 | -1.01 | 0.82 |
| Abies | 1 | -0.41 | 0.31 | Picea | 1 | -0.56 | 0.5 |
| Abies | 1.5 | -0.3 | 0.25 | Picea | 1.5 | -0.41 | 0.39 |
| Abies | 3 | -0.19 | 0.18 | Picea | 3 | -0.22 | 0.23 |
| Acer | 0.5 | -0.83 | 0.73 | Pinus | 0.5 | -0.91 | 0.68 |
| Acer | 1 | -0.44 | 0.39 | Pinus | 1 | -0.53 | 0.41 |
| Acer | 1.5 | -0.32 | 0.29 | Pinus | 1.5 | -0.4 | 0.34 |
| Acer | 3 | -0.16 | 0.18 | Pinus | 3 | -0.24 | 0.23 |
| Betula | 0.5 | -0.73 | 0.61 | Platanus | 0.5 | -1.18 | 0.91 |
| Betula | 1 | -0.4 | 0.35 | Platanus | 1 | -0.67 | 0.55 |
| Betula | 1.5 | -0.3 | 0.27 | Platanus | 1.5 | -0.49 | 0.43 |
| Betula | 3 | -0.16 | 0.18 | Platanus | 3 | -0.27 | 0.26 |
| Carya | 0.5 | -0.88 | 0.72 | Populus | 0.5 | -1.01 | 0.79 |
| Carya | 1 | -0.49 | 0.41 | Populus | 1 | -0.58 | 0.46 |
| Carya | 1.5 | -0.35 | 0.33 | Populus | 1.5 | -0.43 | 0.37 |
| Carya | 3 | -0.19 | 0.21 | Populus | 3 | -0.23 | 0.25 |
| Catalpa | 0.5 | -0.78 | 0.54 | Quercus | 0.5 | -0.79 | 0.69 |
| Catalpa | 1 | -0.47 | 0.37 | Quercus | 1 | -0.43 | 0.36 |
| Catalpa | 1.5 | -0.37 | 0.32 | Quercus | 1.5 | -0.31 | 0.28 |
| Catalpa | 3 | -0.19 | 0.2 | Quercus | 3 | -0.17 | 0.18 |
| Celtis | 0.5 | -0.74 | 0.58 | Robinia | 0.5 | -0.79 | 0.59 |
| Celtis | 1 | -0.44 | 0.34 | Robinia | 1 | -0.46 | 0.36 |
| Celtis | 1.5 | -0.33 | 0.28 | Robinia | 1.5 | -0.34 | 0.28 |
| Celtis | 3 | -0.19 | 0.19 | Robinia | 3 | -0.19 | 0.19 |
| Fraxinus | 0.5 | -0.79 | 0.61 | Salix | 0.5 | -0.75 | 0.56 |
| Fraxinus | 1 | -0.45 | 0.36 | Salix | 1 | -0.4 | 0.38 |
| Fraxinus | 1.5 | -0.34 | 0.29 | Salix | 1.5 | -0.29 | 0.29 |
| Fraxinus | 3 | -0.19 | 0.19 | Salix | 3 | -0.21 | 0.21 |
| Ginkgo | 0.5 | -1.12 | 0.85 | Thuja | 0.5 | -0.91 | 0.71 |
| Ginkgo | 1 | -0.63 | 0.56 | Thuja | 1 | -0.52 | 0.43 |
| Ginkgo | 1.5 | -0.45 | 0.43 | Thuja | 1.5 | -0.38 | 0.34 |
| Ginkgo | 3 | -0.22 | 0.26 | Thuja | 3 | -0.2 | 0.22 |
| Gleditsia | 0.5 | -0.81 | 0.6 | Tilia | 0.5 | -0.77 | 0.59 |
| Gleditsia | 1 | -0.46 | 0.38 | Tilia | 1 | -0.44 | 0.35 |
| Gleditsia | 1.5 | -0.35 | 0.3 | Tilia | 1.5 | -0.33 | 0.28 |
| Gleditsia | 3 | -0.19 | 0.2 | Tilia | 3 | -0.18 | 0.19 |
| Gymnocladus | 0.5 | -0.78 | 0.51 | Ulmus | 0.5 | -0.68 | 0.55 |
| Gymnocladus | 1 | -0.47 | 0.35 | Ulmus | 1 | -0.37 | 0.31 |
| Gymnocladus | 1.5 | -0.36 | 0.3 | Ulmus | 1.5 | -0.28 | 0.25 |
| Gymnocladus | 3 | -0.19 | 0.21 | Ulmus | 3 | -0.15 | 0.16 |
| Juglans | 0.5 | -1.14 | 0.93 | Juglans | 1.5 | -0.45 | 0.43 |
| Juglans | 1 | -0.63 | 0.54 | Juglans | 3 | -0.23 | 0.27 |

# 5  CONCLUSION

As more people live in cities, urban forests will continue to play an important role in human wellbeing. The challenge moving forward for the ecology of urban trees is a continued improvement in our understanding of the interactions between trees and people. We need to use accurate maps of urban trees to better quantify the magnitude and uncertainty of the services and disservices that trees provide, along with a deepening understanding of how trees respond physiologically to the urban environment. These two interrelated concepts – how trees affect us, and how we affect them – are critical to the future design and/or redevelopment of more livable cities.

Projecting the role of urban forests for cities in the future is inherently uncertain. Just 150 years ago, damage to street trees from horses was a major problem that is now non-existent. The future of transportation, housing, and work will alter where trees have space to grow, their potential for providing services and disservices, and the quality of the planting locations – in ways that are unknown. While we have known for decades about design principles to reduce building energy use and how to place trees for maximum benefit with regards to decreasing building energy use, the arrangement of trees around houses still appears to be driven primarily by aesthetic concerns. This may not matter as much in a cold and relatively cloudy city like Madison where better insulation is more important that designing houses for passive solar gain. However, it could be important for cities elsewhere. There is large climatic diversity across the globe and trees may be more suitable in some places than others, and as such, consideration of tree location may be particularly relevant depending on geography. Urban forestry needs to better study how to match species traits to the ecological function required by a city, even as they change in the future. For example, a city with scarce water resources, like Los Angeles, CA, will need trees that transpire less. A cold but sunny city, like Denver, CO, may require species with greater transmissivity in winter. Similarly, better understanding of tree functional response to urban gradients will enable better decision making for improving forest function and the provision of ecosystem services.

Our work has shown that rapidly developing remote sensing technology can be used to effectively monitor the urban forest by providing spatially explicit insight across urban areas that would otherwise be difficult to access because of the thousands of property owners. Many of our results would have been inconclusive without the large sample sizes afforded by remote sensing which allowed for the detection of small effects either of trees on humans or the urban environment on trees. With more and more satellites in orbit or soon to be in orbit providing much finer temporal, spatial, and spectral resolution,

there is great promise to continue improving the remote sensing of urban forests. City-wide individual tree species-specific maps are still very rare. By fusing datasets and taking advantage of spectral and phenological differences of species, these maps will be a promising future extension of the work of this dissertation. Species maps of individual trees can help cities better understand their risk of losing a large amount of tree cover to a species specific pest like we have seen with Dutch elm disease or the emerald ash borer. Species specific maps can also better help quantify ecosystem services and disservices and better identify appropriate planting locations according to species specific tolerances to the urban environment.

Concurrent with the satellite revolution is the rise of Deep Learning (DL) for image classification. DL is the current state of the art for image classification and can produce very high accuracies. Even without the new satellite imagery, DL would be suitable for creating land cover maps from existing NAIP imagery. In chapter 1, accurate prediction of land cover was the primary objective and so machine learning approaches that tend to be black boxes were appropriate. However, in chapters 2 and 3, our key objective was inference about very specific covariates and so the relatively simpler multiple linear regression was more appropriate. In this case, we did not try to fit the model that would have the highest predictive accuracy, but instead we fit models that could help to clearly understand the overall association between tree cover and carbon emissions or between the urban environment and tree height growth.

Key results from the above chapters are listed below:

1. NAIP imagery is a no cost data source capable of generating quality urban tree canopy maps at the state level.

2. Using actual heating and cooling energy use data from Madison combined with our tree canopy map, we showed that that contrary to the predictions of the most commonly used simulations, carbon emissions from residential building energy use were higher for buildings surrounded by trees compared to those with no or few trees nearby (this is likely to be the case in other cool climate cities as well).

3. Tree height growth rates derived from multiple years of bias-corrected LiDAR could largely be explained by initial tree height and genus, but foliar canopy traits derived from imaging spectroscopy could explain much of the same variability in growth if genus information was unavailable.

4. Urban tree height growth varied significantly with urban environmental variables such as topography and percent impervious cover.

## BIBLIOGRAPHY

Aber, J. D., Magill, A., Mcnulty, S. G., Boone, R. D., Nadelhoffer, K. J., Downs, M., and Hallett, R. (1995). Forest biogeochemistry and primary production altered by nitrogen saturation. *Water, Air, and Soil Pollution*, 85(3):1665–1670.

Achanta, R., Shaji, A., Smith, K., Lucchi, A., Fua, P., and Susstrunk, S. (2012). Slic superpixels compared to state-of-the-art superpixel methods. *IEEE Transactions on Pattern Analysis and Machine Intelligence*, 34(11):2274–2282.

Ahles, N., MacFaden, S., O'Neil-Dunne, J., Royar, A., and Engel, T. (2016). Geobia systems for massive data processing.

Akbari, H. (2002). Shade trees reduce building energy use and $CO_2$ emissions from power plants. *Environmental Pollution*, 116(nil):S119–S126.

Akbari, H. and Konopacki, S. (2005). Calculating energy-saving potentials of heat-island reduction strategies. *Energy Policy*, 33(6):721–756.

Akbari, H., Kurn, D. M., Bretz, S. E., and Hanford, J. W. (1997). Peak power and cooling energy savings of shade trees. *Energy and buildings*, 25(2):139–148.

Akbari, H. and Taha, H. (1992). The impact of trees and white surfaces on residential heating and cooling energy use in four canadian cities. *Energy*, 17(2):141 – 149.

Al-Kofahi, S., Steele, C., VanLeeuwen, D., and Hilaire, R. S. (2012a). Mapping land cover in urban residential landscapes using very high spatial resolution aerial photographs. *Urban Forestry & Urban Greening*, 11(3):291–301.

Al-Kofahi, S. D., VanLeeuwen, D. M., Samani, Z. A., and Hilaire, R. S. (2012b). Water budget calculator created for residential urban landscapes in albuquerque, new mexico. *Journal of Irrigation and Drainage Engineering*, 138(6):525–533.

Alonzo, M., McFadden, J. P., Nowak, D. J., and Roberts, D. A. (2016). Mapping urban forest structure and function using hyperspectral imagery and lidar data. *Urban Forestry & Urban Greening*, 17(nil):135–147.

Amthor, J. S. (2003). Efficiency of lignin biosynthesis: a quantitative analysis. *Annals of Botany*, 91(6):673–695.

Andersen, H.-E., Reutebuch, S. E., and McGaughey, R. J. (2006). A rigorous assessment of tree height measurements obtained using airborne lidar and conventional field methods. *Canadian Journal of Remote Sensing*, 32(5):355–366.

Arguez, A., Durre, I., Applequist, S., Vose, R. S., Squires, M. F., Yin, X., Heim, R. R., and Owen, T. W. (2012). Noaa's 1981-2010 u.s. climate normals: An overview. *Bulletin of the American Meteorological Society*, 93(11):1687–1697.

Asner, G. P. (1998). Biophysical and biochemical sources of variability in canopy reflectance. *Remote Sensing of Environment*, 64(3):234–253.

Barker, P. A. (1975). Ordinance control of street trees. *Journal of Arboriculture*.

Bates, D., Mächler, M., Bolker, B., and Walker, S. (2015). Fitting linear mixed-effects models using lme4. *Journal of Statistical Software*, 67(1):1–48.

Beers, T. W., Dress, P. E., and Wensel, L. C. (1966). Notes and observations: aspect transformation in site productivity research. *Journal of Forestry*, 64(10):691–692.

Boone, C. G., Cadenasso, M. L., Grove, J. M., Schwarz, K., and Buckley, G. L. (2009). Landscape, vegetation characteristics, and group identity in an urban and suburban watershed: Why the 60s matter. *Urban Ecosystems*, 13(3):255–271.

Boryan, C., Yang, Z., Mueller, R., and Craig, M. (2011). Monitoring us agriculture: the us department of agriculture, national agricultural statistics service, cropland data layer program. *Geocarto International*, 26(5):341–358.

Cabané, M., Pireaux, J.-C., Léger, E., Weber, E., Dizengremel, P., Pollet, B., and Lapierre, C. (2004). Condensed lignins are synthesized in poplar leaves exposed to ozone. *Plant Physiology*, 134(2):586–594.

Carter, G. A. and Knapp, A. K. (2001). Leaf optical properties in higher plants: linking spectral characteristics to stress and chlorophyll concentration. *American journal of botany*, 88(4):677–684.

Census Bureau, U. D. o. C. (2013). Urban areas tiger/line shapefiles 500k.

Census Bureau, U. D. o. C. (2017). Quickfacts.

Chapin III, F. S., Matson, P. A., and Vitousek, P. (2011). *Principles of terrestrial ecosystem ecology*. Springer Science & Business Media.

Cleve, C., Kelly, M., Kearns, F. R., and Moritz, M. (2008). Classification of the wildland-urban interface: A comparison of pixel- and object-based classifications using high-resolution aerial photography. *Computers, Environment and Urban Systems*, 32(4):317–326.

Cregg, B. M. and Dix, M. E. (2001). Tree moisture stress and insect damage in urban areas in relation to heat island effects. *Journal of Arboriculture*, 27(1):8–17.

Czerniawska-Kusza, I., Kusza, G., and Dużyński, M. (2004). Effect of deicing salts on urban soils and health status of roadside trees in the opole region. *Environmental Toxicology: An International Journal*, 19(4):296–301.

Day, S. D., Eric Wiseman, P., Dickinson, S. B., and Roger Harris, J. (2010). Tree root ecology in the urban environment and implications for a sustainable rhizosphere. *Journal of Arboriculture*, 36(5):193.

DeWalle, D. R., Heisler, G. M., and Jacobs, R. E. (1983). Forest home sites influence heating and cooling energy. *Journal of Forestry*, 81(2):84–88.

Dobbs, C., Kendal, D., and Nitschke, C. R. (2014). Multiple ecosystem services and dis-services of the urban forest establishing their connections with landscape structure and sociodemographics. *Ecological Indicators*, 43(nil):44–55.

Donovan, G. H. and Butry, D. T. (2009). The value of shade: Estimating the effect of urban trees on summertime electricity use. *Energy and Buildings*, 41(6):662–668.

Dubayah, R. O. and Drake, J. B. (2000). Lidar remote sensing for forestry. *Journal of Forestry*, 98(6):44–46.

Duncanson, L. and Dubayah, R. (2018). Monitoring individual tree-based change with airborne lidar. *Ecology and Evolution*, 8(10):5079–5089.

Emissions & Generation Resource Integrated Database (2016). Accessed Jul. 24, 2018.

Erker, T., Wang, L., Lorentz, L., Stoltman, A., and Townsend, P. A. (2019). A statewide urban tree canopy mapping method. *Remote Sensing of Environment*, 229(nil):148–158.

Feller, U., Anders, I., and Mae, T. (2007). Rubiscolytics: Fate of rubisco after its enzymatic function in a cell is terminated. *Journal of Experimental Botany*, 59(7):1615–1624.

Foody, G. M. (2008). Harshness in image classification accuracy assessment. *International Journal of Remote Sensing*, 29(11):3137–3158.

Galvin, M. F., Grove, J. M., and O'Neil-Dunne, J. P. M. (2006). A report on annapolis'present and potential urban tree canopy. Technical report, Maryland Forest Service, Annapolis, MD.

Gelman, A. and Hill, J. (2007). *Data Analysis Using Regression and Multilevel/Hierarchical Models*. Analytical Methods for Social Research. Cambridge University Press.

Grove, J. M., Locke, D. H., and O'Neil-Dunne, J. P. M. (2014). An ecology of prestige in new york city: Examining the relationships among population density, socio-economic status, group identity, and residential canopy cover. *Environmental Management*, 54(3):402–419.

Gu, H., Singh, A., and Townsend, P. A. (2015). Detection of gradients of forest composition in an urban area using imaging spectroscopy. *Remote Sensing of Environment*, 167:168–180.

Haralick, R. M., Shanmugam, K., and Dinstein, I. (1973). Textural features for image classification. *IEEE Transactions on Systems, Man, and Cybernetics*, 3(6):610–621.

Harris, J. R., Day, S. D., and Kane, B. (2008). Nitrogen fertilization during planting and establishment of the urban forest: a collection of five studies. *Urban Forestry & Urban Greening*, 7(3):195–206.

Hastie, T., Tibshirani, R., and Friedman, J. (2009). *The Elements of Statistical Learning*. Springer Series in Statistics. Springer New York.

Heisler, G. M. (1986). Effects of individual trees on the solar radiation climate of small buildings. *Urban Ecology*, 9(3-4):337–359.

Heisler, G. M. (1990). Mean wind speed below building height in residential neighborhoods with different tree densities. volume 96. Proceedings of the American Society of Heating, Refrigeration and Air conditioning Engineers.

Heisler, G. M., Ellis, A., Nowak, D. J., and Yesilonis, I. (2015). Modeling and imaging land-cover influences on air temperature in and near baltimore, md. *Theoretical and Applied Climatology*, 124(1-2):497–515.

Hijmans, R. J. (2016). *raster: Geographic Data Analysis and Modeling*. R package version 2.5-8.

Homer, C., Dewitz, J., Yang, L., Jin, S., Danielson, P., Xian, G., Coulston, J., Herold, N., Wickham, J., and Megown, K. (2015). Completion of the 2011 national land cover database for the conterminous united states–representing a decade of land cover change information. *Photogrammetric Engineering & Remote Sensing*, 81(5):345–354.

Hostetler, A. E., Rogan, J., Martin, D., DeLauer, V., and O'Neil-Dunne, J. (2013). Characterizing tree canopy loss using multi-source gis data in central massachusetts, usa. *Remote Sensing Letters*, 4(12):1137–1146.

Huang, Y. J., Akbari, H., and Taha, H. (1990). The wind-shielding and shading effects of trees on residential heating and cooling requirements. volume 96. Proceedings of the American Society of Heating, Refrigeration and Air conditioning Engineers.

Huang, Y. J., Akbari, H., Taha, H., and Rosenfeld, A. H. (1987). The potential of vegetation in reducing summer cooling loads in residential buildings. *Journal of Climate and Applied Meteorology*, 26(9):1103–1116.

Irani, F. M. and Galvin, M. F. (2002). Strategic urban forests assessment. *Maryland Department of Natural Resources, Baltimore, MD*.

itreetools.org. i–tree software suite.

Ji, L. and Gallo, K. (2006). An agreement coefficient for image comparison. *Photogrammetric Engineering & Remote Sensing*, 72(7):823–833.

Jim, C. Y. (1998). Impacts of intensive urbanization on trees in hong kong. *Environmental Conservation*, 25(2):146–159.

Jo, H.-K. and McPherson, E. (2001). Indirect carbon reduction by residential vegetation and planting strategies in chicago, usa. *Journal of Environmental Management*, 61(2):165–177.

Kabisch, N., Frantzeskaki, N., Pauleit, S., Naumann, S., Davis, M., Artmann, M., Haase, D., Knapp, S., Korn, H., Stadler, J., et al. (2016). Nature-based solutions to climate change mitigation and adaptation in urban areas: perspectives on indicators, knowledge gaps, barriers, and opportunities for action. *Ecology and Society*, 21(2).

Karatzoglou, A., Smola, A., Hornik, K., and Zeileis, A. (2004). kernlab – an S4 package for kernel methods in R. *Journal of Statistical Software*, 11(9):1–20.

King, D. A. (1990). The adaptive significance of tree height. *The American Naturalist*, 135(6):809–828.

Law, N., Band, L., and Grove, M. (2004). Nitrogen input from residential lawn care practices in suburban watersheds in baltimore county, md. *Journal of Environmental Planning and Management*, 47(5):737–755.

Liaw, A. and Wiener, M. (2002). Classification and regression by randomforest. *R News*, 2(3):18–22.

Lim, K., Treitz, P., Wulder, M., St-Onge, B., and Flood, M. (2003). Lidar remote sensing of forest structure. *Progress in physical geography*, 27(1):88–106.

Lindroth, R. L. and Batzli, G. O. (1984). Plant phenolics as chemical defenses: effects of natural phenolics on survival and growth of prairie voles (microtus ochrogaster). *Journal of Chemical Ecology*, 10(2):229–244.

Liu, Y., Arp, H. P. H., Song, X., and Song, Y. (2017). Research on the relationship between urban form and urban smog in china. *Environment and Planning B: Urban Analytics and City Science*, 44(2):328–342.

Liu, Z., He, C., Zhou, Y., and Wu, J. (2014). How much of the world's land has been urbanized, really? a hierarchical framework for avoiding confusion. *Landscape Ecology*, 29(5):763–771.

Lu, D. and Weng, Q. (2007). A survey of image classification methods and techniques for improving classification performance. *International Journal of Remote Sensing*, 28(5):823–870.

Ma, L., Deng, J., Yang, H., Hong, Y., and Wang, K. (2015). Urban landscape classification using chinese advanced high-resolution satellite imagery and an object-oriented multivariable model. *Frontiers of Information Technology & Electronic Engineering*, 16(nil):238–248.

MacFaden, S. W. and O'Neil-Dunne, J. P. (2012). A report on honolulu's existing and possible tree canopy. Technical report, US Department of Agriculture, Forest Service, Northern Research Station.

MacFaden, S. W., O'Neil-Dunne, J. P., Royar, A. R., Lu, J. W., and Rundle, A. G. (2012). High-resolution tree canopy mapping for new york city using lidar and object-based image analysis. *Journal of Applied Remote Sensing*, 6(1):063567–1.

Marinelli, D., Paris, C., and Bruzzone, L. (2019). An approach to tree detection based on the fusion of multitemporal lidar data. *IEEE Geoscience and Remote Sensing Letters*, 16(11):1771–1775.

Martin, M. E. and Aber, J. D. (1997). High spectral resolution remote sensing of forest canopy lignin, nitrogen, and ecosystem processes. *Ecological applications*, 7(2):431–443.

Mathieu, R., Aryal, J., and k. Chong, A. (2007). Object-based classification of ikonos imagery for mapping large-scale vegetation communities in urban areas. *Sensors*, 7(11):2860–2880.

McDonnell, M. J., Pickett, S. T., Groffman, P., Bohlen, P., Pouyat, R. V., Zipperer, W. C., Parmelee, R. W., Carreiro, M. M., and Medley, K. (2008). Ecosystem processes along an urban-to-rural gradient. In *Urban Ecology*, pages 299–313. Springer.

McNeil, B. E., Read, J. M., Sullivan, T. J., McDonnell, T. C., Fernandez, I. J., and Driscoll, C. T. (2008). The spatial pattern of nitrogen cycling in the adirondack park, new york. *Ecological Applications*, 18(2):438–452.

McPherson, E., Simpson, J. R., and Livingston, M. (1989). Effects of three landscape treatments on residential energy and water use in tucson, arizona. *Energy and Buildings*, 13(2):127–138.

McPherson, E. G., Herrington, L. P., and Heisler, G. M. (1988). Impacts of vegetation on residential heating and cooling. *Energy and Buildings*, 12(1):41–51.

McPherson, E. G. and Kendall, A. (2014). A life cycle carbon dioxide inventory of the million trees los angeles program. *The International Journal of Life Cycle Assessment*, 19(9):1653–1665.

McPherson, E. G. and Simpson, J. R. (1999). Carbon dioxide reduction through urban forestry. *Gen. Tech. Rep. PSW-171, USDA For. Serv., Pacific Southwest Research Station, Albany, CA*.

McPherson, E. G., van Doorn, N. S., and Peper, P. J. (2016). Urban tree database and allometric equations.

McPherson, G., Simpson, J. R., Peper, P. J., Maco, S. E., and Xiao, Q. (2005). Municipal forest benefits and costs in five us cities. *Journal of Forestry*, 103(8):411–416.

Mellway, R. D., Tran, L. T., Prouse, M. B., Campbell, M. M., and Constabel, C. P. (2009). The wound-, pathogen-, and ultraviolet b-responsive myb134 gene encodes an r2r3 myb transcription factor that regulates proanthocyanidin synthesis in poplar. *Plant Physiology*, 150(2):924–941.

Mollenhoff, D. V. (2003). *Madison, a history of the formative years*. Univ of Wisconsin Press.

Möller, M., Lymburner, L., and Volk, M. (2007). The comparison index: A tool for assessing the accuracy of image segmentation. *International Journal of Applied Earth Observation and Geoinformation*, 9(3):311–321.

Myeong, S., Nowak, D. J., Hopkins, P. F., and Brock, R. H. (2001). Urban cover mapping using digital, high-spatial resolution aerial imagery. *Urban Ecosystems*, 5(4):243–256.

Myint, S. W., Gober, P., Brazel, A., Grossman-Clarke, S., and Weng, Q. (2011). Per-pixel vs. object-based classification of urban land cover extraction using high spatial resolution imagery. *Remote Sensing of Environment*, 115(5):1145–1161.

Neely, D. (1980). Tree fertilization trials in illinois. *Journal of Arboriculture*, 6(10):271–273.

Nowak, D. J., Appleton, N., Ellis, A., and Greenfield, E. (2017). Residential building energy conservation and avoided power plant emissions by urban and community trees in the united states. *Urban Forestry & Urban Greening*, 21:158–165.

Nowak, D. J. and Crane, D. E. (2002). Carbon storage and sequestration by urban trees in the usa. *Environmental Pollution*, 116(3):381–389.

Nowak, D. J., Crane, D. E., and Stevens, J. C. (2006). Air pollution removal by urban trees and shrubs in the united states. *Urban forestry & urban greening*, 4(3-4):115–123.

Nowak, D. J., Greenfield, E. J., Hoehn, R. E., and Lapoint, E. (2013). Carbon storage and sequestration by trees in urban and community areas of the united states. *Environmental Pollution*, 178(nil):229–236.

Nowak, D. J., Hirabayashi, S., Bodine, A., and Greenfield, E. (2014). Tree and forest effects on air quality and human health in the united states. *Environmental Pollution*, 193(nil):119–129.

Nowak, D. J., Robert III, E., Crane, D. E., Stevens, J. C., and Fisher, C. L. (2010). Assessing urban forest effects and values, chicago's urban forest. *Northern Research Station Resource Bull.*, NRS-37.

Nowak, D. J., Rowntree, R. A., McPherson, E., Sisinni, S. M., Kerkmann, E. R., and Stevens, J. C. (1996). Measuring and analyzing urban tree cover. *Landscape and Urban Planning*, 36(1):49–57.

Nowak, D. J., Stevens, J. C., Sisinni, S. M., and Luley, C. J. (2002). Effects of urban tree management and species selection on atmospheric carbon dioxide.

O'Neil-Dunne, J. P. M. (2009). A report on the city of des moines existing and possible urban tree canopy. Technical report, US Department of Agriculture, Forest Service, Northern Research Station.

O'Neil-Dunne, J. P. M. (2011). A report on the city of philadelphia's existing and possible tree canopy. Technical report, US Department of Agriculture, Forest Service, Northern Research Station.

O'Neil-Dunne, J. P. M., MacFaden, S. W., and Grove, J. M. (2009). A report on washington, dc's existing and possible tree canopy. Technical report, US Department of Agriculture, Forest Service, Northern Research Station.

Ouyang, Z.-T., Zhang, M.-Q., Xie, X., Shen, Q., Guo, H.-Q., and Zhao, B. (2011). A comparison of pixel-based and object-oriented approaches to vhr imagery for mapping saltmarsh plants. *Ecological Informatics*, 6(2):136–146.

Paris, C. and Bruzzone, L. (2015). A three-dimensional model-based approach to the estimation of the tree top height by fusing low-density lidar data and very high resolution optical images. *IEEE Transactions on Geoscience and Remote Sensing*, 53(1):467–480.

Parker, J. H. (1983). Landscaping to reduce the energy used in cooling buildings. *Journal of Forestry*, 81(2):82–105.

Pataki, D. E., Alig, R. J., Fung, A. S., Golubiewski, N. E., Kennedy, C. A., McPherson, E. G., Nowak, D. J., Pouyat, R. V., and Lankao, P. R. (2006). Urban ecosystems and the north american carbon cycle. *Global Change Biology*, 12(11):2092–2102.

Pataki, D. E., Carreiro, M. M., Cherrier, J., Grulke, N. E., Jennings, V., Pincetl, S., Pouyat, R. V., Whitlow, T. H., and Zipperer, W. C. (2011). Coupling biogeochemical cycles in urban environments: Ecosystem services, green solutions, and misconceptions. *Frontiers in Ecology and the Environment*, 9(1):27–36.

Pelletier, K. and O'Neil-Dunne, J. P. (2009). A report on the city of new haven's existing and possible urban tree canopy. Technical report, US Department of Agriculture, Forest Service, Northern Research Station.

Poland, T. M. and McCullough, D. G. (2006). Emerald ash borer: invasion of the urban forest and the threat to north america's ash resource. *Journal of Forestry*, 104(3):118–124.

Pretzsch, H., Biber, P., Uhl, E., Dahlhausen, J., Schütze, G., Perkins, D., Rötzer, T., Caldentey, J., Koike, T., van Con, T., et al. (2017). Climate change accelerates growth of urban trees in metropolises worldwide. *Scientific reports*, 7(1):15403.

R Core Team (2016). *R: A Language and Environment for Statistical Computing*. R Foundation for Statistical Computing, Vienna, Austria.

Reich, P. B. (2012). Key canopy traits drive forest productivity. *Proceedings of the Royal Society B: Biological Sciences*, 279(1736):2128–2134.

Ridgeway, G. (2017). *gbm: Generalized Boosted Regression Models*. R package version 2.1.3.

Riemann, R., Wilson, B. T., Lister, A., and Parks, S. (2010). An effective assessment protocol for continuous geospatial datasets of forest characteristics using usfs forest inventory and analysis (fia) data. *Remote Sensing of Environment*, 114(10):2337–2352.

Romanczyk, P., Kelbe, D., van Aardt, J., Cawse-Nicholson, K., McGlinchy, J., and Krause, K. (2012). Assessing the impact of broadleaf tree structure on airborne full-waveform small-footprint lidar signals. *Silvilaser 2012*.

Roussel, J. and Auty, D. (2018). lidr: Airborne lidar data manipulation and visualization for forestry applications. r package version 1.0. 0.

Roussel, J.-R., Caspersen, J., Béland, M., Thomas, S., and Achim, A. (2017). Removing bias from lidar-based estimates of canopy height: Accounting for the effects of pulse density and footprint size. *Remote Sensing of Environment*, 198(nil):1–16.

Roy, S., Byrne, J., and Pickering, C. (2012). A systematic quantitative review of urban tree benefits, costs, and assessment methods across cities in different climatic zones. *Urban Forestry & Urban Greening*, 11(4):351–363.

Russell G. Congalton, K. G. (1999). *Assesssing the accuracy of remotely sensed data principles and practices*. Lewis Publications.

Ryan, M. G. and Yoder, B. J. (1997). Hydraulic limits to tree height and tree growth. *Bioscience*, 47(4):235–242.

Searle, S. Y., Turnbull, M. H., Boelman, N. T., Schuster, W. S. F., Yakir, D., and Griffin, K. L. (2012). Urban environment of new york city promotes growth in northern red oak seedlings. *Tree Physiology*, 32(4):389–400.

Shoup, S., Reavis, R., and Whitcomb, C. E. (1981). Effects of pruning and fertilizers on establishment of bareroot deciduous trees. *Journal of Arboriculture*, 7(6):155–157.

Simpson, J. and McPherson, E. (1998). Simulation of tree shade impacts on residential energy use for space conditioning in sacramento. *Atmospheric Environment*, 32(1):69–74.

Simpson, J. R. (2002). Improved estimates of tree-shade effects on residential energy use. *Energy and Buildings*, 34(10):1067–1076.

Singh, A., Serbin, S. P., McNeil, B. E., Kingdon, C. C., and Townsend, P. A. (2015). Imaging spectroscopy algorithms for mapping canopy foliar chemical and morphological traits and their uncertainties. *Ecological Applications*, 25(8):2180–2197.

Song, Y., Imanishi, J., Sasaki, T., Ioki, K., and Morimoto, Y. (2016). Estimation of broad-leaved canopy growth in the urban forested area using multi-temporal airborne lidar datasets. *Urban Forestry & Urban Greening*, 16(nil):142–149.

Stamp, N. (2003). Out of the quagmire of plant defense hypotheses. *The Quarterly Review of Biology*, 78(1):23–55.

Stoeckeler, J., Curtis, W. R., et al. (1960). Soil moisture regime in southwestern wisconsin as affected by aspect and forest type. *Journal of Forestry*, 58:892–896.

Stow, D., Hamada, Y., Coulter, L., and Anguelova, Z. (2008). Monitoring shrubland habitat changes through object-based change identification with airborne multispectral imagery. *Remote Sensing of Environment*, 112(3):1051–1061.

Thapa, R. B. and Murayama, Y. (2009). Urban mapping, accuracy, & image classification: A comparison of multiple approaches in tsukuba city, japan. *Applied Geography*, 29(1):135–144.

Thayer Jr, R. L. and Maeda, B. T. (1985). Measuring street tree impact on solar performance: a five-climate computer modeling study. *Journal of arboriculture (USA)*.

Thomas, N., Hendrix, C., and Congalton, R. G. (2003). A comparison of urban mapping methods using high-resolution digital imagery. *Photogrammetric Engineering & Remote Sensing*, 69(9):963–972.

United Nations (2018). 2018 revision of world urbanization prospects.

United State Environmental Protection Agency (2017). Inventory of u.s. greenhouse gas emissions and sinks: Annex 2 methodology and data for estimating $CO_2$ emissions from fossil fuel combustion. (430-P-17-001).

U.S. Census Tract Centroids (2010). Accessed Jul. 24, 2018.

U.S. Department of Energy, E. I. A. (2009). Wisconsin household energy report.

Ustin, S. L., Roberts, D. A., Gamon, J. A., Asner, G. P., and Green, R. O. (2004). Using imaging spectroscopy to study ecosystem processes and properties. *BioScience*, 54(6):523.

van der Walt, S., Schönberger, J. L., Nunez-Iglesias, J., Boulogne, F., Warner, J. D., Yager, N., Gouillart, E., Yu, T., and the scikit-image contributors (2014). scikit-image: image processing in Python. *PeerJ*, 2:e453.

Veldman, J. W., Aleman, J. C., Alvarado, S. T., Anderson, T. M., Archibald, S., Bond, W. J., Boutton, T. W., Buchmann, N., Buisson, E., Canadell, J. G., et al. (2019). Comment on "the global tree restoration potential". *Science*, 366(6463):eaay7976.

von Döhren, P. and Haase, D. (2015). Ecosystem disservices research: A review of the state of the art with a focus on cities. *Ecological Indicators*, 52(nil):490–497.

Walker, J. S. and Briggs, J. M. (2007). An object-oriented approach to urban forest mapping in phoenix. *Photogrammetric Engineering & Remote Sensing*, 73(5):577–583.

Walton, J. T., Nowak, D. J., and Greenfield, E. J. (2008). Assessing urban forest canopy cover using airborne or satellite imagery. *Arboriculture & Urban Forestry*, 34(6):334–340.

Ward, K., Lauf, S., Kleinschmit, B., and Endlicher, W. (2016). Heat waves and urban heat islands in europe: A review of relevant drivers. *Science of the Total Environment*, 569:527–539.

Weissert, L., Salmond, J., and Schwendenmann, L. (2014). A review of the current progress in quantifying the potential of urban forests to mitigate urban co2 emissions. *Urban Climate*, 8(nil):100–125.

Wright, I. J., Reich, P. B., Westoby, M., Ackerly, D. D., Baruch, Z., Bongers, F., Cavender-Bares, J., Chapin, T., Cornelissen, J. H., Diemer, M., et al. (2004). The worldwide leaf economics spectrum. *Nature*, 428(6985):821.

Ye, S., Pontius, R. G., and Rakshit, R. (2018). A review of accuracy assessment for object-based image analysis: From per-pixel to per-polygon approaches. *ISPRS Journal of Photogrammetry and Remote Sensing*, 141(nil):137–147.

Young, R. F. (2011). Planting the living city. *Journal of the American Planning Association*, 77(4):368–381.

Zhou, W. and Troy, A. (2008). An object oriented approach for analysing and characterizing urban landscape at the parcel level. *International Journal of Remote Sensing*, 29(11):3119–3135.

Zipper, S. C., Schatz, J., Singh, A., Kucharik, C. J., Townsend, P. A., and Loheide II, S. P. (2016). Urban heat island impacts on plant phenology: intra-urban variability and response to land cover. *Environmental Research Letters*, 11(5):054023.

Zipperer, W. C. and Guntenspergen, G. R. (2009). Vegetation composition and structure of forest patches along urban-rural gradients. *In: McDonnell, MJ; Hahns, AK; Breuste, JH, eds. Ecology of Cities and Towns. Cambridge, UK: Cambridge University Press. 274-286.*

Ziter, C. D., Pedersen, E. J., Kucharik, C. J., and Turner, M. G. (2019). Scale-dependent interactions between tree canopy cover and impervious surfaces reduce daytime urban heat during summer. *Proceedings of the National Academy of Sciences*, 116(15):7575–7580.

Zvoleff, A. (2016). *glcm: Calculate Textures from Grey-Level Co-Occurrence Matrices (GLCMs)*. R package version 1.6.1.

Żaneta Kaszta, Kerchove, R. V. D., Ramoelo, A., Cho, M., Madonsela, S., Mathieu, R., and Wolff, E. (2016). Seasonal separation of african savanna components using worldview-2 imagery: A comparison of pixel- and object-based approaches and selected classification algorithms. *Remote Sensing*, 8(9):763.